THE REGULATION OF GENE EXPRESSION PROFILES IN CLEAR CELL RENAL CELL CARCINOMA BY TUMOR HETEROGENEITY AND ENVIRONMENTAL EXPOSURE

Samira A. Brooks

A dissertation submitted to the faculty of the University of North Carolina at Chapel Hill in partial fulfillment of the requirements for the degree of Doctor of Philosophy in the Curriculum of Toxicology in the School of Medicine.

Chapel Hill
2015

Approved by:

W. Kimryn Rathmell

Rebecca Fry

Charles Perou

Stephanie Padilla

Mathew Nielsen

ABSTRACT

Samira A. Brooks: The regulation of gene expression profiles in clear cell Renal Cell Carcinoma by tumor heterogeneity and environmental exposure
(Under the direction of W. Kimryn Rathmell)

Currently, the disease management and therapeutic strategies for renal cell carcinoma (RCC) have arisen from cancer biology discoveries, but have evolved fairly independently of individual tumor biology. Thus, a gap has emerged in our understanding of the fundamental paradigms of what core molecular features are important for tissue based biomarker research today. Although extensive effort has been placed on identifying molecular biomarkers for RCC, remarkably, there are few validated biomarkers with substantive impact on managing disease prognosis. The emergence of high-throughput molecular profiling technologies provides the opportunity to explore the underlying molecular features of RCC that will warrant the enhanced understanding of its biology and shed light on future therapeutic methods to treat the disease.

Identifying molecular biomarkers that provide insight towards biological processes, pathogenesis, and response to therapeutics has been at the forefront of current research. The cancer biology field has focused especially on this area in hopes of further understanding the molecular aberrations that contribute to disease development and progression. Prognostic biomarkers are also needed for making personalized treatment decisions, particularly at a time when adjuvant and neoadjuvant options are becoming the mainstay of therapy for many cancers, including Renal Cell Carcinoma (RCC) [1, 2]. Exploiting the genome to uncover

biomarkers that are indicative of disease progression and aggressiveness can improve patient treatment and survival.

In this dissertation, novel gene expression signatures for the predominant subtype of RCC, clear cell Renal Cell Carcinoma (ccRCC), are validated as imperative prognostic signatures, whose underlying biology is driven by distinct metabolic pathways. Furthermore, environmental exposures to the heavy metal Cadmium, alters the kidney genome and epigenome that may influence the kidney to develop into these ccRCC subtypes and thus impact patient prognosis. These biomarkers of ccRCC have the potential to have an impression on the clinical arena and can be used for assessing prognostic and predictive outcomes.

To my family and friends who showered me with words of encouragement and endless support.

ACKNOWLEDGEMENTS

The continuous support from family and friends has facilitated my progress and growth through graduate school, as well as gave me the strength to successfully defend my doctoral thesis. I love you all and thank you for making me believe I can achieve anything.

I would like to extend my gratitude towards my mentor Dr. W. Kimryn Rathmell who allowed me to join her lab and had faith in me to lead a project in which I had little background and expertise. You have made me a well-rounded scientist that will be equipped to take on any career path I choose. Thank you for all your support and mentorship.

I would also like to thank my committee members Dr. Rebecca Fry, Dr. Charles Perou, Dr. Stephanie Padilla, Dr. Joel Parker, and Dr. Mathew Nielsen for your advice and ideas that have substantially improved my critical thinking skills. Thank you Dr. Joel Parker for being an exceptional co-mentor and for having the patience to teach me bioinformatics and answer my numerous questions. Dr. Rebecca Fry and Dr. Stephanie Padilla thank you for your willingness to always offer assistance and expertise to my projects.

The Rathmell lab past and present members made research enjoyable, and offered support and feedback for both personal and scientific issues. Thank you for being my second family. Finally, I would like to thank the BBSP, IMSD, IME, and the curriculum in Toxicology faculty and staff who offered professional and personal support throughout my studies at UNC that has bolstered my success in graduate school.

TABLE OF CONTENTS

LIST OF TABLES

LIST OF FIGURES

LIST OF ABBREVIATIONS

ACACA	acetyl-CoA carboxylase alpha
ACO2	aconitase 2
AKI	acute kidney injury
ALDOB	fructose-bisphosphate aldolase B
AMPK	AMP-activated protein kinase
ARNT	aryl hydrocarbon receptor nuclear translocator
BAP1	BRCA1 associated protein-1
CAF	cytokine and angiogenic factor
CAIX	carbonic anhydrase 9
ccA	clear cell A
ccB	clear cell B
ccRCC	clear cell Renal Cell Carcinoma
Cd	Cadmium
Cdcl2	cadmium chloride
CI	confidence interval
CO2	carbon dioxide
CS	cigarette smoke
CSS	cancer-specific survival
DLD	dihydrolipoamide dehydrogenase
DNA	deoxyribonucleic acid
ECM	extracellular matrix

ENO1	alpha-enolase
FAIRE	formaldehyde-assisted isolation of regulatory elements
FASN	fatty acid synthase
FBP1	fructose 1,6 biphosphase 1
FBS	fetal bovine serum
FDA	Food and Drug Administration
FDG	fluoridated 2-deoxyglucose
FFPE	formalin-fixed paraffin embedded
G6PC	glucose-6-phosphatase
G6PD	glucose-6-phosphate dehydrogenase
GLUT1	glucose transporter 1
GRB2	growth factor receptor-bound protein 2
HIF	hypoxia-inducible factor
HIF1A	hypoxia-inducible factor-1alpha
HIF2A	hypoxia-inducible factor-2apha
HK3	hexokinase 3
HKC	human kidney cell
HR	hazard ratio
IAP	inhibitors of apoptosis
IARC	International Agency for Research on Cancer
IC50	half maximal inhibitory concentration
IMP3	U3 small nucleolar ribonucleoprotein
IRB	institutional review board

JMJD1A	Jumonji domain-containing protein 1A
LAD	logical analysis of data
LDH	lactate dehydrogenase
MAPK	mitogen-activated protein kinases
ME1	malic enzyme 1
miRNA	micro ribonucleic acid
MRI	magnetic resonance imaging
mRNA	messenger ribonucleic acid
MT	metallothinein
MTF1	metal regulatory transcription factor 1
mTOR	mammalian target of rapamycin
NADPH	nicotinamide adenine dinucleotide phosphate
OS	overall survival
PAM	prediction analysis for microarray
PBRM1	protein polybromo-1
PCK1	phosphoenolpyruvate carboxykinas 1
PCK2	phosphoenolpyruvate carboxykinase 2
PDGF	platelet-derived growth factor
PDK2	pyruvate dehydrogenase lipoamide kinase isozyme 2
PDK4	pyruvate dehydrogenase kinase
PECAM	platelet-endothelial cell adhesion molecule
PET	positron emission tomography
PFKL	6-phosphofructokinase

PFKM	phosphofructokinase muscle
PFS	progressive-free survival
PGD	phosphogluconate dehydrogenase
PGK1	phosphoglycerate kinase 1
PGLS	6-Phosphogluconolactonase
PI3K	phosphatidylinositol 3-kinase
PKD	Proteinase K digest
PKLR	pyruvate kinase isozymes R/L
RCC	Renal Cell Carcinoma
RFS	recurrence-free survival
RHEB	Ras homolog enriched in brain
RNA	ribonucleic acid
ROS	reactive oxygen species
SAM	significance analysis of microarrays
SDHB	succinate dehydrogenase complex subunit B
SDHC	succinate dehydrogenase complex subunit C
SETD2	SET domain containing 2
SHC	Src homology 2 domain-containing
shRNA	small hairpin RNA
SSIGN `	Mayo Clinic Stage, Size, Grade, and Necrosis score
SUV	standard uptake value
TCGA	The Cancer Genome Atlas
TF	tissue factor

TKT	transketolase
TMA	tissue microarray
UISS	UCLA Integrated Staging System
uM	micromolar
UTR	untranslated regions
VEGFA	vascular endothelial growth factor alpha
VEGFR	vascular endothelial growth factor receptor
VHL	von Hippel-Lindau

CHAPTER 1[1,2]: INTRODUCTION

Clear cell Renal Cell Carcinoma

The incidence of adult Renal Cell Carcinoma (RCC), or kidney cancer, is on a steady rise in the western world. In the U.S, kidney cancer is the sixth leading cause of cancer among men and the eighth among women[3]. There are multiple subtypes of this disease, however, over 70% of patients with renal tumors have the clear cell (ccRCC) subtype, a tumor postulated to arise in the proximal tubules and is associated with chromosome 3p deletions and inactivation of the Von Hippel-Lindau (VHL) tumor suppressor[4]. VHL mutations lead to the stabilization of hypoxia-inducible factors (HIFs) and thus the activation of the hypoxia pathway, a response that promotes cancer cell survival through increases in angiogenic growth factor production and metabolic reprograming of cellular glucose and energy metabolism [5]. Even with advances in elucidating the underlying molecular biology of ccRCC, the metastatic setting of this disease remains with no curative therapy options; leaving patients with a median survival range of 10-26 months, even using the best therapies[6]. Exploring the underlying molecular features of ccRCC will warrant the enhanced understanding of its biology. Thus, a novel clinically applicable classification and prognostic tool to identify two subtypes of ccRCC, clear cell A (ccA) and clear cell B (ccB), was elucidated and validated[7]. This 34-gene expression signature (ClearCode34) is

[1] Adapted from Brooks, S.A. & Rathmell, W.K. (2014) Uniting Molecular Biomarkers to Advance the Science and Care of Clear Cell Renal Cell Carcinoma. The Journal of OncoPathology 1, 45-54.
[2] Adapted from Halifax Project. (2014) Assessing the carcinogenic effects of low dose exposures to chemical mixtures in the environment. Carcinogenesis, In press.

expounded on in Chapter 2 and can be used as a prognostic tool to assess progression risk for this cancer that has no optimal treatment for metastatic disease.

The majority of ccRCC patients presents with localized Stage I-III disease, with partial or complete nephrectomy being efficient for tumor removal[8]. However, around 17% of ccRCC patients will have metastatic disease and one-third will recur within the first five years following surgery. ccRCC metastases usually develop in the bone, brain, and lungs[9], all having variable survival outcomes. Few therapeutic options are available for these patients due to disease resistance to chemotherapy and radiation, so targeted treatment to the vascular endothelial growth factor receptor (VEGFR) is the predominate treatment option[8]. Some metastatic patients can also be treated through metastasectomy, surveillance, and high dosing of interleukin-2. Nonetheless, primary tumor features have little to no application towards the prognostics of metastatic disease and accurate tools are increasingly needed that predict response to therapy, progression-free and overall survival.

VEGFR inhibitors Sunitinib, Bevacizumab, and Sorafenib have been used independently, as well as in combination with interferon-alpha to treat metastatic ccRCC, but changes in tumor response and survival are not strong enough to make this the mainstay of therapy[9]. Interestingly, these treatments are recommended as first-line therapy options in international treatment guidelines for metastatic patients. Temsirolimus and Everolimus, two mTOR kinase pathway inhibitors, are also recommended as first and second-line treatment options to combat the deregulated metabolic activity of the disease[9]. Further research and clinical trials are ongoing to determine which therapeutic options and timing of administration is best for treating ccRCC. Elucidating prognostic biomarkers of ccRCC will

facilitate the development of more efficient therapeutics and clinicians with determining the optimal treatment for their patients to improve prognostics.

ccRCC Prognostic Biomarkers

Increasingly, genetic markers and signatures of cancer are being explored to define changes to the transcriptome that expand the knowledge of tumor state, progression characteristics, and response to therapy[10]. The oldest prognostic variables for ccRCC are pathologic stage, lymph nodes status, and histologic grade. While the most established biomarker is inactive VHL, which allows HIF stabilization, with tumors expressing HIF2A associated with a poor prognosis compared to tumors expressing both HIF1A and 2A[11] [12], however, this effect is modest, and has not found clinical traction. In addition to individual markers, gene signatures have been revealed through whole genome expression profiling to identify discrete and global changes in transcript expression. Recently, two subtypes of ccRCC, ccA and ccB, were identified, and these biologically defined tumors were associated with a striking difference in overall and cancer specific survival[13, 14]. In my work, I adapted the signature to a core set of genes measurable in crude lysates prepared from formalin-fixed paraffin embedded (FFPE) tissue, as well as high-throughput mRNA transcriptomic data, verifying the two predominant gene expression patterns, and creating a prognostic algorithm that can be applied widely to clinical specimens[7]. Although the new recognition of intratumoral heterogeneity of ccRCC raises a challenge for identifying and validating genetic biomarkers, my data shows stable core gene expression patterns across tumors suggests expression profiles could be instrumental for personalized disease management and elucidating new strategies for individualized therapy.

VHL and HIFs

The gene mutation events most commonly associated with a cancer type often provide the most clear-cut molecular tools for discriminating between heterogeneous disease subsets. In ccRCC, this event is the loss of function of the von Hippel-Lindau (VHL) tumor suppressor gene through deletion, mutation, or hypermethylation and is the oldest and most frequent hallmark of clear cell RCC (ccRCC)[15] [16]. Evidence of VHL gene perturbation can be identified in as many as 92% of renal tumors [17]. It has been postulated that VHL loss is an initiating event for ccRCC, however, sufficient data is still lacking to associate VHL status to prognostic outcomes. There are conflicting studies that show the clinical implications of VHL mutation or loss, and this potential biomarker is challenged by the diversity of mutant alleles, challenges in it's analysis owing to a highly GC-rich region in exon 1, as well as the high frequency of association with this event with ccRCC tumors. However, downstream factors that are dysregulated as a result of VHL loss, such as the hypoxia inducible factors (HIFs) and their targets have been shown promise as biomarkers.

The HIF family of transcription factors (notably, HIF1A and HIF2A) are stabilized following the inactivation of VHL, which allows these proteins to engage a co-factor HIF1B (also known as the aryl hydrocarbon nuclear transporter, ARNT) for translocation to the nucleus. Here, these transcription factors avidly promote the expression of genes involved in numerous cancer promoting activities, such as angiogenesis, invasion, and metastasis [18-22]. It has been established that HIF1A and HIF2A both play a role in ccRCC pathogenesis through these mechanisms, but by inducing the expression of distinct target genes [23]. *In vitro* studies using HCT116 and 786-0 cells that overexpress HIF1A and HIF2A, respectively, revealed that HIF2A inhibited HIF1A-promoted cell cycle activity while increasing HIF2A induced cell cycle progression and c-Myc gene expression [24]. It was

further observed that ccRCC tumors expressing HIF2A alone had c-myc-dependent proliferation, compared to tumors wild type for VHL or expressed both HIF1A and HIF2A that exhibited enhanced MAPK and mTOR signaling, with decreased levels of phosphorylated histone H2AX [25]. The strict observation that tumors could be categorized into three groups based on features of HIF expression (wild type VHL tumors, which lack HIF overexpression, H1H2 indicating expression of both HIF1A and HIF2A, and H2 for tumors expressing only HIF2A) paved the way for these profiles to serve as molecular biomarkers for classification of primary renal tumors.

How tumors harboring a VHL mutation come to express only one or both factors is still under investigation. HIF1A is located on chromosome 14q, in a region that is frequently lost in ccRCC. Recently, it has been observed through high-density single-nucleotide polymorphism arrays that kidney cancer has a higher frequency of 14q deletions compared to other cancers and includes focal deletions located within the HIF-1a locus [26]. This same group further demonstrated that expressing HIF1A in HIF1A null renal cell carcinoma cell lines inhibited cell proliferation, while suppression of HIF1A by shRNAs in lines known to express HIF1A and HIF2A increased proliferation and xenograft growth. In all, these results implicate the reverse roles of HIF1/2A: the novel characterization of HIF1A as a tumor suppressor in ccRCC and HIF2A as the oncogenic tumor promoter. Additional studies are needed to establish the prognostic value of HIF profiling and therapeutic potential of rendering this classification.

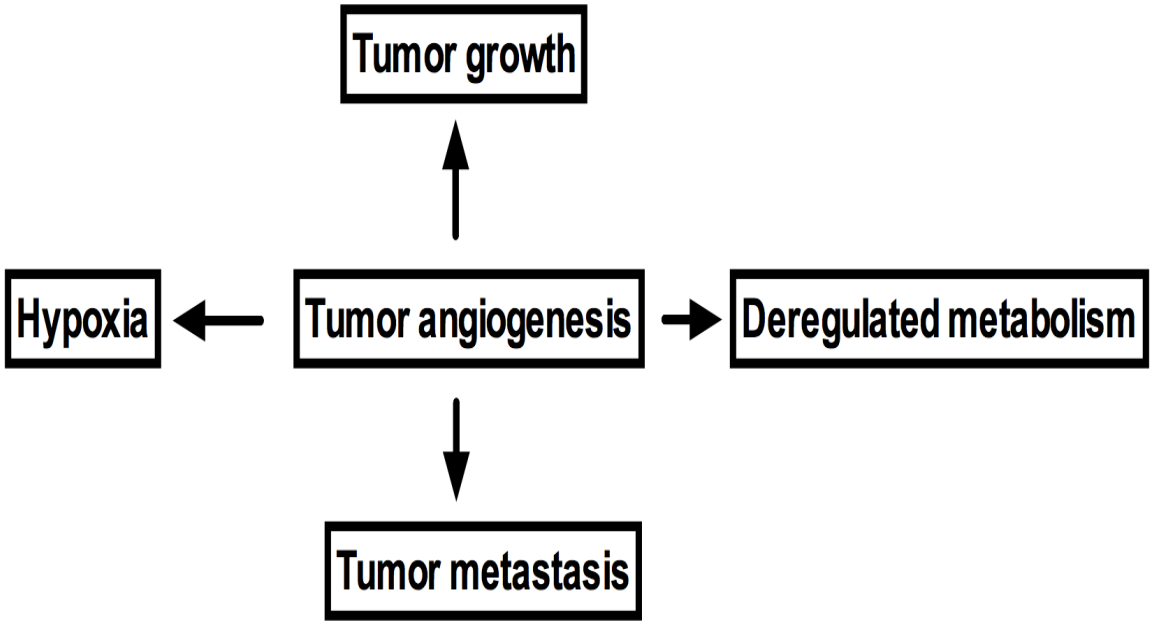

Figure 1.1: Examples of interaction of tumor angiogenesis with tumor microenvironment.

CAIX

CAIX (cG250), a downstream marker of inactive VHL, is transcriptionally regulated by HIF1A. CAIX is not expressed in normal kidney, but is highly expressed in the majority of ccRCC tumors, where this marker has been associated with improved outcomes [27]. To evaluate the prognostic value of CAIX expression in RCC, a tissue microarray of 228 RCC patients was examined for protein levels of CAIX. Significantly higher expression of CAIX ($p<0.001$) was measured in ccRCC compared to papillary and chromophobe RCC [27]. Stratified groups of patients with higher CAIX expression had more favorable prognosis compared to patients with low CAIX expression. CAIX has also been examined in correlation with VHL status [28]. Increased CAIX expression was found in tumors with VHL mutations compared to those without VHL mutations ($p=0.02$). In addition, longer progression-free ($p=0.037$) and disease specific ($p=0.001$) survival was associated with high CAIX expression and mutated VHL. Furthermore, univariate analysis of Ki67 (high staining) and carbonic anhydrase IX (CAIX) (low staining) revealed significant association with overall survival [29]. Multivariate analysis revealed that high Ki67 ($p=0.014$) and low CAIX ($p=0.009$) were significant predictors of disease specific survival and when combined into a single parameter could stratify tumors into risk groups. Finally, this tumor feature has been examined in a clinical trial testing the utility of a cG250 antibody adjuvant therapy. Only patients with the highest level of CAIX staining showed benefits to treatment, indicating the novel use of this marker to provide prognostic or predictive information is on the horizon [30].

VEGF and PDGF

Tumor growth and metastasis require angiogenesis to increase blood supply and recruit activating cells. Angiogenesis is tightly controlled by diverse subsets of ligands and receptors. Enrichment of ligands including growth factors, chemokines, cytokines, and endogenous angiogenesis inhibitors has been extensively observed in extracellular matrix (ECM) during vascularization. As tumor enlarges, hypoxia and nutrient deprivation occur and upregulate the expression of hypoxia inducible factor 1 alpha (HIF1A), VEGF-A, VEGFR-1, angiopoeitin-2 (Ang2), fibroblast growth factor-3 (FGF-3), nitric oxide synthase (NOS), and transforming growth factors (TGF-α, TGF-β1, TGF-β3) [31].

The vascular endothelial growth factor (VEGF) and its receptors, as well as platelet-derived growth factor (PDGF) has been established as key promoters of vascular bed expansion [32] and are aberrantly expressed in RCC. Sunitinib, a potent tyrosine kinase inhibitor of VEGFR 1-3 and PDGF-a/b, has shown strong antitumor properties [33], which have been validated in phase I, II, and III clinical studies [34]. A 2003 phase II study involving sixty-three RCC patients that received prior cytokine therapy of either interferon-alpha alone, interleukin-2 alone, or both interferon alpha and interleukin-2 revealed a partial response and stable disease for three or more months in 40% (95% CI, 28-53%) and 27% of patients following administration of sunitinib, respectively [35]. A complete or partial response was observed in 6% of patients treated with cytokine therapy only. A subsequent phase III study revealed the efficacy and safety of sunitinib as a first-line therapy for metastatic RCC compared to interferon alfa [36]. 750 metastatic RCC patients without prior systemic treatment received either repeated 6-week cycles of sunitinib or interferon alfa. Patients administered sunitinib had significantly longer progression-free survival (PFS) compared to the interferon alfa group (HR, 0.42; 95% CI, 0.32 to 0.54; $p<0.001$). Moreover,

a higher objective response rate (31% vs. 6%, $p<0.001$) and better quality of life ($p<0.001$) was associated with sunitinib compared to interferon alfa, validating that sunitinib is an effective therapeutic strategy for the treatment of metastatic RCC. Studies are ongoing to identify predictive markers to assess clinical outcomes for sunitinib treatment [37, 38].

Predictive biomarkers for sorafenib and pazopanib, two additional tyrosine kinase inhibitors that target VEGFR and PDGF, have been effective in determining outcomes in metastatic cancer. Univariate and multivariate analysis confirmed serum VEGF levels were prognostic for overall survival (OS) and progression-free survival (PFS) in second-line treatment of sorafenib in 903 patients from the Treatment Approaches in Renal Cancer Global Evaluation Trial (TARGET) study [39]. However, no direct link was established between sorafenib treatment and VEGF levels for OS since significant correlation between VEGF and overall survival for patients that received sorafenib were only revealed after censoring post-cross-over placebo patients. Recently, chromosome copy number variations were significantly associated with clinical outcomes in metastatic ccRCC patients treated with sorafenib, sunitinib, or bavacisumab [38]. In addition, a phase II and phase III trial was used to evaluate cytokine and angiogenic factors (CAFs) as prognostic biomarkers for pazopanib treatment [40]. Interleukin 6, interleukin 8, hepatocyte growth factor, tissue inhibitor of metalloproteinases (TIMP)-1, and E-selectin were identified as candidate markers in a screen of 129 pazopanib-treated patients from a phase II trial with the greatest or least tumor shrinkage and confirmed to be associated with tumor response and PFS in 215 patients from the same trial. Furthermore, interleukin 6, interleukin 8, osteopontin, hepatocyte growth factor, and TIMP-1 were validated as prognostic markers for PFS in 344

patients from a randomized, placebo-controlled, pazopanib phase III study. These studies provide potential predictive markers beyond established clinical parameters for assessing response of targeted treatment with advanced RCC.

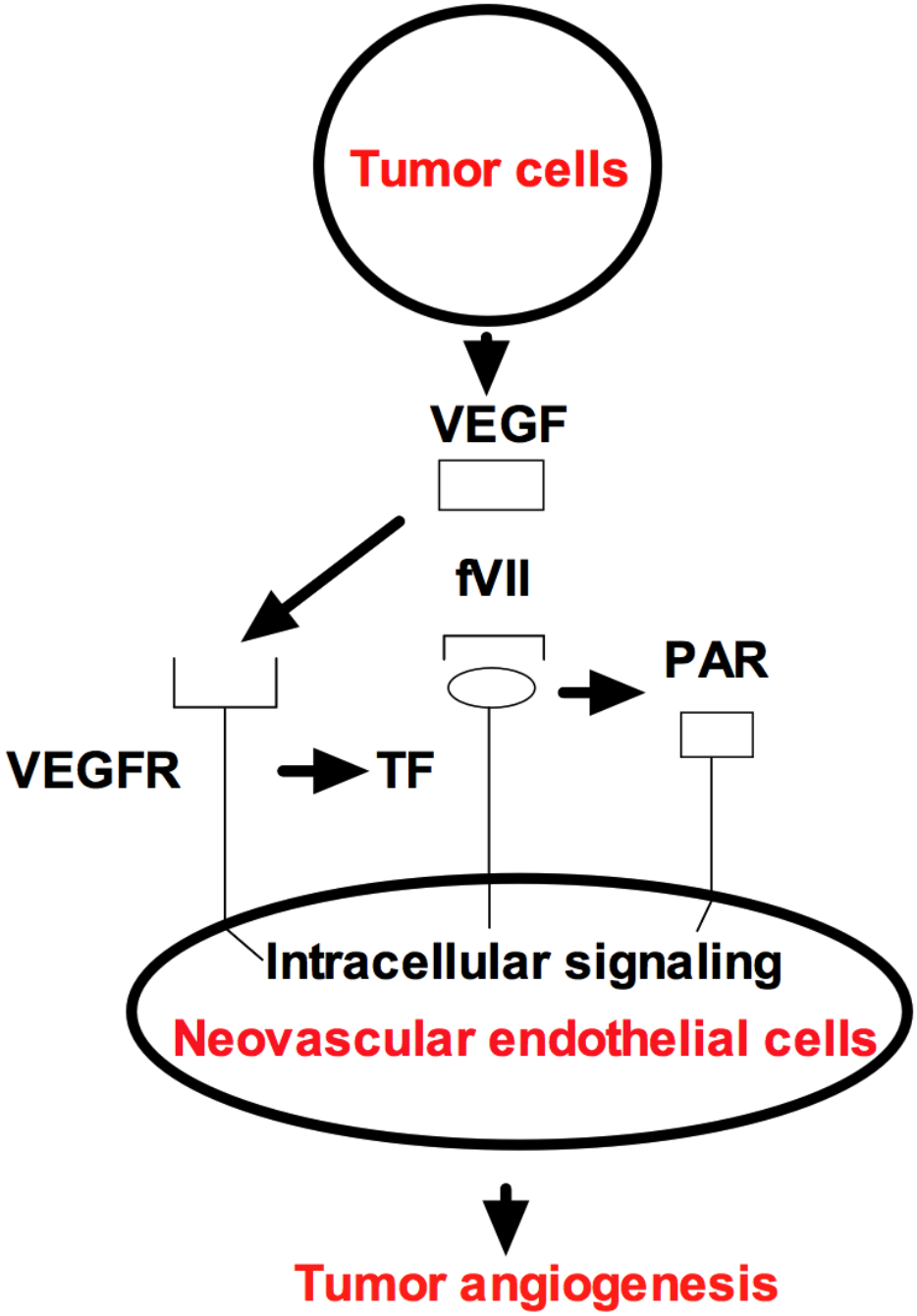

Figure 1.2: VEGFR/VEGF and TF/fVII signaling pathways as prioritized targets in tumor angiogenesis.
The diagram shows VEGF produced by tumor cells binds to VEGFR on vascular endothelial cells to activate VEGF signaling pathways in tumor angiogenesis. In addition, VEGF binding to endothelial cells can induce TF expression, an angiogenic specific endothelial receptor in pathological neovasculature. After its ligand fVII binding, TF could contribute to tumor angiogenesis via proteolysis-dependent pathways through PARs or proteolysis-independent pathway through its cytoplasmic domain. VEGF/VEGFR: Vascular endothelial growth factor/receptor; TF: Tissue factor; fVII: Coagulation factor VII; PAR: Protease-activated receptors.

mTOR

The P13k/Akt pathway plays an essential role in regulating translation, protein degradation, protein signaling, and angiogenesis [41]. This pathway is deregulated in several cancers, including ccRCC [42]. mTOR, a serine/threonine protein kinase, is a downstream component of the P13k/Akt pathway and has been targeted to treat this cancer. A phase II clinical study revealed the mTOR inhibitor temsirolimus produced an objective response rate and minor response rate in 7% and 26% of 111 advanced RCC patients, respectively [43]. Median time to progression was 5.8 months and median survival was 15 months. Temsirolimus, in combination with interferon alfa, displayed antitumor activity in 71 patients with advanced RCC from a phase I/II ascending dose study [44]. The recommended dose resulted in 8% partial responses and 36% stable disease for at lease 24 weeks. A phase III trial further examined the treatment of temsirolimus alone and in combination with interferon alfa as first-line treatments for advanced RCC [41]. In this 626 patient study, a longer median survival was observed in the group that received temsirolimus alone (10.9 months) compared to interferon alfa alone (7.3 months) and temsirolimus with interferon alfa (8.4 months). Furthermore, survival was enhanced in the temsirolimus group compared to the interferon alfa group (HR, 0.73; p=0.0069). Serum levels of LDH have been evaluated as a possible predictive biomarker for temsirolimus-treated patients with metastatic RCC [45]. However, additional studies are needed to validate these findings, as well as determine if temsirolimus is effective with other targeted treatments.

IMP3 and Survivin – Factors Implicated with Poor Prognosis

A variety of factors have been identified through studies specifically screening for features associated with metastasis or very poor outcomes. IMP3 is a member of the insulin-

like growth factor (IGF-II) mRNA binding protein family that's important for biological processes during early stages of embryogenesis, such as RNA trafficking, cell growth, and cell migration [46]. IMP3 was interrogated as a predictor for RCC metastasis and poor prognosis after the association was discovered through a primary screen for factors associated with metastasis [47]. Immunohistochemistry analysis of 501 primary and metastatic RCC tumors revealed stronger expression of IMP3 in metastatic tumors and primary tumors with enhanced metastatic potential. Not only was a shorter metastasis-free survival and overall survival found among patients with primary tumors expressing IMP3 compared to those without IMP3 expression ($p<0.0001$), but patients with IMP3-positive primary tumors had lower 5-year overall and metastasis-free survival than those negative for IMP3. IMP3 was validated as a prognostic marker for ccRCC in an independent dataset of 716 patient samples, showing that IMP3 expression was significantly associated with a 42% increase of disease specific death after multivariate adjustment for known clinical variables (HR, 4.71; $p=0.024$) [48]. These results suggest that IMP3 could potentially be used as a marker to identify patients at risk for metastatic disease.

Survivin or BIRC5 is apart of a gene family of inhibitors of apoptosis (IAP) and is expressed in numerous malignancies, but not in normal adult tissues [49], and is important for cell proliferation in RCC [50]. In a cohort of 49 ccRCC tumors, survivin expression, analyzed by immunohistochemistry, was found to be significantly associated with poor differentiation, advanced stages, and aggressive tumors ($p<0.05$) [49]. Patients with moderate-fair and strong expression had poor survival rates compared to patients with weak positivity ($p=0.0157$). After adjusting for tumor stage, patients with high expression of survivin had increased risk of dying from ccRCC than patients with low expression. Higher

transcript levels of survivin were also detected by RT-PCR analysis in 20 RCC tumors compared to normal renal tissue ($p<0.05$) [51]. Significant correlations between survivin expression and stage ($p=0.028$), grade ($p=0.004$), and lymph node metastasis ($p=0.017$) were identified. Kaplan-Meier analysis revealed that patients with high survivin expression had lower overall survival compared to patients with low expression ($p<.001$). Furthermore, attenuation of survivin in the human RCC cell line ACHN by shRNA resulted in decreased cell proliferation, increased apoptotic rate, and enhanced radiosensitivity, suggesting survivin may be a prospective target for treating RCC.

Chromatin Modifiers

In recent years, three new putative tumor suppressor genes, PBRM1, BAP1, and SETD2, have been identified in ccRCC as the next most frequently mutated genes in this cancer after VHL [52, 53]. The implications of these mutations to tumor outcomes or algorithms to stratify patients according to mutational status are ongoing. BAP1, a nuclear deubiquitinase, was discovered through whole-genome and exome sequencing of seven primary tumors to identify two-hit tumor suppressor genes in ccRCC [54]. An analysis of 176 ccRCC tumors revealed that BAP1 loss highly correlated with Fuhrman nuclear grade ($q=0.0005$). Interestingly, BAP1 mutation was anticorrelated to PBRM1 expression ($p=7x10^{-4}$), suggesting that these two genes may participate in related functions or signaling in cancer cells. The prognostic significance of both BAP1 and PBRM1 were investigated in a retrospective cohort of 145 patients with primary ccRCC that underwent nephrectomy at the University of Texas Southwestern Medical Center (UTSW) and an independent cohort of 327 ccRCC patients from The Cancer Genome Atlas (TCGA) [55]. Median overall survival was decreased for UTSW patients with BAP1 mutations (4.6 years) compared to patients

with PBRM1 mutations (10.6 years). Overall survival were reduced in the TCGA cohort, with patients with BAP1-mutant tumors having a median of 1.9 years and PBRM1-mutant patients having a median of 5.4 years. In addition, a TMA of more than 300 RCC tumor samples found significant correlation of PBRM1 loss with advanced tumor stage ($p<0.0001$), low differentiation grade ($p=0.0002$), and worse outcome ($p=0.025$) [56].

Another study utilized targeted sequencing in 185 ccRCC tumors and matched normal to examine the relationships of these genes to clinical outcomes [57]. Tumors with BAP1, PBRM1, or SETD2 (a H3K36 trimethyltransferase) mutations were found to be more likely stage III or higher. BAP1 mutations were found to be associated with poor cancer specific survival ($p=0.01$) and were present exclusively in Fuhrman grade III-IV tumors. The same group strengthened these results in a subsequent study [58]. PBRM1, SETD2, and BAP1 were frequently mutated in a cohort of 188 ccRCC patients who underwent resection at the Memorial Sloan-Kettering Cancer Center (MSKCC) and in 421 primary ccRCC patients from TCGA. Again, BAP1 was associated with worse cancer specific survival (CSS), with a hazard ratio of 7.71 in the MSKCC cohort ($p=0.002$) and 2.21 in TCGA ($p=0.002$). SETD2 was found to be significantly associated with CSS only in the TCGA cohort ($p=0.036$, HR 1.68). However, PBRM1 was not associated with cancer specific survival in either cohort. These studies present the use of ccRCC subtypes, based on mutational status, as potential markers that can be used to better understand RCC pathogenesis.

Moreover, a novel study elucidated that SETD2 mutations in a cohort of 42 ccRCC primary tumor samples were found to be associated with open chromatin regions in gene bodies by formaldehyde-assisted isolation of regulatory elements (FAIRE) sequencing[59]. Transcriptionally active genes in samples harboring SETD2 mutations expressed RNA

processing defects that involved aberrant splicing, exon skipping, intron retention, and alternative transcription start and termination sites. This study sheds light on the impact chromatin modifier mutations have on the ccRCC genomic landscape.

Clear cell A and clear cell B gene signatures

In addition to individual markers, gene signatures have been revealed through genome expression profiling to identify discrete and global changes in transcript expression. Recently, two subtypes of clear cell RCC, clear cell A (ccA) and clear cell B (ccB), were identified using gene expression consensus clustering to identify complex biological patterns [14]. Using a data set of 177 ccRCC tumors, it was found that tumors displaying the ccA signature were associated with an 8.6-year cancer specific survival as compared to only 2 years for ccB ($p=0.0002$). This relationship is not unexpected, as ccB tumors expression includes panels of genes associated with cell differentiation, mitotic cell cycle, transforming growth factor beta, and Wnt signaling. In contrast, ccA tumors expressed genes associated with angiogenesis, beta-oxidation, and fatty acid and pyruvate metabolism [14]. Moreover, the ccA/ccB signature was robust in a meta-analysis of 480 ccRCC tumors [13]. Unsupervised consensus clustering in this large group revealed an additional cluster that comprised tumors phenotypically wild type for VHL that displayed histological features of a rare supbtype of RCC defined as clear cell-papillary-typed tumors, demonstrating this profile was stable across ccRCC and that expression profiling provided a potential clinical tool for personalized disease management to elucidate rare subgroups.

Furthermore, a 34-gene subtype predictor was developed to classify clear cell tumors according to ccA or ccB subtype[7]. The predictor was developed from a panel of genes significantly expressed in ccA and ccB tumors and associated with prognosis. The

prognostic value of the algorithm was corroborated in RNA-sequencing data from 380 ccRCC samples from The Cancer Genome Atlas (TCGA) and further validated using the NanoString platform with a cohort of 157 fixed archival samples collected at the University of North Carolina. The intrinsic subtypes, ccA and ccB, were classified in the TCGA and NanoString cohorts. Subtype classification showed significant prognostic outcomes for overall survival, cancer-specific survival, and recurrence-free survival and remained significant in multivariate analyses that included pathologic stage and histologic grade. A prognostic model was built for recurrence-free survival for non-metastatic ccRCC patients within the context of subtype and clinical characteristics, which outperformed established algorithms. Moreover, the ccA/ccB signature was found to be the only independent prognostic biomarker in multivariate analysis, establishing the molecular tool adds prognostic value for clinical assessment[60].

Chromosomes 9q and 14q deletions

Cytogenetic abnormalities provide a high level indication of tumor genomics, and can be very valuable in making tumor classifications. In addition to the characteristic chromosome 3p deletion that is a hallmark of this cancer, deletions of chromosomes 9q and 14q have emerged as high frequency copy number changes and as potential prognostic factors for RCC. Fluorescence in situ hybridization and cytogenetics were used with 703 ccRCC tumors to analyze whether chromosome 9p deletions could predict disease-specific survival and recurrence-free survival, as well as associating deletion of 9q with an aggressive tumor phenotype [61]. 13.8% of the tumors had chromosome 9p deletions, and these tumors presented larger, with higher grade and stage, and with lymph node or distant metastases.

Since the HIF1A locus resides within 14q and loss of 14q had also previously been associated with poor outcome, loss of chromosome 14 and corresponding decreased expression of HIF1A were investigated for prognostic potential [62]. Utilizing 112 ccRCC tumor specimens with 250K SNP microarrays, qPCR, and immunohistochemical methods, significant associations were observed between loss of chromosome 14q and high stage ($p=0.001$), recurrence risk ($p=0.002$), and reduced overall survival ($p=0.030$) in non-metastatic patients. However, multivariate analysis revealed that 14q loss was not independent of stage as a prognostic tool in patients with localized disease. In contrast with previous studies, loss of 9p was not associated with overall survival in this cohort of patients with localized or metastatic ccRCC, indicating the prognostic influence of this aberration may be specific to smaller, less aggressive renal tumors. Further research is needed to better understand the effects of these chromosomal aberrations on the molecular architecture of RCC and to validate the prognostic potential of these markers.

ccRCC displays marked variability in risk for developing metastatic disease, and although numerous clinical algorithms exist that can accurately assess risk for disease death using clinical stage-based metrics [63], within the large group of intermediate staged tumors, tissue-based prognostic biomarkers are urgently needed. Furthermore, molecular stratification will most likely add the most value for predictive biomarker algorithms going forward, which can also facilitate the understanding of imperative influences, such as the environment, on the molecular profiles of this disease.

Table 1.1: Prognostic and predictive markers in ccRCC

Prognostic Markers				
Biomarker	Type of study	Patients (n)	Results	References
HIF1A and HIF2A	Basic Research	*In vitro*	786-0s expressing HIF2A inhibited HIF1A-promoted cell cycle and induced cell cycle progression in combination with c-Myc gene expression.	Gordan et al. [24]
	Basic Research	*In vivo*	HIF2A-expression ccRCC tumors exhibited c-myc-dependent proliferation compared to tumors wild type for VHL and expressed both HIF1a and HIF2A. Tumors expressing HIF1A and HIF2A had enhanced MAPK and mTOR signaling, with decreased phosphoryalated H2AX.	Gordon et al. [25]
	Basic Research	*In vitro* and *in vivo*	HIF1A expression in RCC cell lines inhibited cell proliferation. HIF1A-shRNA increased proliferation in xenografts and cell lines expressing HIF1A and HIF2A.	Shen et al. [26]
CAIX	Retrospective	288	Tissue microarray analysis revealed higher expression of CAIX is significantly associated with ccRCC ($p<0.001$) and a favorable prognosis.	Sandlund et al. [27]
	Retrospective	224	Tumors with mutated VHL had enhanced CAIX expression and were associated with longer progression-free ($p=0.037$) and disease specific survival ($p=0.001$).	Patard et al. [28]
	Prospective	864	cG250 antibody adjuvant therapy benefited only ccRCC patients with the highest CAIX staining in the primary tumor.	Belldegrun et al. [30]
IMP3	Retrospective	501	Patients with IMP3-positive primary tumors had shorter metastasis-free and overall survival ($p<0.0001$). Primary tumors expressing IMP3 were associated with a lower 5-year overall and metastasis-free survival compared to IMP3 negative tumors.	Jiang et al. [47]

	Retrospective	716	A 42% risk increase of disease specific death was significantly associated with IMP3 expression (HR, 4.71; p=0.024). IMP3-positivity was associated with a 5-fold increased risk of distant metastases.	Hoffman et al. [48]
Survivin	Retrospective	49	Immunohistochemistry analysis revealed significant association of survivin expression with poor differentiation, advanced stages, and aggressive tumors (p<0.05). Patients with high survivin expression had increased risk of dying from ccRCC compared to patients with low expression after adjusting for tumor stage.	Zamparese et al. [49]
	Retrospective and basic research	20, *in vitro*	High survivin expression was correlated with lower overall survival compared to low expression (p<0.001). Reduction of survivin expression by shRNA in ACHN cells decreased cell proliferation, increased apoptotic rate, and enhanced radiosensitivity.	Lei et al. [51]
B7-H1	Retrospective	196	Tumors expressing high levels of B7-H1 were associated with increased risk of death from RCC, with patients with high B7-H1 tumor expression having 4.5 times the risk of death of RCC compared to those with low levels (RR, 4.53; 95% CI 1.94 to 10.56; p<0.001).	Thompson et al. [64]
	Retrospective	306	Immunohistochemistry analysis showed 41.9% and 82.9% 5-year cancer-specific survival rates for patients with and without B7-H1 expression, respectively. After adjusting for standard clinical variables, B7-H1 tumor expression remained associated with cancer-specific death (RR, 2.00; p=0.0003).	Thompson et al. [65]
	Retrospective	259	Fresh-frozen specimens expressing B7-H4 staining from RCC patients associated with adverse clinical and pathological features.	Krambeck et al. [66]

			Patients expressing B7-H4 were three times more likely to die from RCC compared to patients that didn't express B7-H4 (RR, 3.05; 95% CI, 1.51 to 6.14; p=0.002).	
BAP1 and PBRM1	Retrospective	145, 327	Median overall survival was 4.6 and 1.9 years for patients with BAP1 mutations compared to 10.6 and 5.4 years for those with PBRM1 mutations in the 145 and 327 cohorts, respectively.	Kapur et al. [55]
	Retrospective	300	Tissue microarray analysis revealed significant association between PBRM1 loss with advanced tumor stage (p<0.0001), low differentiation grade (p=0.0002), and worse outcome (p=0.025).	Palowski et al. [56]
	Retrospective	188, 421	Patients with BAP1 mutations were associated with a 7.71 (p=0.002) and 2.21 (p=0.002) hazard ratio for cancer specific survival in the 188 and 421 cohorts, respectively.	Hakimi et al. [58]
ccA and ccB	Genomic, Retrospective	177	Genome expression profiling of ccRCC tumors revealed the ccA and ccB subtypes, which have distinct gene signatures. ccB-typed patients presented with lower cancer specific survival (2 years) compared to patients displaying the ccB signature (8.6 years) (p=0.0002).	Brannon et al. [14]
	Genomic	480	Meta analysis revealed the ccA/ccB gene signature is stable across a large group of samples.	Brannon et al. [13]
Chromosome 9q deletions	Genomic	703	Cytogenetic and survival analysis revealed patients with 9q deletions had decreased median disease specific (37 vs 82 months) and recurrence free survival (53 months vs not reached) compared to patients without mutations.	La Rochelle et al. [61]
Chromosome 14q deletions	Genomic	112	Loss of chromosome 14q was significantly associated with high stage (p=0.001), recurrence risk (p=0.002), and reduced overall survival (p=0.030) using SNP microarray, qPCR, and immunohistochemical analysis, but failed to be independent after adjusting for stage.	Monzon et al. [62]
Predictive Markers				

VEGF and PDGF	Prospective	63	RCC patients who received prior cytokine therapy from a phase II study had a partial (40%; 95% CI, 28-53%) response and stable disease for ≥ 3 months (27%) following sunitinib treatment.	Motzer et al. [41]
	Prospective	750	Metastatic RCC patients experienced longer progression-free survival following sunitinib treatment compared to patients treated with interferon alfa (HR, 0.42; 95% CI, 0.32 to 0.54; p<0.001). A higher objective response rate (31% vs. 6%, p<0.001) and better quality of life (p<0.001) was associated with sunitinib treatment compared to interfon alfa.	Motzer et al. [36]
	Prospective	903	Serum VEGF levels significantly associated with overall survival (17.8 v 14.3 months; HR, 0.78; p=0.029) and progression-free survival in patients that received second-line treatment of sorafenib compared to placebo following censoring of post-cross-over placebo patients.	Escudier et al. [39]
	Genomic, Retrospective	215, 344	Candidate cytokine and angiogenic factors (CAFs) were identified from a screen of 129 patients with the greatest or least tumor shrinkage from a trial of 215 RCC patients treated with pazopanib, which were associated with continuous tumor shrinkage or progression-free survival. A cohort of 344 RCC patients were used to validate selected CAFs and revealed patients treated with pazopanib that had high concentrations of interleukin 8 (p<0.0001), osteopontin (p=0.0004), HGF (p=0.010), and TIMP-1 (p=0.006) were associated with shorter progression-free survival compared to those with low levels.	Tran et al. [40]
mTOR	Prospective	111	A phase II study of advanced RCC patients produced a 7% objective response rate and 26% minor response rate following treatment of temsirolimus.	Atkins et al. [43]

			Patients who received treatment had a median time to progression of 5.8 months and median survival of 15 months.	
	Prospective	71	Advanced RCC patients receiving the recommended dose of temsirolimus and interferon alfa in a phase I/II study resulted in 8% partial responses and 36% stable disease for at least 24 weeks.	Motzer et al. [44]
	Prospective	626	A longer median survival was observed in advanced RCC patients from a phase III study that received first-line treatment of temsirolimus alone (10.9 months) compared to inferno alone (7.3 months) or in combination with temsirlimus (8.4 months). Increased survival was observed in the patients treated with temsirolimus compared to the interferon alfa group (HR, 0.73; p=0.0069).	Armstrong et al. [45]

ccRCC Heterogeneity

Even within a single subtype of the disease, ccRCC, this cancer can present with variable histopathogical and clinical patterns, which significantly impairs accurate clinical prognostication for an individual patient[67]. Moreover, it has recently been reported that these tumors can display significant intratumoral genomic heterogeneity, which further complicates tissue based biomarker development. Tumor Fuhrman grade, one of the key features used to determine the pathology of a tumor and the risk for metastasis, has long been recognized to have regional variation among and within renal tumors[68]. Recent large-scale sequencing analyses, however, have identified that individual tumors have a heightened amount of genomic heterogeneity[53]. Moreover, ccRCC has been observed to be composed of diverse cell populations and to display intratumoral heterogeneous DNA content[69, 70]. Exome sequencing of multiple ccRCC intratumoral biopsies revealed a high level of DNA aneuploidy amongst the samples and that the majority of the somatic mutations were sample-specific[71]. Our own work sampling across tumors has also shown this pattern of mutational heterogeneity in large tumors: however, we also observed that the gene expression features of the sampled sublocations were more generally stable, and that sublocations from a single tumor preferentially clustered together when compared across a larger group of tumors. The recent discovery of intratumoral heterogeneity in ccRCC has substantially altered cancer researchers and clinicians' perspective of this cancer. However, there remains a substantial deficit of information regarding the affects tumor heterogeneity has on driving biological and molecular features of ccRCC tumorigenesis, which is examined in Chapter 2 and 3. Furthermore, understanding the extent of tumor heterogeneity has the potential to facilitate discoveries related to tumor development and extrinsic forces inducing disease progression.

Environmental exposure and RCC

The kidney is a structurally and functionally complex organ that has a significant role of detoxifying blood and excreting chemical compounds to maintain homeostasis, making it vulnerable to chemical insults. Cellular damage due to nephrotoxicity results in acute kidney injury (AKI)[72, 73], and can be worsened if untreated to cause chronic kidney damage or promote or exacerbate tumorigenesis[74-76]. In fact, chronic damage is the leading risk factor for development of renal cancer[76]. Toxicogenomics has been instrumental in revealing early changes in gene expression in response to compounds and environmental factors[77, 78]. These genomic mechanisms have elucidated unique gene patterns from toxicant exposure. While it's known that RCC can be influenced by chemical exposure, we are largely unaware of the sustaining effects exposures have on distinct gene signatures of this disease, and how these exposures relate to tumor heterogeneity and molecular patterns. Thus, in Chapter 4 I investigate the influence cadmium exposure has on core gene expression patterns in clear cell renal cancer, prioritizing the focus to genes in Clearcode34.

Environmental Sources of Cadmium

Cigarette smoke (CS) is one of the oldest environmental exposures linked to cancer [79] and contains numerous carcinogenic compounds, such as Cadmium. Smoking is the predominant source of Cd exposure and the smoking populations experience higher levels of cadmium exposure, as one cigarette may contain 1-2 ug cadmium[80, 81]. Cigarette and second hand smoke have both been shown to induce or be associated with angiogenesis by a variety of mechanisms, although separating angiogenic effects from other carcinogenic activities is a challenge. Mouse models of chronic colitis were found to have increased blood vessel formation following exposure to CS ($P>0.01$) compared to control[82]. Increased

angiogenesis in these models were found to be dose-dependent. In addition, bcl-2 and VEGF protein expression was significantly increased ($p>0.05$) after CS exposure. However, CS in absence of ulcerative colitis failed to induce these pathologic alterations. Tumor growth, capillary density, plasma VEGF levels, and circulating endothelial progenitor cells were significantly increased in mice subcutaneously injected with Lewis lung cancer cells after a 17 days exposure to second hand smoke compared to mice exposed to clean room air [83]. Furthermore, a hospital-based case-control study consisting of 730 urothelial carcinoma cases, 470 bladder cancers, 260 upper urinary tract urothelial carcinomas, and 850 age-matched controls found significant correlations between bladder and upper urinary tract urothelial carcinomas (UUTUC) and both cigarette smoking and arsenic exposure.[84] Patients that smoked and had high arsenic exposure, another RCC risk factor, were found to have increased risk of developing bladder cancer and UUTUC. The risk for both bladder cancer (6.6; 95% cI, 3.1-13.9) and UUTUC (9.9; 95% CI, 4-24.5) were increased with the presence of VEGF polymorphisms associated with increased cancer risk.

Consumption of contaminated water or food is the second most common route of cadmium exposure among non-smokers. Mollusks, crustaceans, seeds (Oil, Sunflower, and flax), peanuts, vegetables, grains, and offals of sea animals are primary food sources for high cadmium concentrations[85]. The World Health Organization set a safe intake limit of 7ug cadmium/week/kg body weight based on a critical renal cadmium concentration between 100 and 200ug/g wet weight that corresponds to a urinary threshold limit of 5-10 ug/g creatinine. However, studies have reported adverse kidney effects at urinary cadmium levels less than 0.5 ug/g creatinine, Furthermore, increased endometrial cancer risk was detected in a Swedish cohort among persons who consume less than 15ug/day of cadmium through

vegetables and cereals[85], suggesting these limits are too high and lower exposures have the potential to induce adverse health effects.

Cadmium can also be absorbed through inhalation from ambiant air and occupational environments, but is the least likely route of exposure. Heavy metal mining, metallurgy and industrial use of manufacturing nickel-cadmium batteries, pigments, plastic stabilizers, and anti-corrosive products are the main reasons for exposures. Although cadmium production has decreased in developed countries due to its toxicity, cadmium pollution has increased due to waste incineration causing its presence in farm fertilizers and during mud purification.

Kinetics and metabolism of Cadmium

The most efficient absorption of cadmium takes place in the lungs where 25-60% is absorbed compared to ingestion where the gastrointestinal tract takes up only 5-10%[86]. On average, adults are estimated to absorb 1.4-8ug of cadmium orally[86]. The cadmium compound and its solubility highly affect the absorption of oral exposure, while inhalation absorption is dependent on compound solubility and particle size. Cadmium can also be absorbed through the skin, but this route is less efficient.

Once absorbed, cadmium binds to red blood cells or high molecular weight proteins in plasma and distributed through out the body. The kidney and liver are the main deposition sites for Cd accumulation, which induces the family of metallothineins (MT) that binds the majority of cadmium[87]. Persons with chronic Cd exposure usually contain high levels of Cd in the renal cortex, levels that increase with body burden and age until 50 to 60 years. Cadmium is absorbed by the liver from the blood and bound to MT, where the complex is then released back into the cardiovascular system and filtered by glomerular in the kidney[81, 86]. Here, Cd is taken up by the renal tubules and cleaved from MT. MT

production is low in the kidney and makes tubules vulnerable to insult or cell membrane destruction through the activation of reactive oxygen species caused by free unbound cadmium[81].

The majority of cadmium ingested is excreted mostly in feces[86]. On the other hand, Cd is excreted in both urine and feces following inhalation. As exposure prolongs, urine excretion will increase, but this will only be a small percentage of the total body burden[86]. Accumulating Cd concentrations over time is the main focus of kidney toxicity and has been linked to numerous adverse effects.

Mechanisms of Cadmium Toxicity

Both acute and chronic cadmium exposures have been linked to adverse health effects, with acute toxicity responsible for injuries to testes, liver, and lungs, while obstructive airway diseases, emphysema, end-stage renal failures, diabetic and renal complications, deregulated blood pressure, bone disorders, and immune-suppression are associated with chronic exposures[88]. The accumulation of cadmium over time and the lack of excretion from the body make it highly toxic and dangerous to human health. In addition to these effects, evidence has shown that cadmium is able to promote cancer. Lung cancer and cadmium exposure has the strongest association compared to prostate and kidney[89]. Cadmium was deemed a category 1 carcinogen by the International Agency for Research on Cancer (IARC)[90]. However, cadmium is not genotoxic and exerts its toxicity through various mechanisms including the induction of reactive oxygen species (ROS), inhibiting DNA repair systems, and altering the genome and epigenome[88].

Probably one of the main mechanisms cadmium influences genome stability is through oxidative stress. The induction of ROS following cadmium exposure is a result of

indirect processes that involve the decrease of cellular antioxidants and exhalation of ROS by mitochondria[91]. Increased hydrogen peroxide levels have been measured with Cd concentrations of less than 50uM up to 15 minutes post exposure and were observed to also affect permeability of the plasma membrane[92]. Furthermore, Cd-induced oxidative stress causes the production of mutagenic lesions, such as 8-oxo-7,8-dihydro-2'-deoxyguanosine adducts, as well as increased production of DNA single-strand breaks[91]. Studies have also shown that cadmium has the ability to influence antioxidant proteins, such as glutathione-S-transferase, which play an important role in eliminating ROS. These effects can cause a heightened oxidative state that can result in DNA damage and aberrant translation. In addition, superoxide anion and hydrogen peroxide release was enhanced in mitochondria upon Cd intoxication, enhancing mitochondrial oxidative stress and lipid peroxidation of mitochondrial membranes[93, 94]. ROS-induced mitochondria damage could result in the alteration of transmembrane potential, release of mitochondrial calcium and upcoupling, activation of caspase-3, DNA fragmentation, and apoptosis[88, 95].

Several studies have shown a correlation between cadmium exposure and disruption of DNA repair mechanisms, such as mismatch repair, nucleotide excision repair, and base excision repair[88]. In human kidney 293T cells, Cd suppressed the mismatch repair-mediated cell cycle arrests in G2 phase after intoxication[96]. Mismatch repair is imperative for reconciling base substitutions and insertion-deletion mismatches that can promote mutations and cancer. Cd also prevents the xeroderma pigmentosum A protein from binding to DNA damage sites, which inhibits the recruitment of nucleotide excision repair proteins. It's postulated that this effect is due to the replacement of zinc in the zinc finger of the structure by Cd[97]. In addition, formamidopyrimidine glycosylase and apurinic

endonuclease 1 is inhibited and modified by Cd exposure preventing the initiation of base excision repair, important for resolution of oxidative-induced base damage and single-strand breaks[88, 98]. It's thought that cadmium targets the zinc finger motif of the formamidopyrimidine glycosylase protein to inhibit DNA binding, however, the mechanism for the inhibition of apurinic endonuclease 1 is unknown.

Cadmium exposure has been shown to regulate cell cycle progression through the activation of cellular signals and inhibition of DNA methylation. These effects are dose dependent, with inhibition of DNA synthesis observed at concentrations above 1uM and increased DNA synthesis and cell proliferation at concentrations lower than 1uM. Moreover, cell cycle genes and proteins, such as GRB2 and SHC, are upregulated after Cd exposure, enhancing the RAS signaling pathway implemented in cell proliferation. The expression of proto-oncogenes C-FOS, C-MYC, and C-JUN has also been induced following Cd exposure. Interestingly, the induction of apoptosis by Cd^{2+} intoxication has been demonstrated in Hela cells, bovine endothelial cells, rat normal kidney tubular epithelial cells, and rat glioma cells[99-101] through either the extrinsic Fas-FADD caspase-8 pathway initiated by the activation of the death receptors at the plasma membrane or the intrinsic pathway induced by cellular stress signals activating caspase-9. The most hallmark genetic effect of Cd exposure is the induction of metallothioneins (MT), cysteine-rich heavy metal-binding proteins. MTs protect against toxicity by binding to metals and preventing cellular damage caused by oxidative stress. Metal response elements located in the proximal promoters of MTs and the metal-responsive six zinc fingers transcription factor (MTF-1) help facilitate this response. MTs bind cadmium with high affinity preventing it from being absorbed and allowing for its detoxification.

Toxicant Exposure and Angiogenesis

Environmental exposures have been found to promote tumorigenesis of multiple cancers through various mechanisms [102-107]. Vascular endothelial growth factor (VEGF) has been established as one of the key promoters of vascular bed expansion [32] and has been targeted for anti-angiogenesis therapy, with numerous VEGF blockers approved by the FDA to treat metastatic colorectal cancer, non-squamous non-small-cell lung cancer, breast cancer, renal cell carcinoma, and recurrent glioblastoma [108]. Thus, VEGF-mediated signal pathways and VEGF-induced tissue factor/factor VII (TF/fVII) signal pathway are prioritized targets, which are believed to be important in pathological angiogenesis.

Cadmium and ccRCC

Cadmium (Cd) is a known environmental and occupational metal compound that has the ability to cause kidney toxicity and damage, as well as associated with cancer [109-113]. The half-life of Cd is very long, with an average of 20 years, due to the lack of biochemical mechanisms to excrete it from the body and reabsorption by the kidney[76]. More specifically, heavy metals like cadmium can induce nephrotoxicity altering gene expression in the kidney, and thus increasing the risk of developing RCC [81, 87, 114]. In addition to transcript alterations, numerous studies have found that Cd exposure can result in epigenetic deregulation by changing DNA methylation levels, histone modifications, and miRNA expression [84, 115-117], which further suggests a possible connection between cadmium and ccRCC due to epigenetic modifiers being highly affected in this cancer. Moreover, treatment of Nickel, another heavy metal, was shown to induce the expression of the histone demethylase Jumonji domain-containing protein 1A (JMJD1A), a hypoxic response gene that regulates HIF1A, and the hypoxia pathway in RCC [118]. Exploring toxicant-induced global

expression and epigenetic changes can enhance our understanding of the genetic interactions that drive the biological responses to these exposures and their influence on prognostic signatures of RCC.

Concluding Remarks

Conducting clinically relevant research has become increasingly imperative for understanding the underlying biology of diseases. This dissertation provides the foundations for risk stratification and ultimately possible therapeutic strategies. I've focused exclusively on clear cell type RCC, which is a highly distinct molecular entity compared with other renal cell carcinoma histologic subtypes. This work attempts to integrate the genetic and functional/morphological heterogeneity of primary tumors and molecular influence of environmental exposures to develop new theories regarding toxicant exposure and heterogeneous disease progression.

The identification of key molecular profiles of ccRCC and the entities that influence them presents the opportunity to make novel and substantive discoveries regarding RCC tumor genetics that will advance the field and expand our knowledge of this cancer.

CHAPTER 3[3]: CLEARCLODE34: A PROGNOSIC RISK PREDICTOR FOR LOCALIZD CLEAR CELL RENAL CELL CARCINOMA

Introduction

The majority of Renal Cell Carcinoma (RCC) or kidney cancer patients have the clear cell RCC (ccRCC) subtype. Although extensive effort has been devoted to identifying molecular biomarkers for RCC, there are few validated markers that aid disease prognosis, and none are used routinely in clinical practice[31, 119-123]. Thus, transcriptional biomarkers present a potentially target-rich environment towards the goal of improving our understanding of underlying ccRCC biology.

Recently, we identified two subtypes of clear cell RCC, ccA and ccB, based on patterns of differential gene expression, which revealed distinct biological signatures[14]. These subtypes appear to provide prognostic information, with tumors classified as ccA associated with significantly better survival compared to ccB in a retrospective cohort[14]. The ccA/ccB classification was subsequently validated in a meta-analysis of 480 ccRCC tumors, suggesting this profile may have value for risk stratification[13].

Building on this foundation, in the present study we demonstrate the utility of a novel tool to identify the ccA and ccB groups in ccRCC. This molecular tool comprises a 34-gene expression signature (ClearCode34) and an accompanying protocol for ccA/ccB classification. Clinical utility of the classifier is demonstrated by 1) accurate and reproducible

[3] Adapted from Samira A. Brooks**,** A. Rose Brannon, et al. (2014) ClearCode34: A prognostic risk predictor for clear cell renal cell carcinoma. *European Urology, 66:77-84.*

classification of ccRCC tumors into ccA and ccB molecular subtypes, 2) validation of prognostic classification in ccRCC samples from The Cancer Genome Atlas (TCGA)[124] ccRCC project, 3) adaptation of ClearCode34 to a NanoString probeset for validation in an independent cohort of 163 formalin-fixed paraffin-embedded (FFPE) clinical ccRCC samples, and 4) constructing a more precise unified model of ccRCC subtype and standard clinical variables to assign individual ccRCC patients into clinically informative risk categories.

Table 2.1: Expression of ClearCode34

Gene	ccRCC Subtype
MAPT	ccA
STK32B	ccA
FZD1	ccA
RGS5	ccA
GIPC2	ccA
PDGFD	ccA
EPAS1	ccA
MAOB	ccA
CDH5	ccA
TCEA3	ccA
LEPROTL1	ccA
BNIP3L	ccA
EHBP1	ccA
VCAM1	ccA
PHYH	ccA
PRKAA2	ccA
SLC4A4	ccA
ESD	ccA
TLR3	ccA
NRP1	ccA
C11orf1	ccA
ST13	ccA
ARNT	ccA
C13orf1	ccA
SERPINA3	ccB
SLC4A3	ccB
MOXD1	ccB
KCNN4	ccB
ROR2	ccB
FLJ23867	ccB
FOXM1	ccB
UNG2	ccB
GALNT10	ccB
GALNT4	ccB

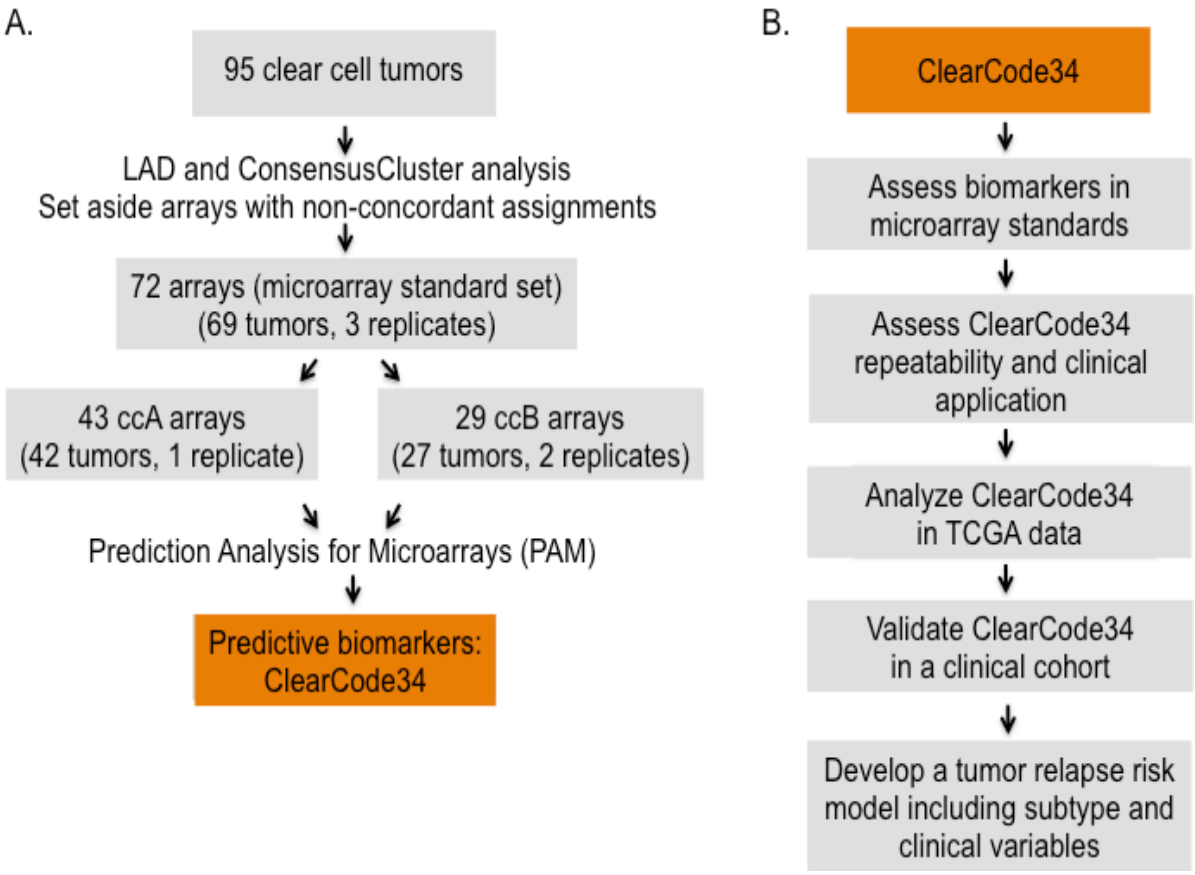

Figure 2.1. Workflow for biomarker discovery and order of analyses.
(A) Steps taken to identify the 34 genes that classify ccA and ccB tumors.
(B) Diagram of analyses to validate the efficiency of the biomarkers to classify tumors and predict prognostic outcomes.

Results

Subtype comparison for prognosis and recurrence in the TCGA dataset

To evaluate the prognostic utility of the 34-gene classifier (**Table 2.1**), ClearCode34, for ccA and ccB ccRCC tumors, Kaplan-Meier analysis was used to assess tumor recurrence and survival rates by subtype assignment in tumor samples from 380 non-metastatic ccRCC patients from the TCGA dataset (**Table 2.2**). Univariate analysis revealed ccB patients experienced tumor recurrence earlier and more frequently than ccA (HR, 2.3; 95% CI, 1.6 to 3.3; *P*=4.3e-06) (**Figure 2.2A**). Moreover, ccB patients had almost three times the risk of death from disease (HR, 2.9; 95% Cl, 1.6 to 5.6; *P*=0.0005) and more than two times the risk of death from any cause compared to ccA (HR, 2.4; 95% CI, 1.6 to 3.7; *P*=2.3e-05) (**Figure 2.2B and C**). Competing risk analysis further validated the differences in survival between the two subtypes, which showed their specificity as prognostic tools for clear cell renal disease (cancer specific survival, *P*=0.002; overall survival, *P*=0.037).

Table 2.2: Patient Demographics and Clinical Characteristics of TCGA Cohort

Characteristic	No.	%
Sex		
Male	240	64
Female	136	36
Age		
Median	61	
Range	29-90	
Ethnicity		
Caucasian	326	87
African American	17	5
Hispanic	20	5
Asian	8	2
Unknown	5	1
Grade		
1	6	2
2	181	48
3	148	39
4	36	10
Unknown	5	1
Staging (TNM)		
I	213	56
II	44	12
III	116	31
IV	3	1

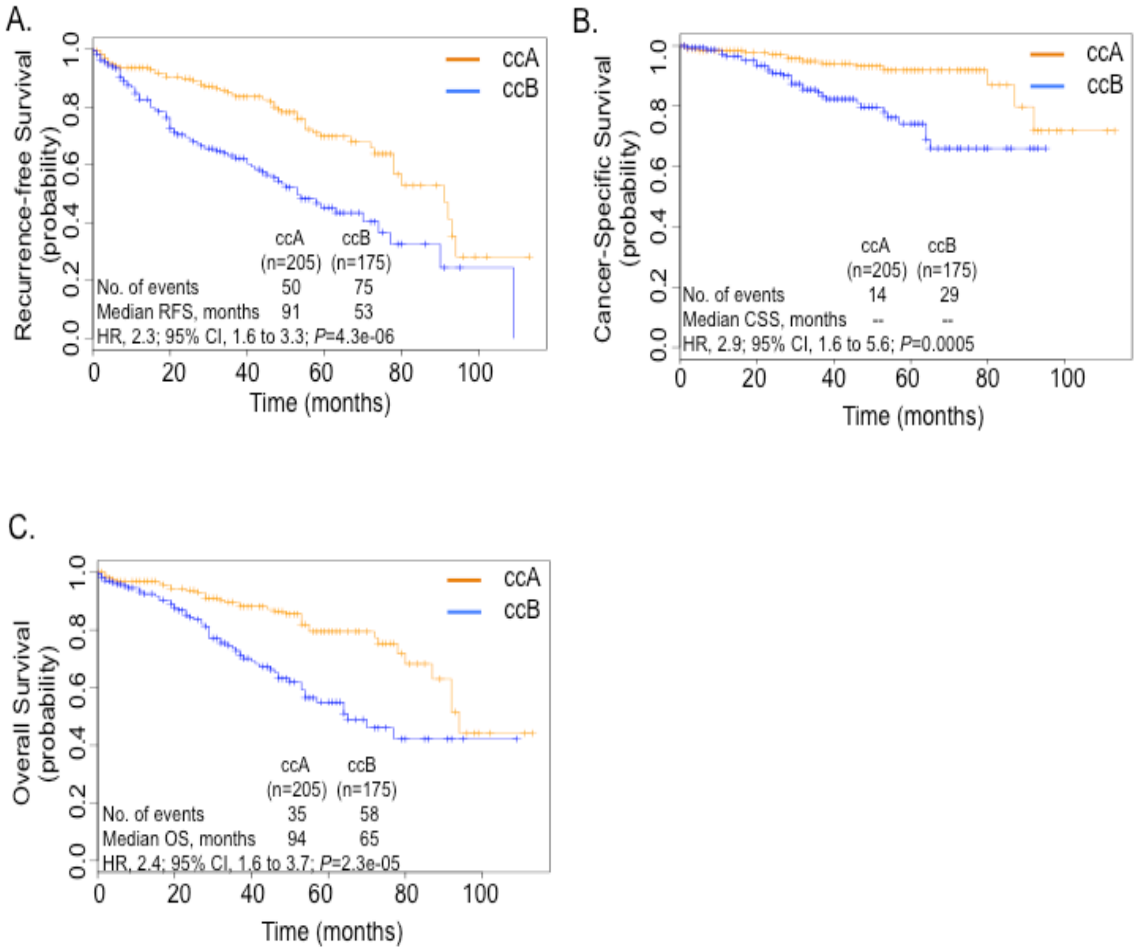

Figure 2.2: Tumor classification from TCGA shows distinct prognostic outcomes.
Prediction Analysis for Microarray (PAM) classified 380 untreated, non-metastatic ccRCC tumors from the Cancer Genomic Atlas (TCGA) as either ccA or ccB using the 34-gene classifier ClearCode34. Kaplan-Meier curves were used to calculate recurrence-free survival (RFS) (A), cancer-specific survival (CSS) (B), and overall survival (OS) (C) for ccA and ccB patients. ccB-typed patients had a median RFS and OS of 53 and 65 months, respectively, while patients with ccA-typed tumors had a 50% survival probability of 91 and 94 months for RFS and OS.

Biomarker validation in an independent cohort

Since ClearCode34 demonstrated prognostic value in the TCGA cohort from known clinical samples, we next attempted to validate the classifier in an independent group of clinical specimens using the NanoString platform. Applying the classifier to a cohort of 163 non-metastatic ccRCC archived FFPE samples (**Table 2.3**), 71 samples were assigned as ccA subtype and 92 as ccB, and again, the subtype classifications followed survival patterns seen previously (**Figure 2.3**). In this cohort, ccB cases experienced tumor relapse after nephrectomy more frequently (HR, 2.2; 95% CI, 1.4 to 3.4; $P<0.0005$) (**Figure 2.3A**) and had higher risk of both cancer-specific and overall mortality compared to patients classified as ccA (**Figures 2.3B** (HR: 3.1) and C (HR: 2.2), respectively). Additionally, cancer-specific deaths ($P= 0.008$), but not overall deaths ($P=0.398$), remained significant between subtypes after competing risk analysis.

Table 2.3: Patient Demographics and Clinical Characteristics of Clinical Cohort

Characteristic	No.	%
Sex		
Male	96	59
Female	67	41
Age		
Median	58	
Range	19-82	
Ethnicity		
Caucasian	106	65
African American	46	28
Hispanic	5	3
Asian	1	1
Native American	5	3
Grade		
G1	3	2
G2	72	44
G3	72	44
G4	15	9
Unknown	1	1
Staging (TNM)		
I	76	47
II	28	17
III	50	31
IV	2	1
Unknown	7	4

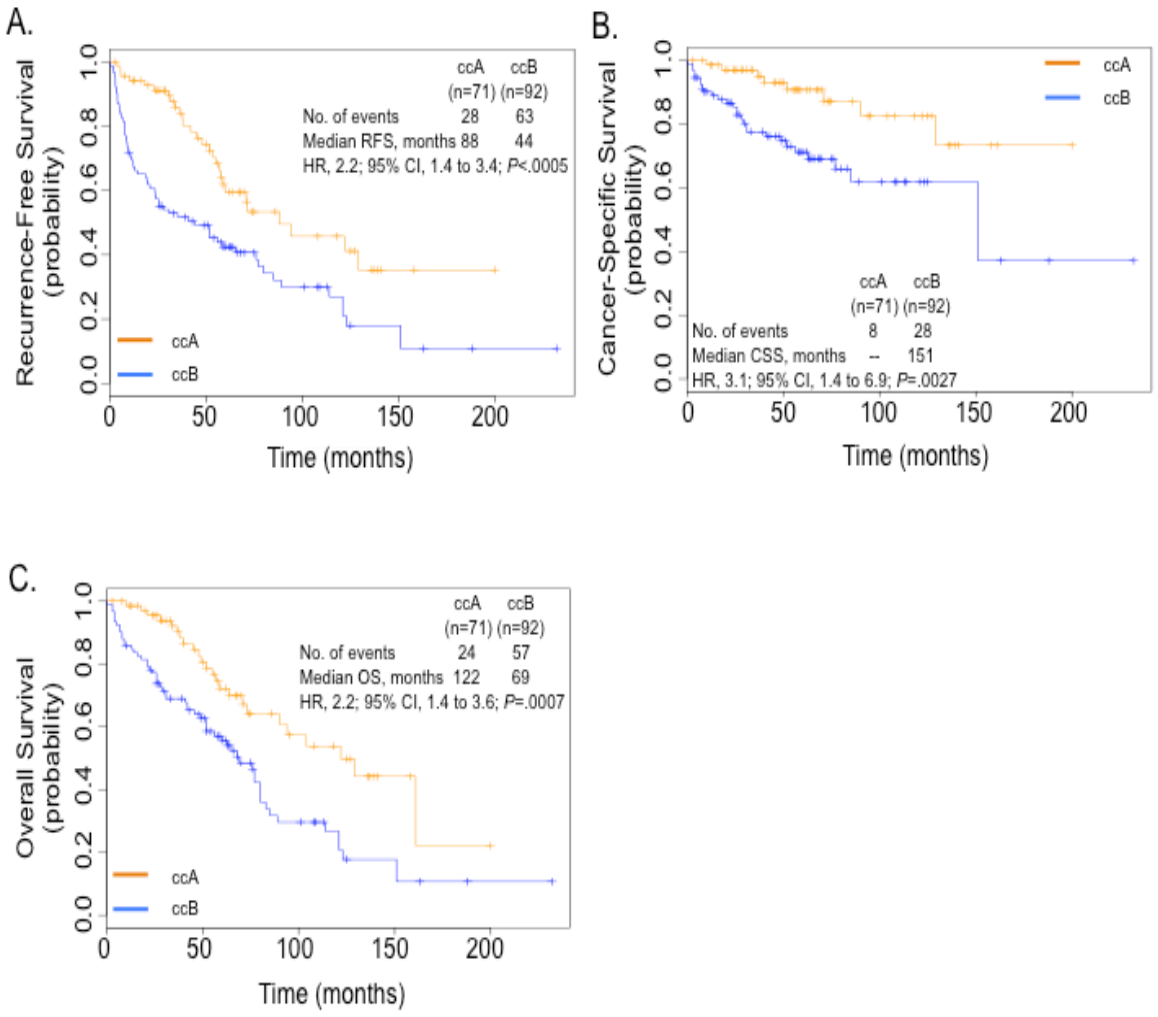

Figure 2.3: ccRCC classifier recapitulates survival outcomes for subtypes in clinical cohort. Whole lysates from 163 non-metastatic archived ccRCC primary tumor samples were subjected to NanoString gene expression analysis. Kaplan-Meier plots of the independent cohort using ClearCode34 show ccB patients have significantly lower probabilities of recurrence-free (A), cancer-specific (B), and overall survival (C) compared to ccA.

Prognostic risk models for recurrence in non-metastatic ccRCC patients

We next sought to determine if a recurrence risk model encompassing both ClearCode34 ccRCC subclassification along with stage and grade could be utilized to enhance the assessment of patient risk. A Cox model for recurrence was assembled using a combined cohort including both the TCGA and clinical cohorts. In the final model, subtype classification (P=0.04), grade (G1/2 v. greater) (P=<0.001), and stage (Stage I v. greater) (P<0.001) were found to be significant independent variables for predicting recurrence-free survival (RFS) (**Appendix Table 2.2A**). Likelihood ratios verified that subtype status was a prognostic factor even after adjustment for stage and grade.

A training set was randomly selected from the combined cohort and used to train the risk prediction model, focusing on recurrence. Thresholds for identifying patients for high probability of recurrence within five years following surgical resection were determined by Ridge regression, fit to the training set, and used to stratify low, intermediate, and high risk groups of relapse (P< 4e-15) (**Figure 2.4A**). The high-risk- and intermediate test-set groups had a median time to recurrence of 19 and 151 months, respectively. The low-risk group failed to reach a 50% relapse probability. Similarly, the three risk groups showed similar survival trends for cancer-specific death after applying the thresholds determined for RFS (P=1.21e-13) (**Figure 2.4B**).

Furthermore, we compared our risk assessment tool with existing clinical tools to predict death from ccRCC utilizing multivariate (**Figure 2.4C**) and C-index analysis (**Figure**

2.4D). Our analyses show a clear superiority in assessing risk of ccRCC death using prognostic classification (three-risk group model) (**Figure 2.4C and D**) or raw risk scores (**Figure 2.4D**) compared to the UCLA Integrated Staging System[125] (UISS) and Mayo Clinic Stage, Size, Grade, and Necrosis (SSIGN) score[126]. Thus, utilizing ClearCode34 enhances risk stratification.

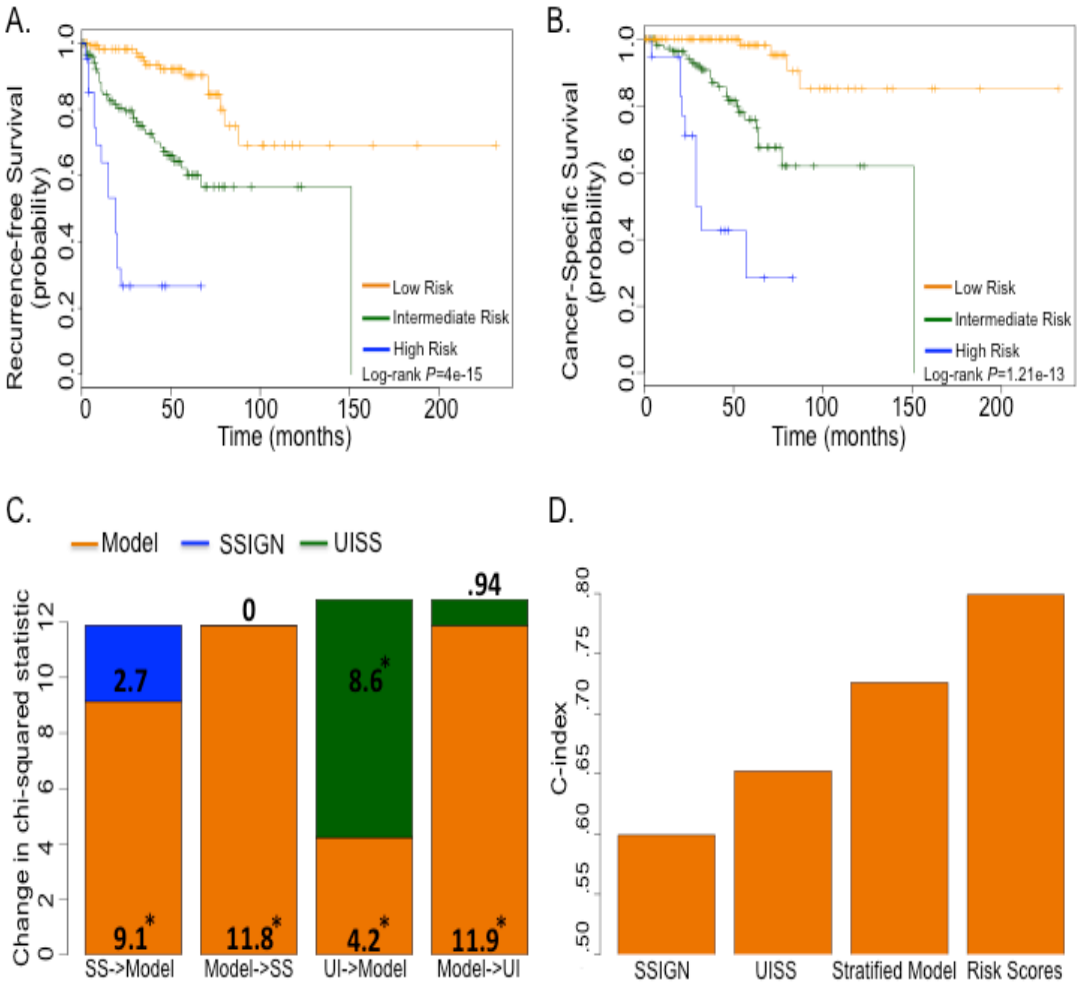

Figure 2.4: ClearCode34 prognostic model can evaluate patient risk.
A randomized training set of 266 patients from the TCGA and clinical cohorts were used to train a model to identify low, intermediate, and high-risk groups for tumor recurrence using ccRCC subtype status (ccA/ccB), tumor stage, and histologic grade. The model was applied to the test set (n=267) to predict recurrence (A) and cancer-specific death (B), revealing a highly significant risk profile integrating clinical and biological features. Cox regression (C) and C-index (D) analysis validated the efficacy of the model using the three risk groups or raw risk scores to predict risk of ccRCC death over the established algorithms UISS (UI) and SSIGN (SS) score.

Discussion

We developed ClearCode34 to adapt the ccA/ccB ccRCC classification to the real world of clinical practice. ClearCode34 is translatable to multiple gene expression platforms and clinically available specimens, which has added value to predicting risk above standard clinical and pathologic variables as well as standard ccRCC risk algorithms. The TCGA and clinical cohorts afforded testing of the prognostic value of ClearCode34 in independent datasets. The intrinsic subtypes were significantly associated with disease recurrence (RFS), cancer-specific survival (CSS), and overall survival (OS), independent of standard clinical risk factors. Multivariate analysis for risk of tumor recurrence suggested that the risk prediction model including subtype, stage, and grade provided the best model, given the available variables. The model was trained to predict risk groups for tumor recurrence and after being applied to a test set, revealed prognostic low, intermediate, and high-risk groups, and was also able to predict disease-specific death. Moreover, the model was shown to be a better predictor for CSS than established algorithms.

The primary value of this proposed classification system would be for clinicians caring for the majority of patients who present with non-metastatic disease seeking guidance regarding post-surgical management. In addition, it must be considered that primary tumors from which samples in the current studies are derived may be genetically heterogeneous, or clonally divergent from metastases, which may present a challenge in developing tools for predicting the behavior of metastatic disease[71].

Gene expression-based tools have dramatically altered the landscape of many cancers. Such tools are widely used in the classification, risk assessment, and therapeutic selection of breast cancers[127-129], and are becoming standard also for the classification of diffuse

large B cell lymphoma[130] as well as colon cancer[131, 132]. Other expression-based systems have examined ccRCC, and have demonstrated similar patterns associated with risk[133]. [22] Because several individual transcripts had previously been associated with risk in ccRCC[31, 119-123], we specifically incorporated those features in our model and many were included in the final ClearCode34 codeset, validating their relevance in ccRCC risk prediction.

Conclusions

This work presents a novel integration of molecular profiling with standard clinical features to significantly enhance prognostication in ccRCC, thus re-defining the subset of patients at greatest risk for recurrence for risk-stratified patient care.

Patients and Methods

Patients and Clinical Samples

95 ccRCC samples were previously analyzed by gene expression microarray, and clustered to define the ccA and ccB classifications[14]. From the 95, 72 arrays were chosen as references that had previous concordant subtype classifications determined by two bioinformatic methods: logical analysis of data (LAD) and ConsensusCluster[13, 14] (Figure 1A).

RNA-sequence data of The Cancer Genome Atlas (TCGA) cohort and clinical data (last modified on August 23, 2013) were downloaded from https://tcga-data.nci.nih.gov. Pathological re-evaluation was performed at the time of analysis by expert members of the TCGA Analysis Working Group, and cases that did not definitively represent clear cell histology were excluded from further analysis. [9] Recurrence and survival data were taken

from the TCGA Biotabs database, with appropriate permissions, with supplementation by the clinical TCGA working group database (version April 11, 2013).

Specimens for the clinical cohort were collected between 1992 and 2010 at the University of North Carolina at Chapel Hill (UNC) from patients with non-metastatic ccRCC.

Only patients with localized disease at the time of nephrectomy were used for the study. This did include a small number of patients with T4 (locally advanced) lesions, who have extensive local disease classified by AJCC as stage IV. No patients received systemic therapy for ccRCC before nephrectomy or prior to clinical recurrence. All samples and data were obtained with appropriate institutional review board (IRB) approvals.

TCGA Data Analysis

TCGA RNA sequence data were normalized to the upper quartile of normal counts. For analysis, the data were log-transformed (base 2) and the genes median-centered.

FFPE Sample Preparation

FFPE samples were sliced 5-7 microns onto slides or prepared as 10-20 micron scrolls. Surface of the tissue sectioned was a minimum of 1 cm^2. Xylene was added and washed twice with 100% ethanol. Pellets were suspended in 10mM 2-(N-morpholino) ethanesulfonic acid (MES) pH 6.5 or Qiagen's (Maryland, USA) Proteinase K digest (PKD) buffer. 0.5% SDS and 5µl Proteinase K (20mg/ml) was added. Suspensions were incubated at 55ºC, proteinase K inactivated at 80ºC, and supernatant collected.

NanoString Analysis

The UNC genomics core processed 5µl lysate or 100 nanograms RNA for hybridization against NanoString probes, post-hybridization in the nCounter Prep Station, and data collection with the nCounter Digital Analyzer (NanoString, Seattle, WA, USA).

Sample-specific background was subtracted using values from included negative controls. Data were normalized using the geometric mean of housekeeping genes and log transformed (base 2). See Appendix methods for details.

NanoString assay development and quality assessment

We performed a series of quality controls using five tumors from the microarray standards to confirm that NanoString nCounter Analysis System[134] reports transcript abundance similarly to microarray (Appendix Figure 2.1A). Equivalent RNA detection was found comparing lysates prepared from FFPE to RNA from snap frozen tissue of the same tumor. A 20.2% failure rate was observed for preparing adequate lysate for analysis from FFPE specimens, with the majority of failures occurring in samples provided as scrolls, in which the tumor area could not be estimated.

Development of a gene expression classifier of ccA or ccB

To develop a minimal geneset classifier for assigning ccA or ccB subtype, prediction analysis of microarray (PAM)[135], a centroid-based classification algorithm, was applied to the microarray reference data (Figure 1A). PAM was used due to its reproducibility in subtype classification compared to other centroid-based prediction methods[129]. We utilized a list of genes (Appendix Table 2.1A) that encompassed those previously associated with ccA/ccB classification[14]**,** genes differentially expressed between the ccA/ccB subtypes using significance analysis of microarrays (SAM), and other published markers[31,

119, 120, 122, 123]. Ninety-four percent of the tumors were classified correctly (68 out of 72) using a PAM model of 34 genes (Table 1) based on nearest centroids. This gene list was labeled ClearCode34.

Cross-validation (random 10% left out in each of 50 cycles) was applied to the microarray reference set to evaluate the accuracy of the classifier and anticipated performance on independent sample cohorts. In addition, unsupervised clustering and ConsensusCluster[136] were used to further assess assignment accuracy by the minimized gene panel in the microarray standard set by comparing PAM-derived subtype assignments with those determined previously[14].

A set of 56 biological replicates of the microarray standard set (derived from 32 cases) was collected, and these samples were analyzed by NanoString to evaluate the concordance of subtype classification by ClearCode34 with previous methods[14]. These samples consisted of RNA from frozen and formalin-fixed paraffin embedded tissues and whole lysates prepared from either MES or Qiagen's PKD buffer. After removing 16 misclassified samples (derived from 8 cases), PAM correctly classified 95% of the samples and final subtype assignments were determined. This sample set, consisting of 40 replicates derived from 24 cases, became the reference set for subtype classification. This set forms the tool used to make ccA/ccB calls for specimens analyzed by ClearCode34 on all platforms. Replicate samples were treated as individual samples for classification.

Statistical Analysis

All continuous variables were described with median and range. Recurrence, or relapse, was defined as the date from nephrectomy to the date that recurrence or metastasis was detected by imaging or pathology report. Cancer-specific survival (CSS) was defined as

the time from nephrectomy, to death resulting specifically from ccRCC; patients who remained alive, died from other reasons, or had unknown causes of death were censored for this outcome at the date of last follow-up or death. Overall survival (OS) was defined as the time from the nephrectomy to death of any cause. The probability of death or recurrence was determined by using the Kaplan-Meier method, with log-rank tests assessing the differences between the groups. CSS was analyzed using the competing risk method, utilizing the "cmprsk" R package. Cox proportional hazard models and likelihood ratio using overall survival, cancer-specific survival, and recurrence outcomes were used to compare competing survival models. ccRCC subtype, grade, age, gender, and stage, were modeled as additive predictors of outcome. Cox proportional hazard models were used to estimate hazard ratios (HR) and 95% CIs.

Developing a relapse risk model and identifying risk groups

The combined TCGA and clinical cohort consisted of 532 patients, after removing 11 patients with missing stage or grade information. The combined cohort was randomly split into two sets of equal size for use as training and evaluation cohorts for the prognostic model. A multivariable Cox model with ccA/ccB subtype, stage, and Fuhrman grade as additive terms was fit with Ridge regression. Ten-fold cross-validation was performed in the training set to optimize the penalty parameter. A final model was fit to the entire training set using the optimized parameter. All variables are coded as binary, and the sum of the weighted variables produce the recurrence risk score (0.3251862 * subtype + 0.2918120 * grade 3 + 1.0072706 * grade 4 + 0.9506794 * stage II + 1.1947564 * stage III/IV).

For every case subject, subtype ccA, grade 1/2, and stage I were all given a value of zero, while a value of one was assigned for being either ccB-subtyped, grade 3 or 4, or stage

II or III/IV. Thresholds of this score were optimized in the training set to identify a group at risk for having tumor relapse within 5 years following nephrectomy. Case subjects with a score of .5 or less were assigned to the low-risk group, subjects between .5 and 2 were assigned to the intermediate risk group, and subjects with a score of 2 or greater were determined to have high-risk of RFS. All weights and thresholds optimized in the training set remained fixed to provide unbiased estimates of performance in the evaluation set.

Methods

Housekeeping Gene Calculations

Agilent microarrays of renal cell carcinoma tumors from previously published data[14, 122] were analyzed to identify stably expressed genes for use as housekeepers. For identification of SNRPD2, the antilog (2) of the data was calculated, and the coefficient of variation (CV=Standard Deviation (SD)/average) and maximum fold change (MFC=maximum/minimum) were calculated. For the remaining five housekeeping genes, expression data was culled for the suggested housekeepers from NanoString and the top 100 of [Popovici et al., BMC Bioinformatics 2013] kidney list. The top two overall (C14orf166 and RPLP1) and top two NanoString probes (TBP and ABCF1) were chosen. SD, CV and MFC were calculated; genes were sorted on each of these variables and ranked accordingly. Duplicate probes with lower SD were removed, to keep worse-case scenario. A stability score was calculated according to [Popovici et al., BMC Bioinformatics 2013] and [de Jonge et al., PLoS One 2007] PSS =αLOG(MAX(average-ß,0),2)-stdev, where α is a coefficient to control mean expression vs. SD (we set it to 0.25 as the paper did) and ß is the mean expression cutoff, which we set to the 25th percentile following the paper or -0.3908466934. The PSS was sorted and ranked, with genes that had calculation errors due to negative values

being given a rank of 87. The rank product was then calculated as RP=product(ranks)^(1/(n)), where n is the number of ranks available, and RP was sorted. The top two overall (C14orf166) and top two NanoString probes (TBP and ABCF1) were chosen. Additionally, CD63 was chosen for having the highest mean value.

NanoString Data Analysis

Sample-specific background was subtracted by adding the average of all the negative controls to the standard deviation of all the negative controls multiplied by two and subtracting this value from the raw values for each gene. Data were normalized using previously selected housekeeping genes. The geometric mean of the housekeeping genes for each sample was calculated and summarized across samples. The overall geometric mean was divided by each sample's geometric mean to create a housekeeping correction factor for every sample. The housekeeping correction factor was then multiplied against the background-subtracted values. Data were log transformed (base 2) for analysis. The overall failure rate for the validation cohort using the NanoString platform was 20%, with the majority of these failures associated with a subset of FFPE samples that were scrolls, which had low amounts of RNA due to the difficulty to measure the amount of tissue.

ConsensusCluster

ConsensusCluster was performed using the same methods previously published in Brannon et al, 2010[14, 122] and Brannon et al, 2012[13] using K-Means.

CHAPTER 3: ALTERNATE METABOLIC PROGRAMS DEFINE REGIONAL VARIATION OF RELEVANT BIOLOGICAL FEATURES IN RENAL CELL CARCINOMA PROGRESSION

Introduction

The heterogeneous biology of most cancers challenges tools that rely on single biopsy criteria for making disease-wide assessments. Sporadic clear cell renal cell carcinoma (ccRCC) has recently been recognized to display a high level of genetic heterogeneity, based on high-throughput sequencing studies of subsampled tumors. These findings reveal a core mutational signature, which likely represents early or initiating events, coupled with variable secondary mutations, some of which are presumed to be associated with disease progression[71, 137]. In addition, recent studies have implicated changes in hypoxia regulated gene expression, and key enzymes involved in cellular metabolic programs, as potential features linked with progression. In particular, the recent finding of lost fructose 1,6 bisphosphatase 1 (FBP1) expression in renal tumors implies that metabolic diversions are central to ccRCC activity. The regional variation of these and other relevant protein features of ccRCC, or the associations with regional metabolic variation has not been previously explored. Here, we use positron emission tomography (PET) with fluoridated 2-deoxyglucose (FDG) in combination with magnetic resonance imaging for structural and anatomic resolution, to evaluate the potential for functional metabolic imaging to provide a comprehensive and relevant assessment of the disease biology based on regional variation in key prognostic and biologic features.

Results

Medical imaging technologies, such as FDG-PET and magnetic resonance imaging (MRI), have advanced the field of oncology by characterizing tumor morphology, functional activities, and disease monitoring. The fused MRI/PET technology has further improved the assessment of soft-tissue for diagnostic purposes[138, 139]. Functional imaging using FDG-PET has previously been evaluated in ccRCC to predict and evaluate response to systemic treatment[1, 140], but such studies have been challenged by the variable uptake of glucose by this tumor type, and reporting that was developed around tumors that display homogeneous intense FDG uptake. Accordingly, this methodology has yet to be adopted into general practice as a screening or disease assessment modality, precisely because of the variability in glucose uptake by these tumors[141, 142]. In this study, we used MRI/FDG-PET imaging to identify and evaluate heterogeneous regions of ccRCC (**Figure 3.1**). MRI was used for its greater tissue resolution, and FDG-PET for mapping regional uptake variation throughout the tumor. We observed a wide range of contrast patterns in ccRCC tumors, including patterns displaying low or no FDG uptake (**Figure 3.1a**), as measured by SUV, standardized uptake value, and tumors that were uniformly high in FDG SUV (**Figure 3.1b**). Interestingly, metastatic sites expressed higher FDG-PET intensity compared to the primary tumor (**Figure 1c**). Various histologic morphologies were observed within these heterogeneous regions, which ranged from the hallmark lipid-filled epithelial cells with distinct cell membranes to granular cells with regional necrosis (**Figure 3.1d**), although notably, regional variation in SUV did not strictly correspond to regional necrosis.

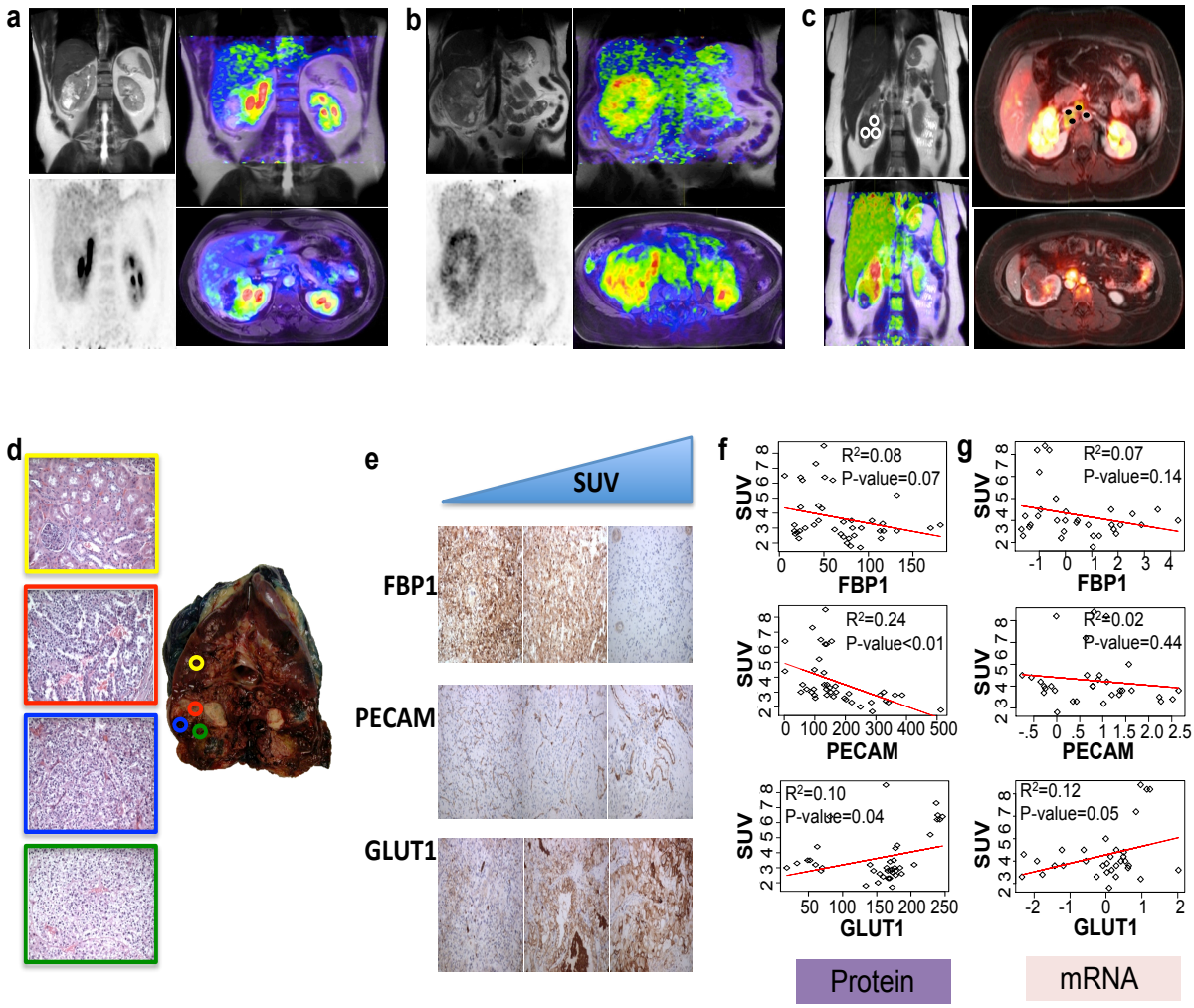

Figure 3.1: PET/MR imaging characterizes heterogeneous regions of ccRCC that correlate to tumor biology.
Representative PET, MR, and PET/MR fused images depicting low (a), high (b), and heterogeneous (c) metabolic activity in clear cell Renal Cell Carcinoma (ccRCC). (c) Five to eight tumor samples were obtained from eight ccRCC patients for hematoxylin and eosin (d), immunohistochemistry (e and f), and microarray (g) analysis. (d) Normal kidney cortex architecture was observed in the normal tissue (yellow) compared to ccRCC (red, blue, and green) that displayed various architectures that ranged from classical epithelial cells with clear cytoplasm and distinct membranes to a granular cell morphology. Samples with increased Glut1 protein (e and f) and gene expression (g) correlated with higher Fluorodeoxyglucose uptake (SUV), suggesting a possible mechanism that supports the greater metabolic activity. In contrast, protein (e and f) and gene expression (g) of the fructose-1,6-bisphosphatase 1 (FBP1) enzyme and the platelet endothelial cell adhesion molecule (PECAM) were anti-correlative to SUV. Images in (e) were captured using a 20X magnification.

We also evaluated levels of key proteins implicated in ccRCC in selected tumor regions. Hypoxia inducible factors (HIF1A and HIF2A), are commonly stabilized in ccRCC due to the high frequency of *VHL* mutation in this disease[10, 16] and promotes the expression of genes that support tumor progression, such as angiogenic factors like the vascular endothelial growth factor (VEGF) and the platelet endothelial cell adhesion molecule (CD31/PECAM)[18-20]. Metabolic reprogramming is also key in tumor progression, especially in ccRCC[15, 143], with both glucose transporters (GLUT1) and key metabolic enzymes regulated by the HIF factors. We detected regional variation in these features, and in particular we observed reduced protein (**Figure 3.1e and f**) and mRNA (**Figure 3.1g**) levels of the critical glycolytic enzyme FBP1, as well as a marker of tumor vascularity, CD31/PECAM in tumor samples with increased SUV[143]. Specifically considering factors that directly regulate glucose metabolism, it was noteworthy to find that samples from FDG-PET avid regions expressed higher expression of the glucose transporter GLUT1 and lower expression of FBP1 (**Figures 3.1e-g**), potentially indicating a switch from producing glycogen for energy storage to obtaining additional glucose to support increased metabolic activity. Downregulation of FBP1 was recently found to be a critical feature of progressive ccRCC[144] by enabling glycolytic flux in renal tubular epithelial cells, and this data further supports this molecular mechanism.

In addition, gene expression profiles which define distinct risk patterns of ccRCC, clear cell A (ccA) and B (ccB)[13, 14][7] have also been observed to display regional heterogeneity[71], possibly reflecting the same clonal evolution revealed in DNA sequencing studies. Samples from these regions also displayed distinct gene expression profiles (**Figure 3.2a**) of the clear cell A (ccA, good risk) and clear cell B (ccB, poor risk) ccRCC subtypes[7,

13, 14]. Similar to previous findings[71], intra-tumor gene expression heterogeneity was sometimes evident among samples from the same patient, although most tumors demonstrated a majority feature profile (**Figure 3.2a**), as well as more concordant profiles than those from different patients (**Appendix Figure 3.2A**). In an effort to minimize the uncertainty surrounding the influence of tumor heterogeneity on gene expression between tumor biopsies[145, 146], we examined the relationship of the ccA/ccB subtyping with multiple parameters of the MRI/PET imaging, identifying FDG-PET standardized uptake value (SUV) to be the best radiographic parameter for dichotomizing ccA patients from ccB (**Figure 3.2b**). Patients who expressed a complete or predominately ccB subtype had SUVs of 2.0 or higher in 50% or more of the tumor volume compared to only 20% or less in tumors of ccA patients (**Figure 3.2c**). Moreover, individually ccB-typed samples had significantly higher maximum SUV than ccA. This maximum SUV also correlated with HIF1A (not HIF2A, **Appendix Figure 3.3A**) and GLUT1 protein levels, which could account for the shift toward glucose uptake, whereas in good risk ccA classified samples and tumors, FBP1 protein levels were significantly higher (**Figure 3.2d**), suggesting possible alternate metabolic pathways driving these two subtypes.

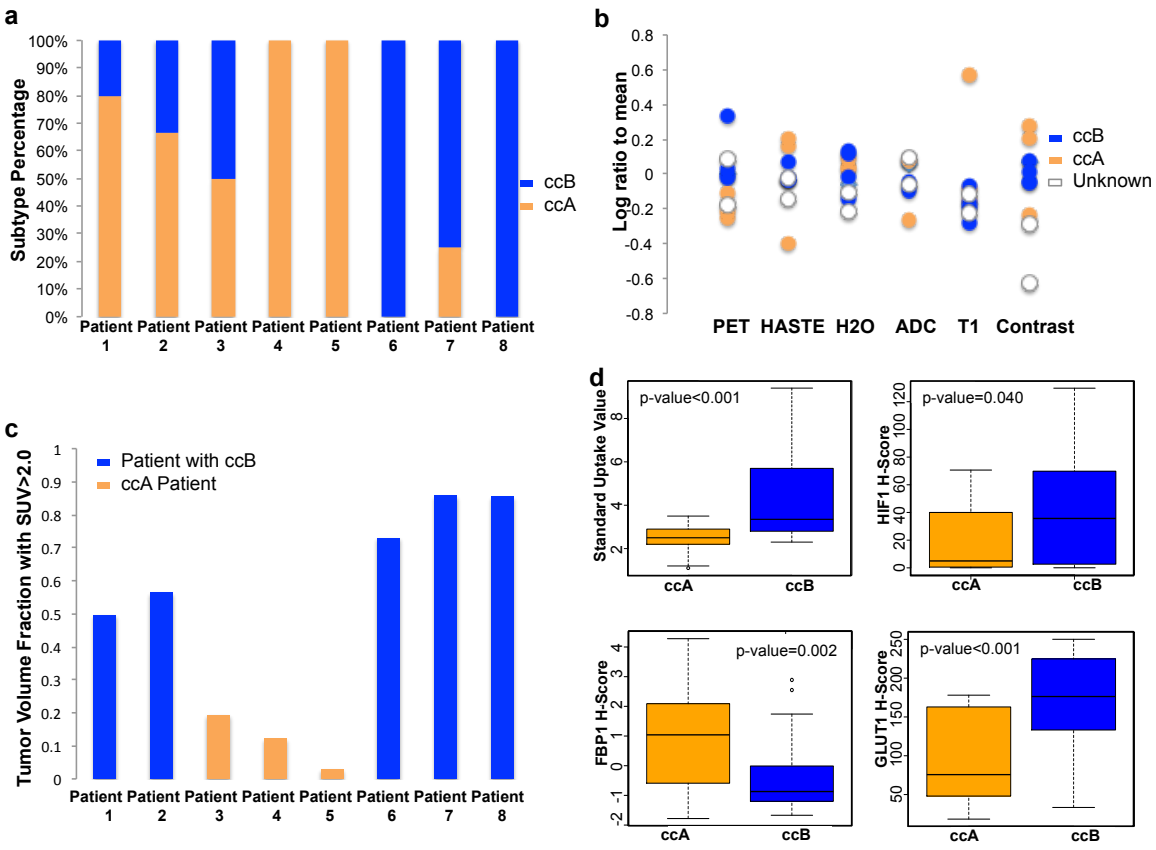

Figure 3.2: PET dichotomizes ccRCC subtypes by metabolic activity.
Heterogeneous subtype classification was evident among samples from the same patient (**a**). However, an overall classification trend was observed with all patients. All primary tumor samples from Patient 3 were of the ccA subtype and metastatic samples ccB. (**b**) The uptake of Fludeoxyglucose (FDG), a glucose analogue, best distinguished ccA patients from ccB compared to MR radiological parameters (Haste, Water, ADC, T1, and Contrast). Patients who largely expressed the ccA classification profile were considered ccA and those expressing mostly ccB were considered ccB. Only the primary tumor was used to measure tumor means, so Patient 3 was annotated as a ccA patient (**b** and **c**). Standardized Uptake Value (SUV) of primary tumors was greater than 2.0 in at least 50% of tumor volume for tumors with a ccB classification while those absent of ccB exceeded SUV of 2.0 in 20% or less of tumor volume. (**c**). (**d**) ccB samples had significantly higher maximum SUV compared to ccA, as well as increased expression of HIF1 and activation of the glucose transporter GLUT1. Interestingly, ccA and ccB-typed samples expressed distinct levels of FBP1, suggesting discrete metabolic reprogramming within these two groups.

Metabolic dysregulation has widely been considered as a key event in ccRCC tumorigenesis due to the high frequency of *VHL* inactivation and resulting activation of hypoxia inducible transcription factors[17, 147], which regulate numerous genes involved in metabolism. Therapeutics are being developed and used to target enhanced metabolic pathways, such as the mTOR pathway. However, these agents produce either inefficient or varied patient responses, underscoring the need for a greater understanding of the complex relationships between tumor and host metabolic activities[36, 41, 121, 148]. Recently, the ccRCC cancer genome atlas (TCGA) elucidated that patients with unfavorable survival outcomes had higher expression of genes involved in early steps of glucose utilization, the oxidative pentose phosphate pathway, fatty acid synthesis, and downregulation of the PI(3)K pathway, whereas patients with better survival expressed genes involved in glycolysis, Krebs Cycle, and AMPK signaling[15]. In our analysis, the ccA and ccB subtypes, and FDG-PET glucose uptake patterns, followed similar trends, as ccB (SUV high) samples significantly displayed higher expression levels of oxidative pentose phosphate pathway genes whereas ccA samples had higher levels of glycolytic and Krebs Cycle genes (**Figure 3.3a**). Surprisingly, FBP1 and other glucose storage genes showed marked differential expression between ccA (SUV low) and ccB (SUV high)-typed samples. It was recently demonstrated that FBP1 is frequently depleted in ccRCC and may act as a critical mediator of tumor progression[144]. We observed that the majority of ccB-typed samples have depleted FBP1 transcript levels, as compared to ccA, consistent with FBP1 corresponding to steps in disease progression or an aggressive phenotype.

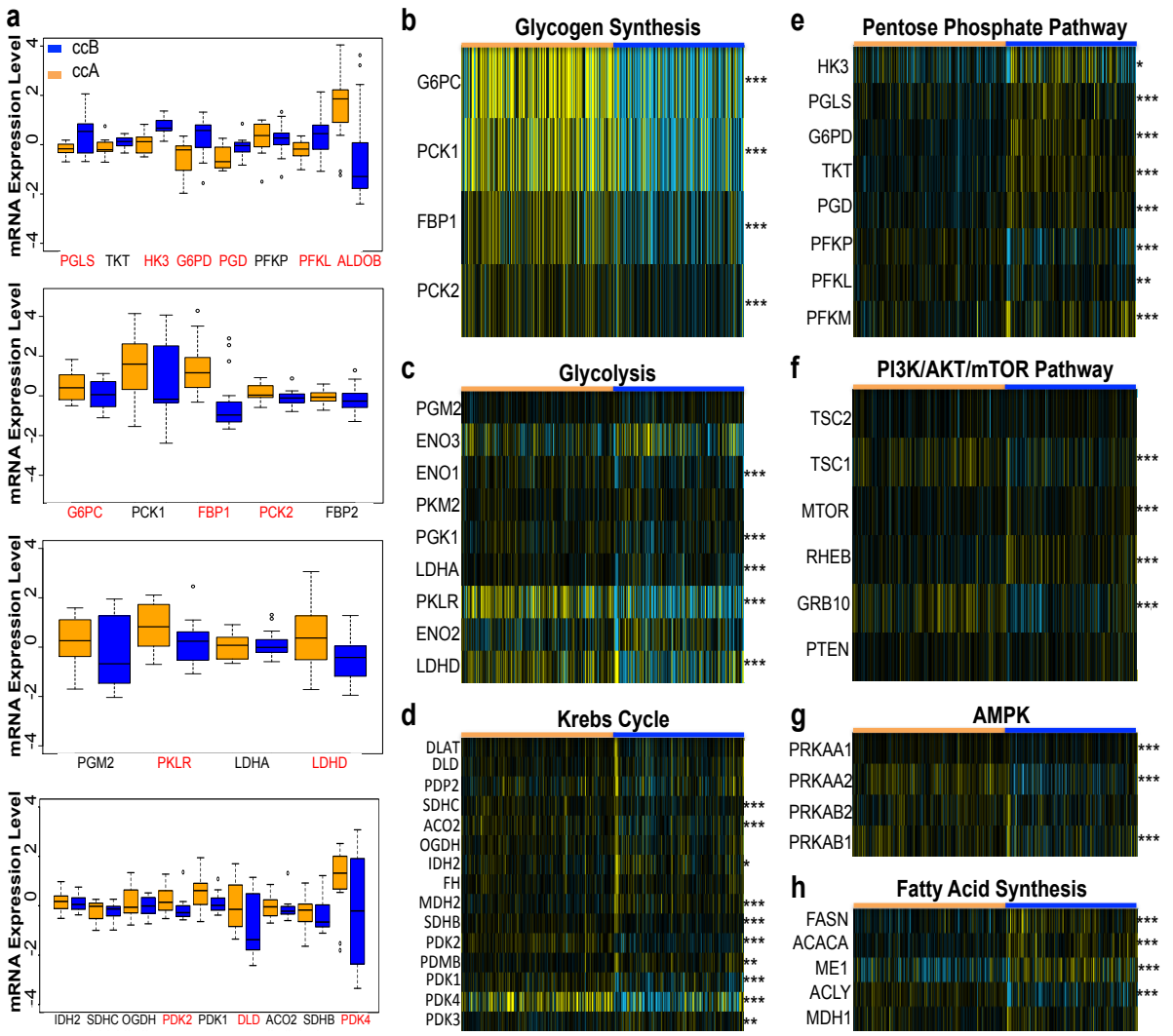

Figure 3.3: ccRCC subtypes are involved in distinct metabolic pathways.
Increased metabolic activity is a key event in ccRCC progression and has been postulated to be a future target for personalized treatment. (a) ccB patients had significantly higher expression of genes associated with the oxidative pentose phosphate pathway (PGLS, HK3, G6PD, PGD, PFKL, and ALDOB), while having lower levels of genes involved in glucose storage (G6PC, FBP1, and PCK2), showing a shift in metabolism towards glucose synthesis. On the other hand, glycolytic activity (PKLR and LDHD) was enhanced in ccA samples compared to ccB, as well as Kreb Cycle genes (PDK2, DLD, and PDK4). Red genes were found statistically significant (p-value>0.05) between ccA and ccB samples by a Welsh t-test. Similar to the patients in the study, ccA and ccB patients from the ccRCC Cancer Genome Atlas (TCGA) (b-h) separated by the activation of distinctive metabolic pathways. ccA patients had higher expression of genes associated with glucose storage (b), glycolysis (c), and the Krebs Cycle (d) compared to ccB patients. Much like ccB patients in Figure 3a, ccB patients had higher expression of genes involved in the oxidative phase of the pentose phosphate pathway (e). Interestingly, ccA patients significantly increased expression of genes inhibiting the PI(3)K, AKT, and MTOR pathway (f and g), while ccB patients had activation of the mTOR pathway and fatty acid synthesis (h), suggesting a possible mechanism for increased HIF1 and GLUT1 expression in ccB patients (Figure 2d). Welsh t-test was performed to analyze significance of gene expression between subtypes (* = p-value>0.05, ** = p-value>0.01, *** = p-value>0.001).

Similarly, a metabolic switch was evident between ccA and ccB assigned samples in the TCGA dataset. ccA samples demonstrated notably higher glycogen synthesis (**Figure 3.3b**), glycolysis (**Figure 3.3c**), and Krebs Cycle (**Figure 3.3d**) activity compared to ccB samples that had enhanced oxidative pentose phosphate (**Figure 3.3e**) and mTOR pathway (**Figure 3.3f**) activation. The trend towards a "Warburg effect"-like state identified in the ccRCC TCGA was evident with ccA patients who experienced increased AMPK signaling (**Figure 3.3g**) and expression of mTOR pathway inhibition, as compared to the upregulation of fatty acid synthesis in ccB patients (**Figure 3.3h**).

We performed logistic regression on ccA and ccB samples from our study (**Figure 3.4a**) and 380 patient samples from the TCGA (**Figure 3.4b**) to identify biological variables significantly correlated to and predictive of subtype. In our study, ccA samples were best defined by genes (pink) and proteins (purple) involved in glucose storage and glycolysis (**Figure 3.4a**). On the other hand, enhanced expression of pentose phosphate pathway genes distinguished ccB samples. Higher standard uptake values trended towards ccB (p-value=0.06), however the sample size limited statistical power. We were able to further evaluate metabolic trends that characterized the two subtypes by using RNA-seq data from the TCGA (**Figure 3.4b**). Similar to previous findings, the most significant genes associated with the ccA subtype involved the upregulation of glycogen synthesis (G6PC, FBP1, PCK1, and PCK2), glycolysis (PKLR, ENO1, LDHD, LDHA, and PGK1), and Krebs Cycle (PDK2, PDK1, ACO2, SDHC, SDHB) in contrast to ccB samples which had significant association with the oxidative pentose phosphate pathway (HK3, PGLS, G6PC, TKT, PGD, and PFKM) and fatty acid synthesis (FASN, ACACA, and ME1). Interestingly, the PI(3)K pathway inhibitors TSC1 and GRB10 were highly associative to the ccA subtype, while mTOR genes

(mTOR and RHEB) were enhanced in ccB subtype, again, highlighting metabolic redirection in these two prognostic groups (**Appendix Figure 3.1A**).

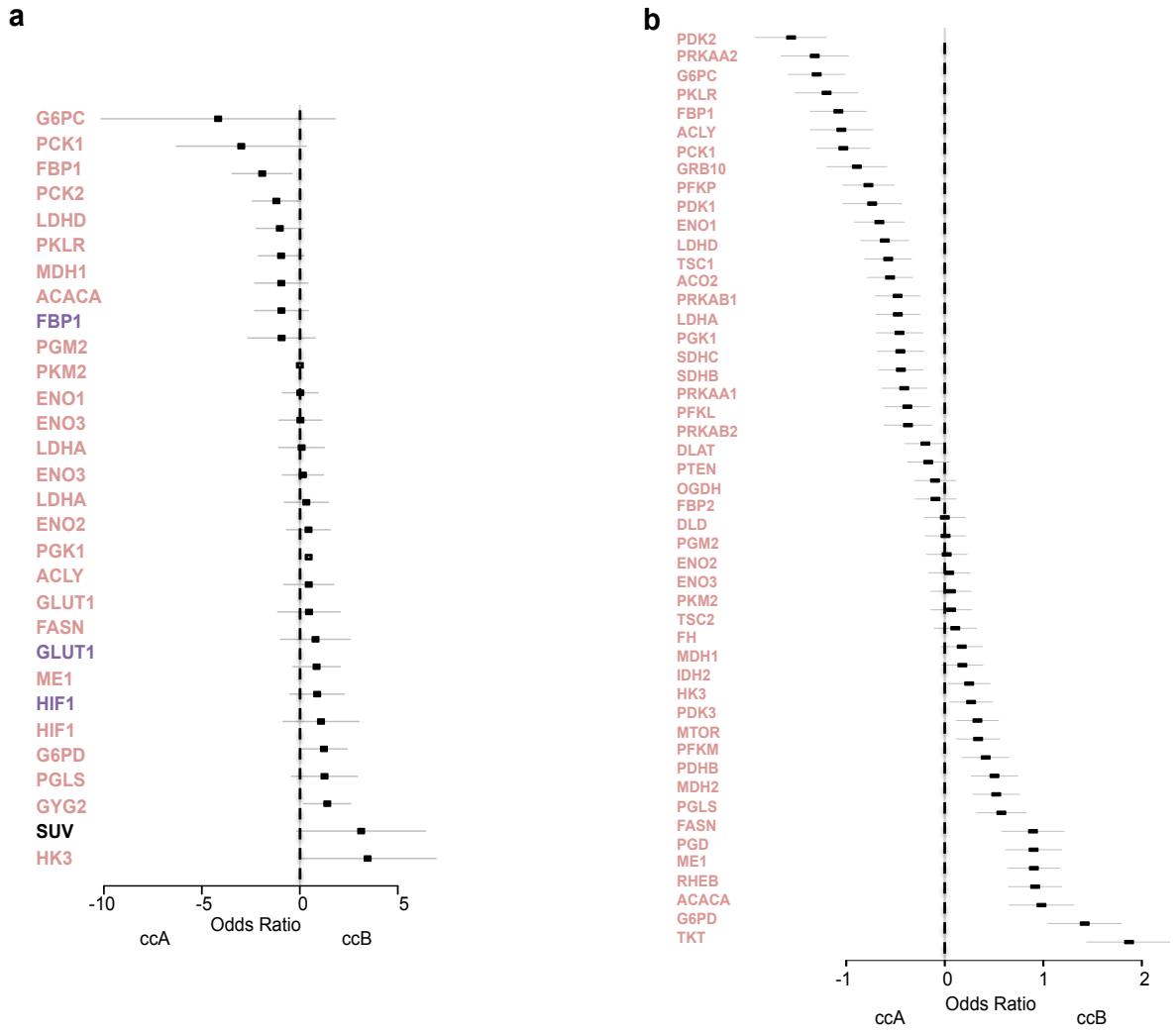

Figure 3.4: Distinct pathways support ccRCC metabolism.
Logistic regression was performed to assess which biological features were significantly correlated to the ccA and ccB subtypes, with the exclusion of patient effect. (a) A forest plot depicts the association of effect estimates (odds ratios) of genes (pink), proteins (purple), and standard uptake values (black) with ccA (odds ratios between -10 and -1) and ccB subtypes (odds ratios between 1 and 5). The G6PC and PCK1 genes were highly associated with ccA samples, but weren't significantly valuable. However, FBP1 gene expression was significantly correlated and higher in (p-value=0.014) ccA samples. In contrast, ccB samples were associated with the gene expression of G6PD (p-value=0.042) and HK3 (p-value=0.052), as well as SUV (p-value=0.06). (b) Similar metabolic trends were associated with subtype in the ccRCC TCGA, where enhanced expression of glycogen synthesis (G6PC, FBP1, PCK1, and PCK2), glycolysis (PKLR, ENO1, LDHD, LDHA, and PGK1) and Krebs Cycle (PKLR, ENO1, LDHD, LDHA, and PGK1) genes were associated with ccA, while oxidative pentose phosphate pathway (HK3, PGLS, G6PC, TKT, PGD, and PFKM) and fatty acid synthesis (FASN, ACACA, and ME1) genes were upregulated in ccB. (c) Model illustrating the different metabolic pathways driving the ccA and ccB subtypes. ccAs generate NADH for the electron transport pathway mainly through glycolysis and Krebs Cycle, while fatty acid synthesis is enhanced to generate energy through the oxidative pentose phosphate pathway in ccBs. The mTOR pathway activity is also enhanced in ccBs driving the expression of HIF1 and thus the target gene GLUT1, resulting in higher glucose uptake.

Discussion

Intratumor heterogeneity has been shown to significantly impact the genome of ccRCC creating difficulties in revealing underlying molecular events that promote tumorigenesis and progression[71, 137]. Thus, biomarkers are urgently needed that provide insight towards tumor biological processes, and which have the potential to comprehensively assess the whole disease, and which could guide selection of treatment[121, 149, 150]. In this study, we provide a novel methodology that incorporates radiographic imaging with multiregional gene expression profiling to facilitate the assessment of intratumor heterogeneity and tumor progression. The ccRCC subtypes, ccA and ccB, even as defined based on single tissue sample specimens, have been validated as prognostic tools for the evaluation of cancer-specific death. ccA patients have substantially better recurrence-free, cancer-specific, and overall survival than patients of the ccB subtype. Here, we have identified that ccB samples express higher glucose uptake compared to ccA and ccB-typed tumor present with higher overall SUV tumor means compared to ccA. This technique can potentially facilitate a comprehensive assessment of the tumor, and the overall disease, without using invasive alternatives, especially where biopsy bias is a concern[146]. More importantly, these data suggest that a metabolic transition accompanies the differences between ccA and ccB, with FBP1 expression as a key factor, and further, that alternate mechanisms for energy processing in ccA and ccB tumors that may contribute to their antagonistic survival outcomes. ccA tumor cells appear to produce energy through increased glycolysis and Krebs Cycle activity, while storing additional glucose through FBP1-controlled glycogen synthesis, in keeping with the glycogen-rich histology that is classic for lower grade ccRCC tumors. In contrast, metabolic activity in ccB patients is substantially enhanced, with glucose uptake and

synthesis increased and storage decreased. The oxidative pentose phosphate pathway is elevated and potentially functions as a generator of NADPH for ccB patients, which is likely supported via the mTOR pathway (**Appendix Figure 3.1A**). Future studies are required to validate the metabolic mechanisms of the ccA and ccB subtypes. However, this study suggests novel therapeutic targets that may improve assessment for prognostic and predictive outcomes for ccRCC.

Methods

Patients and clinical samples

All patients were enrolled to an investigator-initiated trial, LCCC1213, using a UNC Biomedical IRB approved consent. Enrollment criteria consisted of adequate organ function, radiographic confirmation of a renal mass of sufficient size to allow subsampling, and a scheduled surgery date. Patients were encouraged to be fasting at the time of the scan, and blood sugar was tested prior to imaging. No patients were excluded due to hyperglycemia. In total, 13 patients were imaged, but only clear cell RCC patients were included in the primary analysis (supplemental table 1), due to the markedly differing biology of other subtypes such as papillary RCC[15, 151, 152].

Specimens were collected from October 2012 through September 2013 at the University of North Carolina directly from the pathology grossing area using the MR-PET image map as a guide to select samples corresponding to the desired region of interest. At least five fresh kidney specimens were obtained from each patient and were transported back to the lab, relabeled, and stored as flash frozen or paraffin embedded specimens for batched analysis. Stage was classified using the American Joint Committee on Cancer's Cancer

Staging Manuel, 7th edition (AJCC-7). A genitourinary oncologist verified pathologic clinical variables.

MRI/PET Acquisition

Prior to the PET/MR imaging session, 5mCi of FDG was infused intravenously. During the FDG uptake period, patients were kept in a quiet room. 40 min after FDG infusion, patients were asked to empty their bladder prior to the imaging session. All images were acquired using a hybrid PET/MR scanner (Biograph mMR, Siemens HealthCare) housed in the Biomedical Research Imaging Center. A spine coil together with 2 anterior body coils were used to cover liver through kidneys. After acquiring localization images, MR attenuation images were acquired first, followed by a breath-hold T2 half-Fourier acquisition single-shot turbo spin-echo (HASTE) sequence. These included multiplanar T2 weighted images obtained sequentially 5mm in thickness with a 2 mm gap and pre and post contrast enhanced T1 weighted images obtained as a volume and reviewed as 3mm contiguous images in multiple planes. The dose of Gadolinium chelate was 0.1 mg/kg. This sequence was repeated twice along the coronal (cor) and axial orientations, respectively. The image parameters for the coronal orientation were as follows: repetition time, 2sec; echo time (TE) 94msec; slice thickness, 8 mm for 28 slices with 20% gap; matrix size, 256x256; acceleration factor of 3 using GRAPPA; flip angle, 150-degree; and voxel size 2x1.6x8mm3. In contrast, with the exception of TE=95msec, number of slices = 24, acceleration factor = 2, and voxel size = 1.7x1.4x8mm3, images acquired using an axial orientation used identical parameters as that for coronal orientation. The HASTE images were used for the placement of ROIs throughout the tumors. In contrast to MR imaging, a 4 min single-bed PET acquisition covering the kidneys was acquired simultaneously with the above outlined

HASTE sequence. PET images were obtained on the same table again using standard techniques. Post procedure fusion of the MR and PET images was performed using a dedicated workstation (Siemens Medical Solutions, Malvern, PA).

Image review

Two physicians reviewed images, one a genitourinary imaging specialist with 20 years experience and the other a nuclear medicine specialist with 15 years of experience. Cases were reviewed using a standardized hanging protocol. The high-resolution MR images were used to identify anatomic structures. Location of FDG and Gd uptake were identified, focusing on the kidney tumor and local metastases. FDG uptake was quantified using standard SUV. An increase of 2 SUV was considered increased avidity.

Antibodies and Immunohistochemistry

Rabbit polyclonal antibodies against CD31 (ab28364), FBP1 (HPA005857) and Glut-1(07-1401) were from Abcam (Cambridge, MA), Sigma Aldrich Corp. (St. Louis, MO) and Millipore (Billerica, MA)) respectively. Mouse monoclonal HIF1A clone 54 (610959) was from BD Biosciences (San Jose, CA).

IHC was carried in the Bond Autostainer (Leica Biosystems Inc. Norwell, MA). Slides were dewaxed in Bond Dewax solution (AR9222) and hydrated in Bond Wash solution (AR9590). Antigen retrieval for all antibodies was performed for 30 min at 100ºC in Bond-Epitope Retrieval solution1 pH-6.0 (AR9961). After pretreatment slides were incubated with FBP1 (1:1500) and Glut-1 (1:2000) for 30 min, CD31 (1:200) for 1h and HIF1A (1:100) for 3h. Detection of CD31, FBP1 and Glut-1 was performed using Bond™ Polymer Refine Detection (DS9900) and Bond™ Polymer Refine Red Detection (DS9390) for HIF1A.

Stained slides were dehydrated and coverslipped. Positive and negative controls (no primary antibody) were included for each antibody.

Digital imaging and image analysis

IHC stained slides were digitally imaged in the Aperio ScanScope XT (Leica) using 20x objective. HIF1A, Glut-1 and FBP1 slides were analyzed using Aperio Image analysis algorithms and Definiens Tissue Studio software (Munich, Germany) was used to measure the microvessel density in CD31 stained slides.

Quantitative Image Analysis

For each subject, one PET image and five MRI images were analyzed as follows. The PET image was scaled to units of Standard Uptake Value (SUV). The MR images used included a T2-weighted HASTE sequence (referred to as "HASTE"), a water-content image from the Dixon sequence used for attenuation correction (referred to as "Water"), an apparent diffusion coefficient image (referred to as "ADC"), a t1-weighted image (referred to as "T1"), and a contrast image produced from the subtraction of pre-contrast from a post-contrast image (Referred to as "Contrast"). The ADC image was already quantified as an estimate of a physical quantity, the apparent diffusion coefficient, and was used unchanged. The other MRI images in their raw forms were quantified in arbitrary intensity units and so were normalized to the average intensity in a cortical region of the opposite healthy kidney.

Because the PET-MR scanner gives images that are already aligned, the PET and MRI images generally did not require an additional alignment step. However, in two cases, some images had to be rigidly translated to align the tumor sites; generally this appeared to be due to respiratory motion. All images were then resampled to the grid of the PET image (2.086

mm x 2.086 mm x 2.031 mm). Regions of interest encompassing the tumors were drawn by hand to isolate the tumor volume.

For each voxel, a set of six image quantities (PET, HASTE, Water, ADC, T1, and Contrast) were derived. Means of these six quantities within the tumor volume were computed for each subject. Further analysis of the PET image included computation of the percent of tumor volume exceeding certain SUV thresholds, which were found to be related to pathology outcomes.

Microarray Analysis

mRNA was extracted from fresh frozen ccRCC tissue specimens using the Qiagen AllPrep DNA/RNA Mini Kit (Valencia, CA), amplified, labeled and hybridized against a reference[153] on Agilent Whole Human Genome (4 x 44k) Oligo Microarrays. Missing data was imputed, log transformed (base 2), and median centered.

Subtype Classification

Samples were classified as either ccA or ccB using a reference microarray data set and centroid-based classification algorithm previously described[7].

The Cancer Genome Atlas (TCGA) data analysis

TCGA RNA sequence data were obtained from dbGAP and normalized to the upper quartile of normal counts. For analysis, the data were log-transformed (base 2) and genes were median centered.

Statistical Analysis

All statistical analyses were performed using the R program (R Project for Statistical Computing, Vienna, Austria). A two-sample Welch t-test was used to assess differences

between subtypes, with all p-values lower than 0.05 considered significant. Gene and protein (H-Scores log2 transformed) expression data were fit with a mixed effects regression model using fixed effects for each variable of interest, and a random effect for the patients (nlme and lme4 R Packages). Standard errors of the effect estimates were calculated and illustrated as a forest plot. Intra-class correlation (ICC) was utilized to measure concordance between samples from the same patient and between patients. ICC was calculated for each pair and then summarized by mean for each group of paired samples. ICC values for unpaired groups were estimated from all samples in the group. Further analysis and plotting of paired and unpaired analyses were performed identically. The "irr" R package was used to generate ICC estimates.

CHAPTER 4: CADMIUM EXPOSURE INFLUENCES ccRCC HETEROGENEITY THROUGH AN EPIGENETIC MECHANISM

Introduction

Cadmium (Cd) is a known environmental and occupational metal compound that has been linked to various adverse health effects, including cancer[88] [89, 109-113]. Exposure to cadmium can occur through multiple sources, however, the most common source is through smoking cigarettes. Smoking populations experience higher levels of cadmium exposure, as one cigarette may contain 1-2 ug cadmium[80, 81]. The long half-life of Cd of approximately 20 to 21 years results in the accumulation of the metal over time, which is detrimental to persons with numerous or chronic Cd exposures. The kidney is one of the main deposition sites of Cd due to reabsorption from filtered blood by the proximal convoluted tubules[86]. More specifically, heavy metals like cadmium can induce nephrotoxicity altering gene expression in the kidney, and thus increasing the risk of developing Renal Cell Carcinoma (RCC) [81, 87, 114]. In addition to transcript alterations, numerous studies have found that Cd exposure can result in epigenetic deregulation by changing DNA methylation levels, histone modifications, and miRNA expression [84, 115-117], which have all been found to be novel hallmark features of the clear cell Renal Cell Carcinoma (ccRCC) subtype[15, 59]. Exploring toxicant-induced global expression and epigenetic changes can enhance our understanding of the genetic interactions that drive the biological responses to these exposures and their influence on signatures of RCC that are imperative for prognostics.

Clear cell Renal Cell Carcinoma, the most prevalent subtype of RCC or kidney cancer in adults, has been established as a highly heterogeneous disease, displaying various subpopulations of cells, assorted cell and tumor morphology, and distinct genetic signatures[71, 124]. The enhanced genetic heterogeneity of this disease has made it difficult to elucidate which mutations are imperative for ccRCC initiation and progression. Nonetheless, molecular features of ccRCC have recently emerged that shed light towards understanding its underlining biology. Clearcode34, a novel 34-gene risk predictor for ccRCC tumor recurrence and cancer-specific death, was recently elucidated and validated to classify two subtypes of ccRCC, clear cell A (ccA) and clear cell B (ccB). These subtypes conveyed a prognostic value, with tumors displaying the ccA signature associated with better recurrence-free, cancer-specific, and overall survival compared to ccB[7]. ccRCC is a tumor closely linked to environmental toxicant exposure, and heavy metals like cadmium can induce nephrotoxicity altering gene expression in the kidney, and thus increasing the risk of developing RCC. Furthermore, ccRCC is associated with chromosome 3p deletions and inactivation of genes within that region, such as the Von Hippel-Lindau (VHL) tumor suppressor and epigenetic modifiers PBRM1, SETD2, and BAP1[12, 154, 155]. Even with the elucidation of these genetic features, the contributions of other 3p genes involved in ccRCC are less well understood, but additional effects on gene transcription would be expected as a result of chromatin modulating activities. Thus, we aim to evaluate the relationship of cadmium exposure to epigenetic reprogramming in ccRCC that may influence gene expression heterogeneity and core expression patterns.

Here, we 1) explore for the first time the influence distinct DNA methylation profiles have on the ccA and ccB gene signatures, 2) examine epigenetic alterations in both ccRCC

primary tissue and kidney cell lines induced by acute Cd exposure and their affects on the expression profile of the cancer, by measuring changes in DNA methylation, which could provide a possible mechanism for gene expression changes in target genes associated with tumorigenesis. Identifying exposure-related epigenetic changes will inform us of the dynamic nature of the regulation of gene expression in ccRCC.

Results

ccRCC subtypes express distinct DNA methylation profiles

Since ccRCC is influenced by epigenetic alterations, we decided to first focus on DNA methylation and examine the methylation profiles of ccA and ccB within the prognostic tool ClearCode34. Multiple primary tumor subsamples taken from 8 patients that underwent complete nephrectomy at UNC were subjected to DNA methylation and gene expression analysis. Interestingly, samples classified as ccA expressed a hypomethylated signature among loci corresponding to ClearCode34 genes expressed higher in ccA-typed samples and a hypermethylated profile of loci corresponding to genes enhanced in ccB-typed samples (**Figure 4.1A and B**). In contrast, the ccB-classified samples in our cohort expressed increased methylation of ccA-associated ClearCode34 genes and decreased methylation for ccB (**Figure 4.1A and B**). These methylation profiles correlated to the mRNA expression, with increased expression of ccA genes in ccA samples and elevated expression of ccB genes in ccB samples (**Figure 4.1C**).

Table 4.1: Patient demographics and clinical characteristics.

Patient	Stage	Grade	Overall Subtype Classification	Smoking Status
Patient 1	II	2	ccA	Non-Smoker
Patient 2	II	2	ccA	Non-Smoker
Patient 3	IV	3	ccA	Smoker
Patient 4	I	2	ccA	Non-Smoker
Patient 5	I	2	ccA	Smoker
Patient 6	II	3	ccB	Non-Smoker
Patient 7	I	2	ccB	Non-Smoker
Patient 8	IV	4	ccB	Smoker

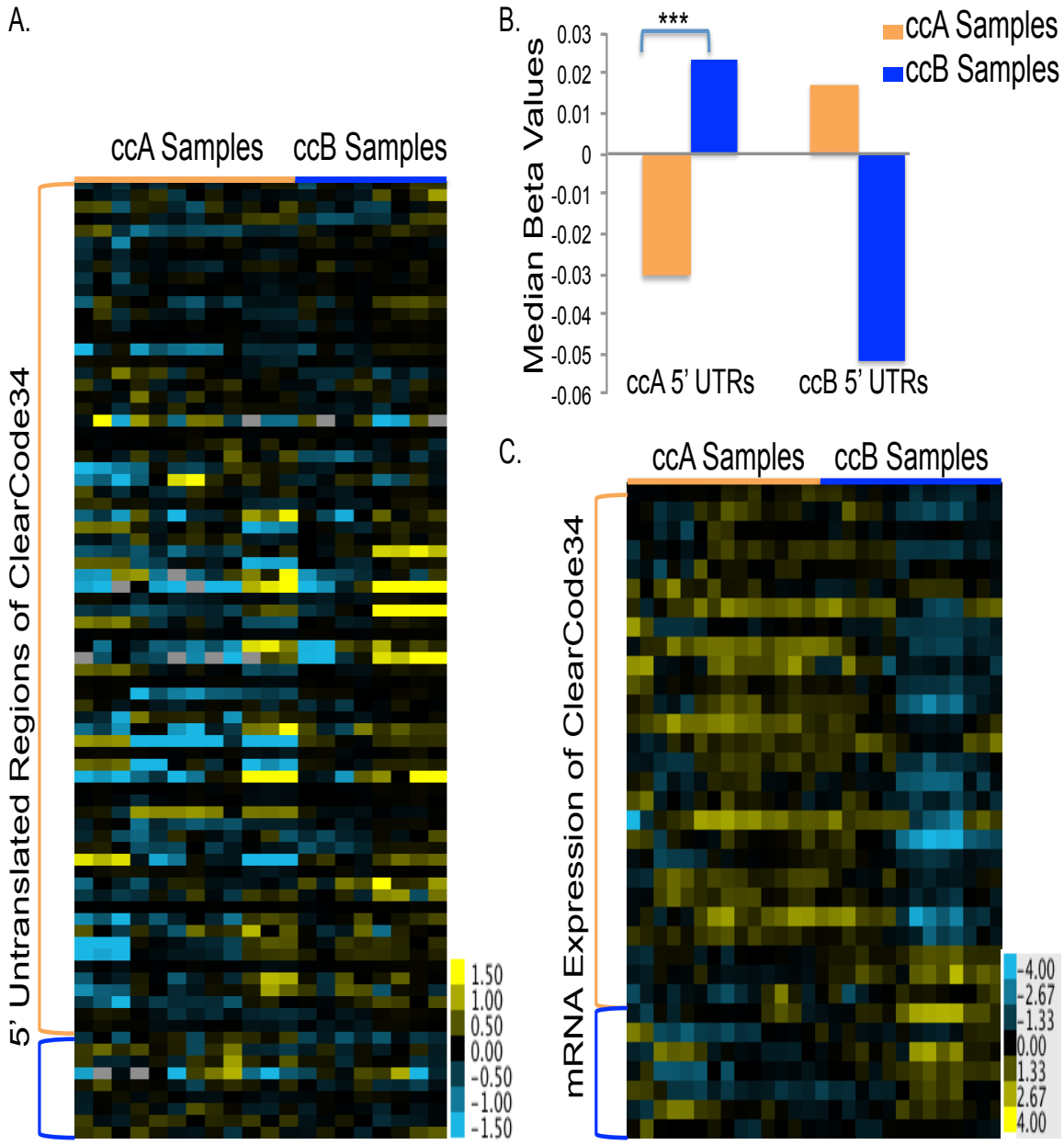

Figure 4.1. ccRCC subtypes express distinct DNA methylation profiles.A. Methylation profiles of 5' untranslated regions corresponding to loci of ClearCode34 genes. ccA-associated genes were hypomethylated in ccA samples and hypermethylated in ccB samples, while loci of genes highly expressed in ccB samples were hypermethylated in ccA samples and hypomethylated in ccB samples. B. The distinct DNA methylation profiles between ccA and ccB-typed samples were found significant among ccA-associated genes ($p<0.001$), but not ccB. C. Gene expression profiles of ccA samples were contradictory to ccB, with ccA genes enriched in ccA samples and ccB genes upregulated in ccB classified samples.

ccRCC subtypes are associated with cadmium exposure

We wanted to evaluate the relationship of cadmium exposure to epigenetic reprogramming in ccRCC that may influence gene expression heterogeneity, so we performed ICP-mass spectrometry to measure Cd concentrations in both normal and ccRCC tissues. As expected, normal (**Figure 4.2A**) and tumor tissues (**Figure 4.2B**) of patients that smoked had higher concentrations of Cd compared to non-smokers. Notably, higher concentrations of Cd was detected in normal tissue compared to ccRCC, which has been previously observed, maybe due to higher metabolic rates in ccRCC expelling out excess Cd. However, no significant trend was observed with smoking status between ccA and ccB-typed patients (**Figure 4.2C**).

We next examined the relationship between cadmium concentrations and the ccA and ccB prognostic signatures. Surprisingly, ccB samples had increased concentrations of Cd compared to ccA, suggesting a possible mechanism between exposure and ccRCC heterogeneous gene expression profiles (**Figure 4.3A**). Samples with higher cadmium concentrations tended to display a "ccB-like" DNA methylation profile of hypermethylation of 5' UTR loci of ccA-associated genes of ClearCode34 and hypomethylated loci of ccB-associated genes compared to low-Cd samples (**Figure 4.3B**), further bolstering the link between Cd and epigenetic alterations in ccRCC.

Table 4.2: Quantity of patient samples used for microarray, DNA methylation, and mass spectrometry analysis.

Patient	Microarray	DNA Methylation	Mass Spectrometry
Patient 1	5	5	3
Patient 2	3	NA	2
Patient 3	2	3	2
Patient 4	2	1	NA
Patient 5	2	2	2
Patient 6	6	4	6
Patient 7	4	NA	5
Patient 8	4	4	4

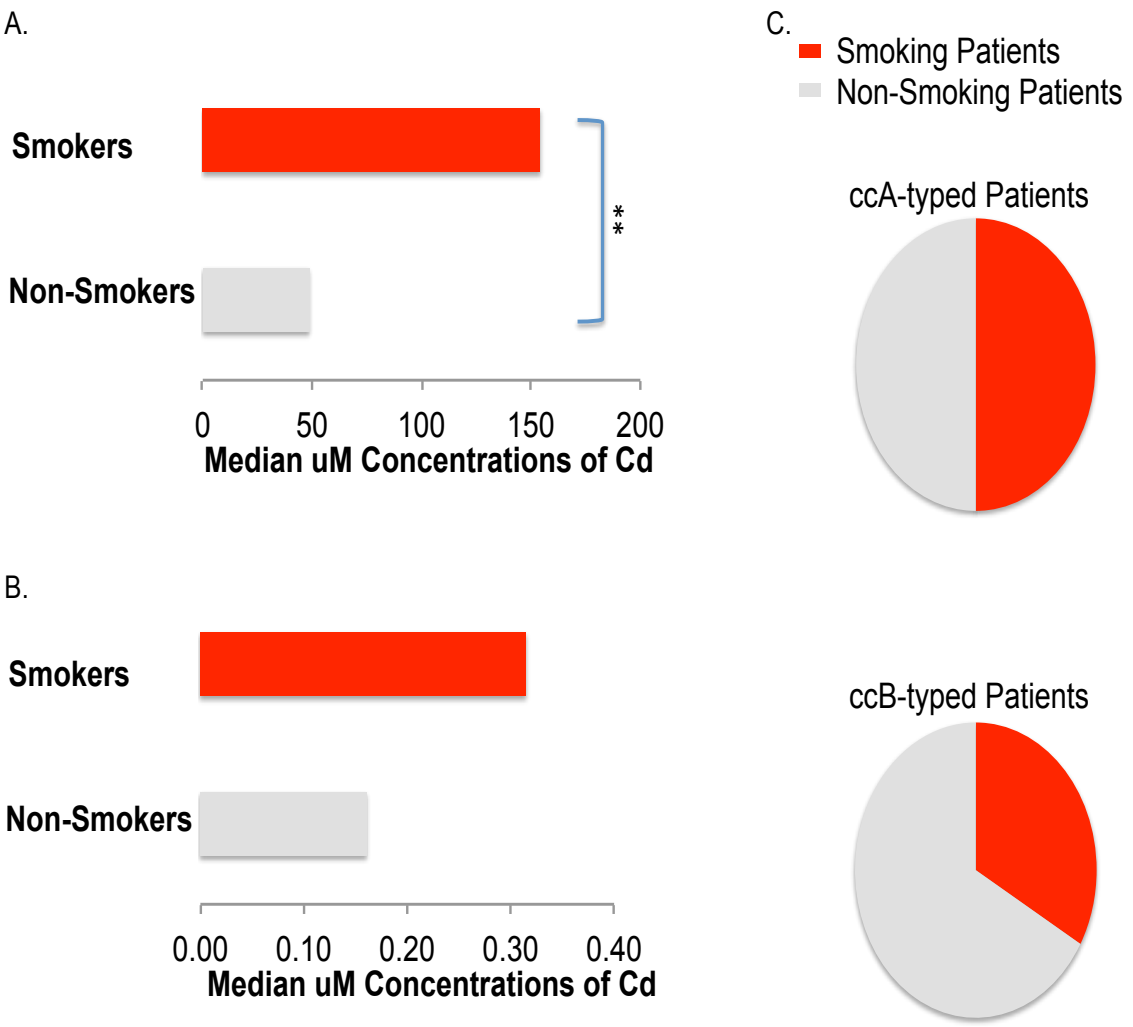

Figure 4.2: Cadmium concentrations correlate with smoking status.
Cadmium (Cd) exposure is a RCC risk factor and is found in high levels in cigarettes and smoking populations. Higher concentrations of Cd were detected by ICP-mass spectrometry in (**A**) normal and (**B**) ccRCC tissues of smokers compared to non-smokers. **C.** No correlation was identified between smoking status and ccA and ccB-typed patients.

Cadmium exposure alters ccRCC epigenome

Multiple exposures besides cadmium could have contributed to the altered epigenome between ccA and ccB in the clinical samples, so we wanted to explore the direct effects of Cd-induced DNA methylation profiles and whether they associated with prognostic markers of ccRCC. Human kidney cells (HKCs) were exposed to 4uM (low dose) and 40uM (high dose) $Cdcl_2$ up to two weeks (**Figure 4.4A**). The low dose was chosen because it represented the average micromole measured in ccRCC tissue among the patient cohort and 40uM was low enough below the half maximal inhibitory concentration (IC_{50}) (**Figure 4.5**) to prevent cell death. However, no significant differences were observed between the two concentrations or the 1-week and 2 weeks exposures.

After exposure to $Cdcl_2$, there was a marked increase of metallothioneins (MT), cysteine-rich proteins that have the capacity to bind cadmium to protect against metal toxicity and oxidative stress (**Figure 4.4B**). No expressions of MTs were detected in untreated HKCs. Moreover, there was an upregulation in the expression of DNA methyltransferases following exposure to cadmium, again suggesting cadmium induces epigenetic rearrangement in the kidney (**Figure 4.4C**). Significant hypermethylation of loci corresponding to genes in ClearCode34 was evident in cadmium-treated cells compared to untreated (**Figure 4.4D**), which correlated to heterogeneous expression of ClearCode34 genes (**Figure 4.4E**).

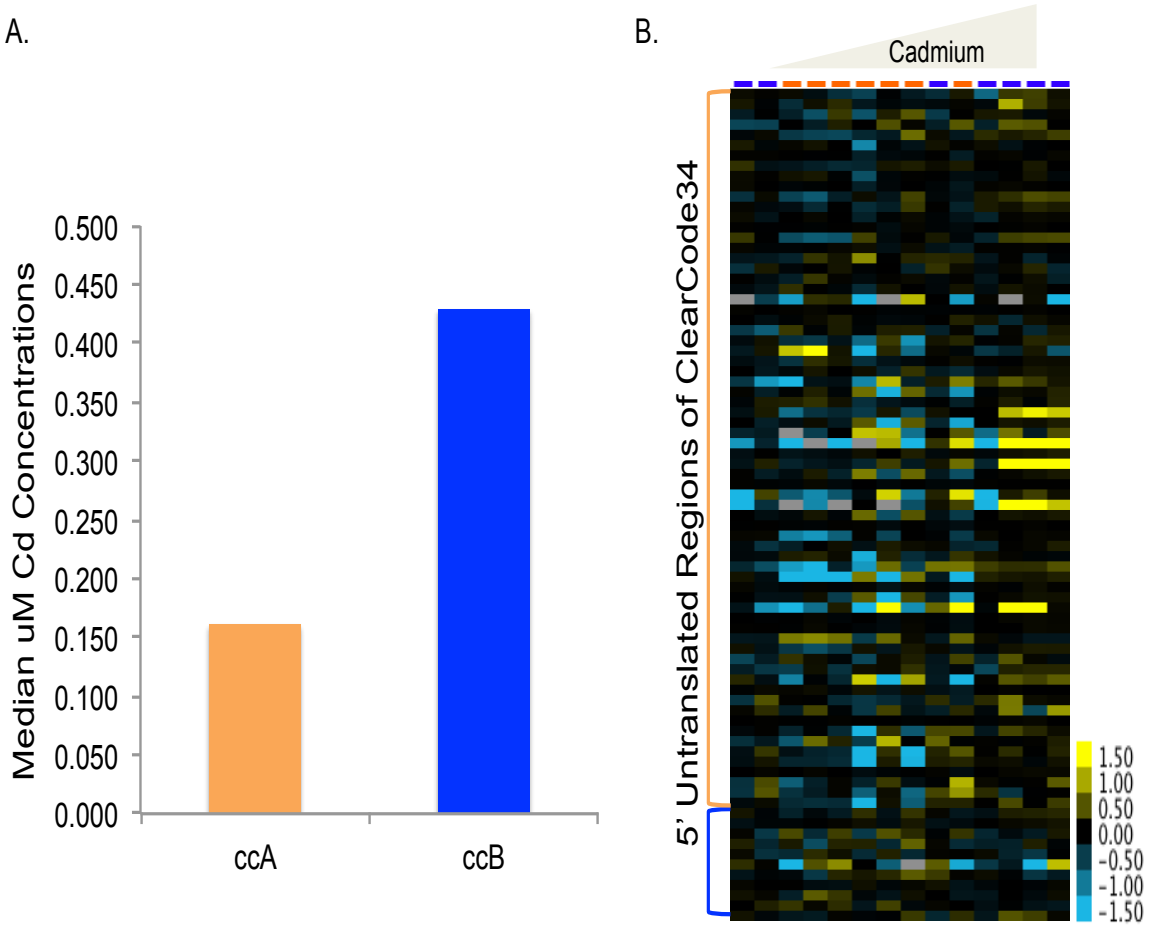

Figure 4.3: ccRCC poor prognostic marker associated with increased cadmium.
A) Higher concentrations of cadmium were measured in ccB classified primary ccRCC samples compared to ccA. B) Hypomethylation of genes significantly associated with the ccB subtype was evident in samples with higher Cd concentrations, while samples with lower Cd expressed DNA methylation profiles similar to ccA subtype.

Discussion

Cellular damage due to nephrotoxicity results in acute kidney injury (AKI) [72, 73], and can be worsened if untreated to cause chronic kidney damage or promote or exacerbate tumorigenesis [74-76]. While it is known that ccRCC can be influenced by chemical exposure, it is largely unknown whether there are sustaining effects exposures have on distinct gene signatures of this disease, and how these exposures relate to tumor heterogeneity and molecular patterns. We propose to use ClearCode34 as a baseline metric to elucidate specific effects of toxicants, such as heavy metals like cadmium, on renal tumor gene expression signatures that can provide insight into the molecular phenotypes of ccRCC.

For the first time, we highlight epigenetic mechanisms supporting the prognostic tool ClearCode34, which has been validated as a risk predictor for ccRCC cancer-specific death and tumor progression. ccA and ccB samples express distinct DNA methylation profiles that inversely correlate to gene expression patterns in ClearCode34 associated with each subtype. Variant methylation was observed in the 5' untranslated regions of loci of the 34 genes corresponding to ClearCode34. This region is upstream of transcription start sites and has been implemented in regulating transcription and translation[156]. Here, loci associated with genes upregulated in ccA-typed samples are demethylated in ccA-classified samples within our cohort compared to enhanced methylation of loci corresponding to genes enhanced in ccB-typed samples. In contrast, samples classified as ccB in our cohort had higher methylation of loci corresponding to ccA genes and lower methylation of loci of genes associated with the ccB subtype. These same DNA methylation profiles were observed in samples with lower and higher concentrations of cadmium, respectively. Furthermore, normal kidney cells exposed to cadmium expressed significantly higher transcript levels of

metallothioneins and DNA methyltransferases, regardless of a 4uM or 40uM dose. As a result, increased methylation was observed in cells following exposure to cadmium, with similar effects between 1 week and 2 week durations, suggesting longer exposures may be needed to measure dose-specific responses. Moreover, heterogeneous ClearCode34 gene expression profiles of cadmium-treated and untreated cells further bolster the cadmium-induced influence on the kidney genome and epigenome. This study will help elucidate the roles of ccRCC heterogeneity and toxicant exposure on gene expression and epigenetic patterns and its potential effects on this cancer. Exploring the range of genome-wide expression alterations as a result of tumor heterogeneity and toxicant exposure will enhance the understanding of this disease and shed light on future methods to provide a personalized care plan for patients with ccRCC.

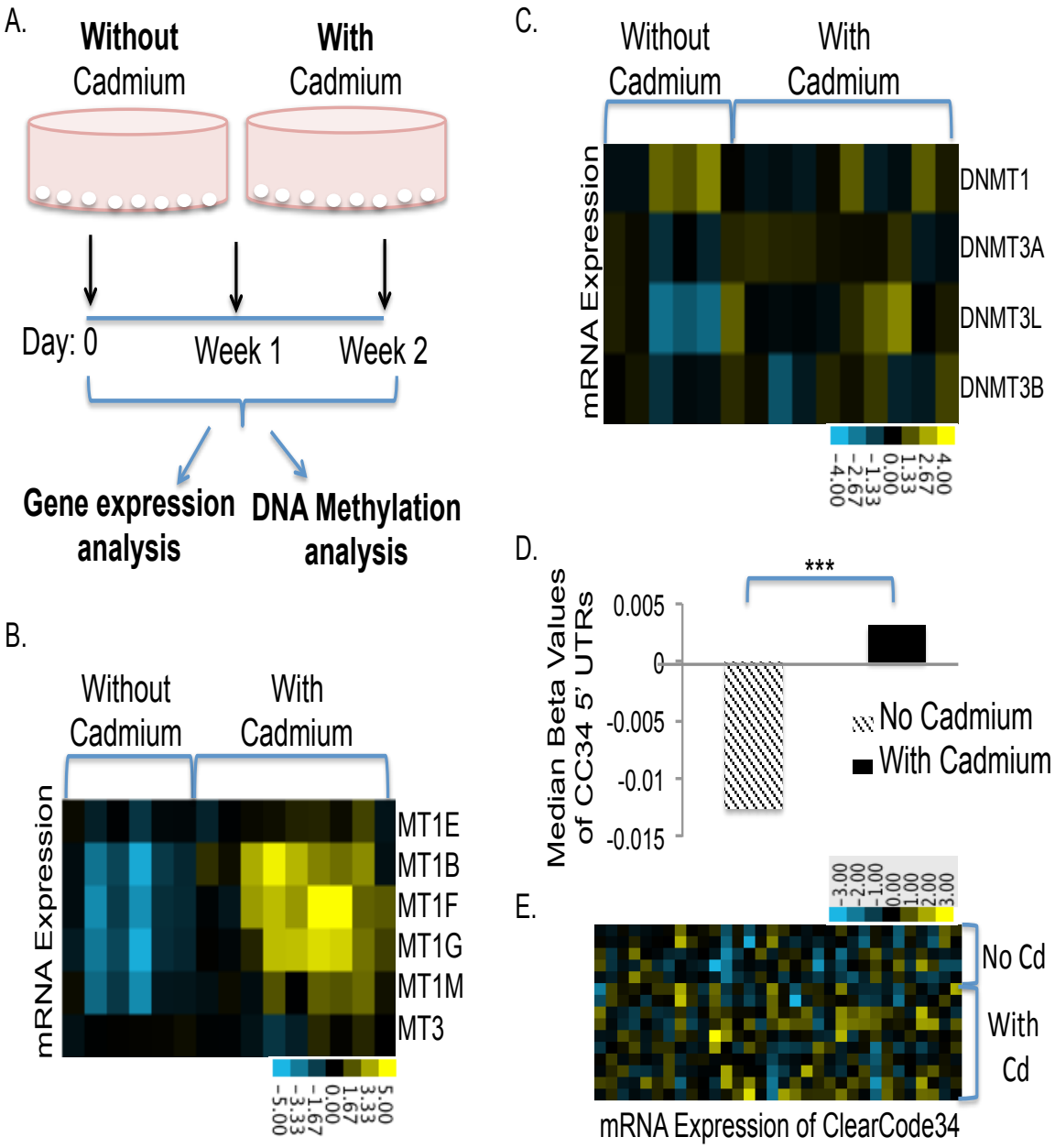

Figure 4.4. Cadmium exposure alters epigenome of primary kidney cells.
A) HKC cells were cultured with and without cadmium (4 or 40 uM) for two weeks. After every 7 days, cells were retrieved for DNA/RNA extraction to perform DNA methylation and gene expression analysis. B) Following cadmium exposure, transcript levels of metallothioneins were upregulated compared to cells untreated. C) Gene expression of DNA methyltransferases increased post cadmium exposure, which corresponded to increased methylation of loci in ClearCode34 (D). E) Heterogeneous gene expression levels of genes in ClearCode34 between genes with and without cadmium.

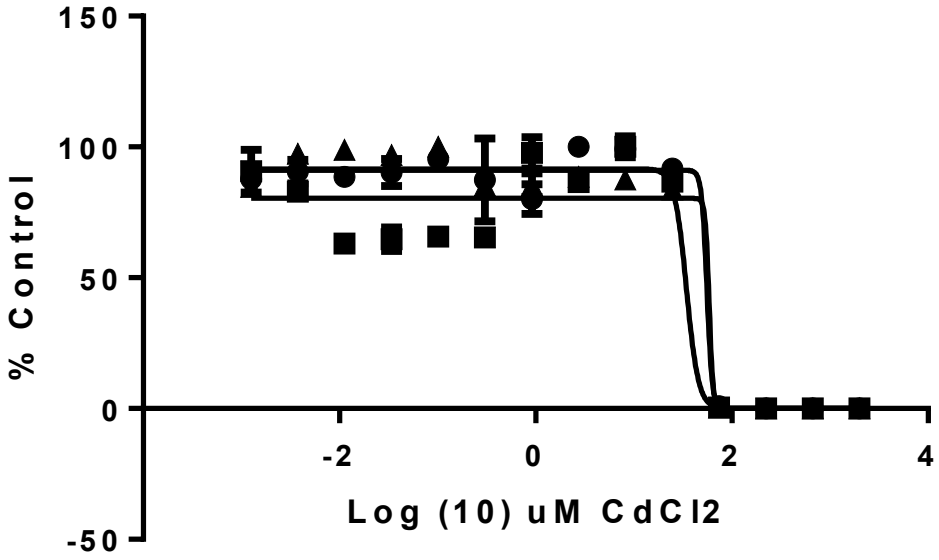

Figure 4.5: HKC cells half maximal inhibitory concentrations of cadmium.
Results of three independent experiments of HKC cell viability following exposure to cadmium chloride for 18 hours. Average inhibitory concentration was 49.6uM.

Methods

Patients and Clinical samples

Specimens were collected from October 2012 through September 2013 at the University of North Carolina directly from the pathology grossing area to select samples corresponding to the desired region of interest. At least five fresh kidney specimens were obtained from each patient and were transported back to the lab, relabeled, and stored as flash frozen or paraffin embedded specimens for batched analysis. Stage was classified using the American Joint Committee on Cancer's Cancer Staging Manuel, 7^{th} edition (AJCC-7). A genitourinary oncologist verified pathologic clinical variables.

Cell Culture

Human Kidney Cells (HKCs) are a renal proximal tubular cell line. *In vitro* studies were performed at 37°C with 5% CO_2. Cells were grown in Dulbecco's modified Eagle media with 10% FBS, nonessential amino acids, L-glutamine, and penicillin/streptomycin. Cadmium chloride was dissolved into the media by vortex to equal 4 and 40 micromolar concentrations. Cells were plated in triplicate with medium without cadmium, 4uM, and 40uM concentrations at 1 x 10^6 in 10cm plates with 10mL of media. Cells were collected for DNA/RNA extraction every 7 days for two weeks. After collections, cells were reseeded at 1 x 10^6 with and without cadmium.

Bisulfate Conversion

DNA was extracted from fresh frozen ccRCC tissue specimens and HKC cells using the Qiagen AllPrep DNA/RNA Mini Kit (Valencia, CA). Bisulfite conversion of DNA was

completed using the Zymo Research EZ DNA Methylation Kit (Irvine, CA). 75ng/uL of DNA was used for DNA methylation analysis.

DNA Methylation Analysis

DNA Methylation was performed by following the Infinium HD Methylation protocol for the HumanMethylation 450K BeadChip as written by the manufacturer (Illumina, San Diego, CA). Data was generated as averaged beta values.

Microarray Analysis

mRNA was extracted from fresh frozen ccRCC tissue specimens using the Qiagen AllPrep DNA/RNA Mini Kit (Valencia, CA), amplified, labeled and hybridized against a reference[153] on Agilent Whole Human Genome (4 x 44k) Oligo Microarrays. Missing data was imputed, log transformed (base 2), and median centered.

IC50 calculation

HKC cells were seeded in 96-well black clear bottom plates at 10,000/mL. 200uL of media with and without cadmium was added to each well. Cadmium concentrations started at 2000 uM and were diluted 3-fold until the concentration of .001uM was reached. Triplicates of cells were subjected to each concentration. Following an 18-hour incubation, media was removed and cell viability measured by the CellTiter-Glo Luminescent Cell Viability Assay (Promega, Madison, WI). Luminescence was measured using a Wallac Envision microplate luminometer.

Subtype Classification

Samples were classified as either ccA or ccB using a reference microarray data set and centroid-based classification algorithm previously described[7].

Mass Spectrometry

Kidney tissue (150 mg) was digested in 7 mL polypropylene screw caps vials with 125 µL 70% nitric acid at room temperature for 5 hours before overnight incubation in an 85°C heating block. After samples reached room temperature, 100 µL of 30% hydrogen peroxide was added and samples put on a 85°C heating block for 4 hours. Vials were cooled and vented every twenty minutes for the first hour of incubation. Following incubation, samples were diluted to 3 mL with 18Ω ohm deionized water.

The Agilent Technologies 7500cx (ICP-MS) (Santa Clara, CA. USA) was used to quantify total cadmium (Cd). Analytes were quantified according to published protocols[157]. The isotope measured was ^{111}Cd. External calibration and quality control standards were prepared from NIST traceable solutions (High Purity Standards, Charleston, SC. USA). Levels are reported as ng analyte/g kidney.

Statistical Analysis

A two-sample Welch t-test was used to assess differences between subtypes, with all p-values lower than 0.05 considered significant. Average Beta values were log transformed (base 2) and median centered to generate heat maps. Heat maps were produced with Java TreeView.

CHAPTER 5: SUMMARY AND DISCUSSION

Summary

In the U.S, kidney cancer is the sixth leading cause of cancer among men and the eighth among women[3]. There are multiple subtypes of this disease, however, over 70% of patients with renal tumors have the clear cell (ccRCC) subtype, a tumor associated with chromosome 3p deletions and inactivation of the Von Hippel-Lindau (VHL) tumor suppressor[4]. This dissertation focused on expanding two recently recognized features of ccRCC **1)** the genetic and functional/morphological heterogeneity of primary tumors, specifically renal tumor prognostic subsets, and **2)** the association of renal exposure to toxicants and their influence on expression features of renal tumors. Investigating ccRCC heterogeneity and possible environmental influences will enhance insight into the molecular phenotypes of ccRCC and their correspondence to patient outcome, as well as elucidate response to this disease.

ClearCode34

Clear cell renal cell carcinoma (ccRCC) displays variability in risk for developing metastatic disease. Thus, tissue-based prognostic biomarkers are needed to better understand the underlying biology that supports tumor progression. Recently, we've elucidated two subtypes of ccRCC, clear cell A (ccA) and clear cell B (ccB). These subtypes conveyed a prognostic value, with tumors displaying the ccA signature associated with better survival compared to ccB. We developed and validated a 34-gene subtype predictor (ClearCode34) to

classify clear cell tumors as ccA and ccB using RNA-sequencing data from ccRCC samples from The Cancer Genome Atlas (TCGA) and the NanoString platform using samples collected at the University of North Carolina. This molecular tool can be used to analyze risk for cancer-specific death and developing metastatic disease. In addition, an algorithm including ClearCode34, pathological stage, and Fuhrman grade can efficiently stratify patients by risk of tumor recurrence within 5 years following nephrectomy, which was shown to perform above and beyond other established risk predictors. ClearCode34 can be used as a baseline metric to provide insight into gene expression signatures and molecular phenotypes of ccRCC tumors.

ccRCC Heterogeneity

The novel magnetic resonance/positron emission tomography (MR/PET) image modality was employed to enrich our understanding of how tumor heterogeneity involving hypoxia signaling, metabolism, and vascularity can influence gene expression and thus provide fortitude towards predicting clinical outcome and defining individualized treatment. In our findings, tumors with increased heterogeneous metabolic derangement and highly angiogenic phenotypes on image analysis expressed the ccRCC ccB (poor risk) gene signature while those more homogenous expressed the ccA (good risk) gene signature. The ccB-typed samples expressed higher levels of fludeoxyglucose (FDG) uptake, the glucose transporter GLUT1, and expression of the hypoxia inducible factor alpha-1 (HIF1A), while ccA samples expressed significantly higher levels of the gluconeogenic regulatory enzyme fructose 1,6-bisposhate (FBP1) and lower FDG uptake, suggesting a possible metabolic paradigm that can provide insight towards the physiological mechanisms that drive tumorigenesis and tumor heterogeneity. Moreover, glycolytic activity, the Krebs Cycle, and

glucose synthesis was enhanced in ccA samples. In contrast, ccB samples expressed increased oxidative pentose phosphate pathway activity, elevated fatty acid synthesis, and PI(3)K/AKT/mTOR pathway activation, postulating an alternate method of producing energy for these samples. Utilizing these tools prior to surgical resection has the potential to create functional 3D maps to link biological correlates with imaging parameters that will enable enhanced knowledge of the biological relationships of heterogeneity and ccRCC.

Cadmium and ccRCC

Heavy metals can increase the risk of developing RCC by inducing nephrotoxicity and altering gene expression in the kidney, as well as epigenetic deregulation, so we investigated the specific effects of heavy metals on renal tumor gene expression signatures that can provide insight into the molecular biology of ccRCC. The heavy metal cadmium (Cd) has been found to disrupt transcript expression and change DNA methylation levels. We first observed that the ccRCC subtypes ccA and ccB have distinct DNA methylation profiles of genes corresponding to ClearCode34. ccA samples expressed a hypomethylated profile of ccA-associated genes in ClearCode34, which were hypermethylated in ccB samples. On the other hand, ClearCode34 genes highly expressed in ccB-classified samples were hypermethylated in ccA samples and hypomethylated in ccB samples. Furthermore, we measured cadmium concentrations in clinical RCC tissues collected at UNC and observed higher Cd concentrations in normal kidney tissue compared to ccRCC, as well as from smokers compared to non-smokers. Smoking populations experience higher levels of cadmium exposure, as one cigarette may contain 1-2 ug cadmium. Interestingly, samples with higher Cd concentrations were of the ccB subtype and expressed DNA methylation profiles similar to ccB-classified samples, suggesting a possible correlation between

cadmium exposure and aggressive disease. Similar to clinical samples, primary kidney cells exposed to Cd expressed significantly different DNA methylation profiles from untreated cells, with heterogeneous methylation of genes in ClearCode34, which correlated with higher levels of metallothioneins and DNA methyltransferases. Exploring toxicant-induced gene expression and epigenetic reprogramming can enhance our understanding of the biological processes that drive ccRCC.

Discussion

This dissertation aims to establish a novel link between intratumoral heterogeneity and the related genomic consequences of toxicant exposure that drives ccRCC tumorigenesis. Narrowing this gap will enrich the field's understanding of how tumor heterogeneity involving metabolism and vascularity can not only influence gene expression, but also provide fortitude towards predicting clinical outcome and determining individualize treatment. This body of work integrates a number of innovative elements to tackle this problem. 1) I have shown that we can take core elements of complex expression signatures and apply them to fixed clinical specimens using NanoString technology. This technology will enable my findings to potentially be applied widely in patient populations. 2) My analysis of transcription-level intratumoral heterogeneity took place in the context of a highly novel clinical trial, using sophisticated technology (MR-PET) that is only available at fewer than five institutions in the US. No other strategy has the potential to create a functional 3D map of a tumor to link biological correlates with imaging parameters. The innovative strategies we have employed have the impact of relating functional imaging findings with biological correlates, which may alter clinical practice paradigms across a variety of clinical disciplines, as well as developing genetic tools for the future that we have the ability to apply

to clinical specimens. 3) I established the novel finding that environmental exposure to cadmium can alter the kidney epigenome and influence gene expression signatures through epigenetic mechanisms. While it was known that ccRCC could be influenced by chemical exposure, we were largely unaware of the effects exposures have on distinct gene signatures of this disease, and how these exposures related to tumor heterogeneity and molecular patterns. Together, these findings further inform us of the nature of tumor heterogeneity on both core gene expression patterns, and functionally significant variations, and inform how these expression patterns relate to overall tumor biology.

Increasingly, genetic markers and signatures of cancer are being explored to define changes to the transcriptome that expand the knowledge of tumor state, progression characteristics, and response to therapy. Inactive VHL is the most established biomarker found in ccRCC and allows HIF stabilization, with tumors expressing HIF2A associated with a poor prognosis compared to tumors expressing both HIF1A and 2A[11, 12], however, this effect is modest, and has not found clinical traction. Thus, clinical tools like ClearCode34 are urgently needed and may thereby enhance patient treatment planning. Further large-scale studies will be mandatory to finalize biological features within the ClearCode34-inclusive algorithm to efficiently predict tumor recurrence risk.

Primary RCC tumors display abundant heterogeneity at multiple levels. This heterogeneity may arise from subclonal populations of cells that display various gene mutations[69, 71], and I believe that this extends to different molecular features that influence metabolism and angiogenesis. MRI and FDG-PET imaging can measure these features radiographically by detecting metabolic derangement and angiogenic phenotypes. Utilizing these tools to identify and define regions of tumors prior to surgical resection will

enable enhanced knowledge of the biological relationships of ccRCC heterogeneity, such as the amount of ccA or ccB present within a tumor, which can possibly guide clinicians towards specific treatment options. Nevertheless, additional studies are needed to identify the thresholds of FDG uptake that can correctly determine the prognostic outcomes of patients.

I hypothesized that toxicant exposures influence the epigenetic patterns of RCC, specifically those of HIF targets, contributing to the heterogeneity of this cancer by changing core signatures of overall tumor biology. Investigating downstream targets of hypoxia-inducible factors would be imperative to identifying exposure-related epigenetic changes that inform us of the dynamic nature of the regulation of gene expression in ccRCC. For example, samples classified as ccB had higher expression of the PI(3)K/AKT/mTOR pathway and HIF1A expression, so it would be important to investigate whether ccA samples have epigenetic silencing of HIFA and genes within this pathway. The molecular influences of other heavy metals and toxicants on renal core signatures should be further examined. Trichloroethylene (TCE) is a known compound that has the ability to cause kidney toxicity and damage, as well alter global gene expression changes in the kidney[109, 111, 158]. Moreover, TCE had been established as a likely human carcinogen by the EPA and National Toxicology Program, due to studies showing S-(1,2-dichlorovinyl)-L-cysteine (DCVC), the main metabolite produced by TCE, and other metabolites induce renal damage that alters genes that are key to kidney pathogenesis[78]. Additionally, nickel treatment was shown to induce the expression of the histone demethylase Jumonji domain-containing protein 1A (JMJD1A), a hypoxic response gene that regulates HIF1A, and the hypoxia pathway in RCC[118]. Exploring the specific effects of acute and chronic exposure to renal toxicants on

ccRCC gene-expression signatures will help elucidate the roles of toxicant exposure on gene expression and epigenetic patterns of ccRCC.

This dissertation has outlined for the first time the role of tumor heterogeneity and toxicant exposure on gene expression profiles of Renal Cell Carcinoma. I have developed a molecular tool capable of identifying ccRCC prognostic subtypes and predicting risk for developing progressive disease, as well as shed light on the metabolic processes supporting these distinct signatures and the specific effects of cadmium-induced DNA methylation profiles of ClearCode34. This unique study provides an exclusive way to globally map tumors, and specifically collect biologic material from regions of the tumor that are functionally defined by MR and PET imaging quantitative parameters. This work attempts to integrate gene expression signatures and environmental exposures to develop new theories regarding toxicant exposure and heterogeneous disease progression of ccRCC to enhance insight into the molecular phenotype of ccRCC tumors and their correspondence to patient outcome and response.

APPENDIX

Chapter 2

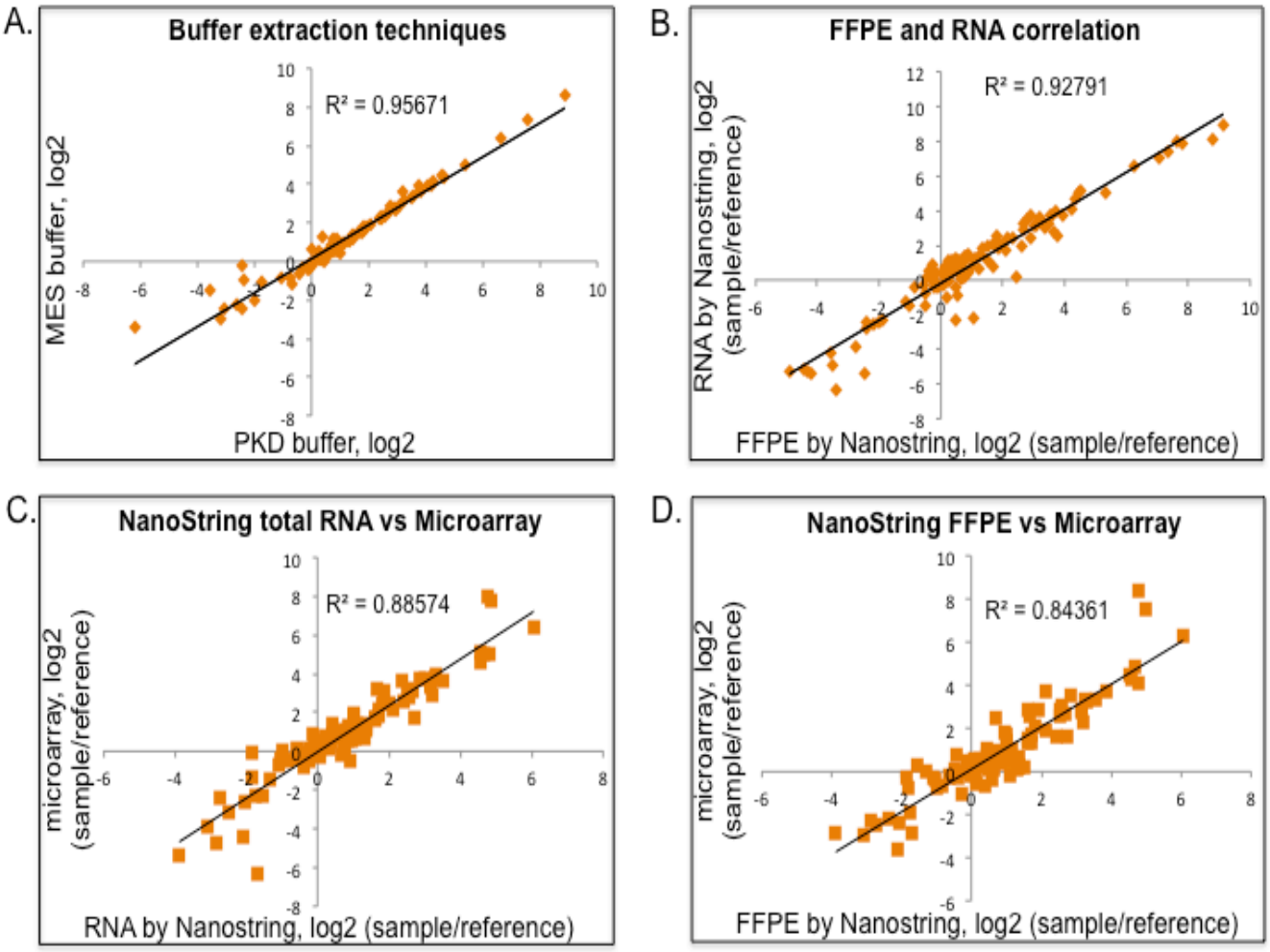

Figure 2.1A: Quality analysis of NanoString gene expression data.
(A) Linear regression plots of one tumor lysate extraction replicates (B) and five FFPE and frozen RNA extractions show strong correlations with the NanoString platform using 101 genes corresponding to the LAD-derived probes. Equivalent RNA measurement was observed between RNA extracts from five fresh frozen tumor samples examined by microarray and NanoString (C) and between biological replicates of matched FFPE samples (D).

Table 2.1A: 121 gene list used to identify 34-gene ccRCC classifier.

Category	Genes
120 Probes	ACAA2, ACADL, ACAT1, ACBD6, ADFP, AFG3L2, ALDH1A2, ALDH3A2, AP4B1, AQP11, ARSE, B3GNT6, B3GALT7, BAT4, BCL2L12, BNIP3L, C5orf19, C11orf1, C13orf1, C9orf87, CDH3, CWF19L2, CYB5R2, DREV1, DSCR5, ECHDC3, EHBP1, ESD, FAHD1, FAM44B, FLJ11200, FLJ11588, FLJ13646, FLJ14054, FLJ14146, FLJ14249, FLJ22104, FLJ23867, FLT1, FZD1, GALNT4, GALNT10, GHR, GIPC2, HIRIP5, HOXA4, HOXC10, HSPA4L, IMP-2, ITGA6, KCNE3, KIAA0436, KCNK6, KCNN4, LEPROTL1, LOC119710, LOC134147, LOC57146, LOC90624, MAOB, MAP7, MAPT, MATN4, MGC32124, MGC33887, MGC40405, MRPL21, NETO2, NCE2, NMT2, NPM3, NPR3, NUDT14, OSBPL1A, PDGFD, PHYH, PMM1, PRKAA2, PTD012, RAB3IP, RBMX, RDX, RNASE4, SAA4, SLPI, SLC1A1, SLC4A1AP, SLC4A4, ST13, STK32B, SYTL1, TCEA3, TCN2, TIGA1, TLR3, TPM4, TUSC1, UNG2, USP4, YME1L1, ZADH1
SAM	FOXM1, GPR87, LAMB3, MOXD1, SERPINA3, SLC4A3, SRPX2, TGFB1
Prognostic Markers	ARNT, BIRC5, CDH5, EDNRB, ENG, EPAS1, KDR, NRP1, RGS5, ROR2, VEGFC, VCAM1

Table 2.2A: Models of Recurrence-free Survival.

Variable	Univariate Model HR	Univariate Model *P*	Multivariate Model HR	Multivariate Model *P*	Final Model *P*
Subtype*	2.3	<.001	1.66	.02	.04
Age#	1.6	.01		.06	--
Stage$		.00			<.001
II	3.7	<.001	3.36	<.001	<.001
III/IV	5.2	<.001	4.12	<.001	<.001
Grade||		<.001			.003
3	1.8	.00		.31	.33
4	5.8	<.001	2.45	<.001	<.001

Table 2.3A: TCGA sample classification determined by PAM.

Sample ID	ccA Probability	ccB Probability	Subtype Classification
TCGA-DV-5575	9.98E-01	1.72E-03	ccA
TCGA-A3-3347	1.96E-13	1.00E+00	ccB
TCGA-A3-3349	9.38E-01	6.20E-02	ccA
TCGA-A3-3382	3.92E-06	1.00E+00	ccB
TCGA-A3-3306	1.00E+00	4.22E-06	ccA
TCGA-A3-3307	1.00E+00	1.16E-10	ccA
TCGA-A3-3308	4.23E-07	1.00E+00	ccB
TCGA-A3-3311	4.09E-04	1.00E+00	ccB
TCGA-A3-3313	1.05E-02	9.90E-01	ccB
TCGA-A3-3316	1.07E-10	1.00E+00	ccB
TCGA-A3-3317	2.52E-06	1.00E+00	ccB
TCGA-A3-3319	9.61E-09	1.00E+00	ccB
TCGA-A3-3320	1.00E+00	2.17E-11	ccA
TCGA-A3-3322	1.00E+00	3.97E-08	ccA
TCGA-A3-3323	1.06E-02	9.89E-01	ccB
TCGA-A3-3324	1.00E+00	2.62E-11	ccA
TCGA-A3-3325	1.00E+00	5.59E-06	ccA
TCGA-A3-3328	1.05E-03	9.99E-01	ccB
TCGA-A3-3329	1.00E+00	6.96E-10	ccA
TCGA-A3-3331	1.00E+00	1.09E-09	ccA
TCGA-A3-3335	7.85E-04	9.99E-01	ccB
TCGA-A3-3343	1.00E+00	7.68E-11	ccA
TCGA-A3-3351	1.00E+00	5.72E-05	ccA
TCGA-A3-3352	1.00E+00	4.83E-10	ccA
TCGA-A3-3357	1.00E+00	1.08E-06	ccA
TCGA-A3-3358	1.37E-04	1.00E+00	ccB
TCGA-A3-3359	1.00E+00	1.10E-10	ccA
TCGA-A3-3362	1.00E+00	1.28E-06	ccA
TCGA-A3-3363	3.75E-02	9.63E-01	ccB
TCGA-A3-3365	9.98E-01	1.90E-03	ccA
TCGA-A3-3367	1.00E+00	5.25E-08	ccA
TCGA-A3-3370	1.00E+00	4.47E-07	ccA
TCGA-A3-3372	1.00E+00	2.76E-09	ccA
TCGA-A3-3373	1.00E+00	8.69E-07	ccA
TCGA-A3-3374	3.78E-07	1.00E+00	ccB
TCGA-A3-3378	2.17E-07	1.00E+00	ccB
TCGA-A3-3380	1.00E+00	2.40E-06	ccA

TCGA-A3-3385	1.00E+00	9.32E-10	ccA
TCGA-A3-3387	1.61E-10	1.00E+00	ccB
TCGA-AK-3426	2.28E-11	1.00E+00	ccB
TCGA-AK-3427	2.15E-02	9.79E-01	ccB
TCGA-AK-3428	1.00E+00	4.65E-04	ccA
TCGA-AK-3429	1.00E+00	6.79E-09	ccA
TCGA-AK-3431	1.34E-05	1.00E+00	ccB
TCGA-AK-3433	8.04E-04	9.99E-01	ccB
TCGA-AK-3434	1.00E+00	1.61E-07	ccA
TCGA-AK-3440	1.35E-06	1.00E+00	ccB
TCGA-AK-3443	8.14E-04	9.99E-01	ccB
TCGA-AK-3445	8.67E-10	1.00E+00	ccB
TCGA-AK-3450	1.00E+00	3.71E-04	ccA
TCGA-AK-3451	9.93E-01	7.37E-03	ccA
TCGA-AK-3453	9.15E-01	8.55E-02	ccA
TCGA-AK-3454	1.00E+00	1.26E-10	ccA
TCGA-AK-3455	1.00E+00	1.02E-05	ccA
TCGA-AK-3456	2.41E-04	1.00E+00	ccB
TCGA-AK-3458	1.00E+00	3.21E-05	ccA
TCGA-AK-3460	1.00E+00	2.46E-06	ccA
TCGA-AK-3461	3.57E-02	9.64E-01	ccB
TCGA-AK-3465	2.31E-05	1.00E+00	ccB
TCGA-AS-3777	4.69E-07	1.00E+00	ccB
TCGA-B0-4693	1.00E+00	4.89E-06	ccA
TCGA-B0-4694	6.59E-08	1.00E+00	ccB
TCGA-B0-4696	3.32E-07	1.00E+00	ccB
TCGA-B0-4698	3.62E-08	1.00E+00	ccB
TCGA-B0-4707	7.54E-08	1.00E+00	ccB
TCGA-B0-4713	3.65E-06	1.00E+00	ccB
TCGA-B0-4718	9.99E-01	1.12E-03	ccA
TCGA-B0-4810	7.07E-09	1.00E+00	ccB
TCGA-B0-4811	4.31E-01	5.69E-01	ccB
TCGA-B0-4813	1.09E-09	1.00E+00	ccB
TCGA-B0-4815	1.52E-13	1.00E+00	ccB
TCGA-B0-4816	9.85E-01	1.51E-02	ccA
TCGA-B0-4817	8.79E-08	1.00E+00	ccB
TCGA-B0-4818	1.00E+00	6.47E-10	ccA
TCGA-B0-4821	2.27E-09	1.00E+00	ccB
TCGA-B0-4823	7.28E-02	9.27E-01	ccB
TCGA-B0-4824	1.00E+00	5.52E-09	ccA

TCGA-B0-4827	2.91E-06	1.00E+00	ccB
TCGA-B0-4833	1.00E+00	3.41E-07	ccA
TCGA-B0-4834	2.58E-05	1.00E+00	ccB
TCGA-B0-4837	1.67E-07	1.00E+00	ccB
TCGA-B0-4838	1.00E+00	3.92E-07	ccA
TCGA-B0-4839	1.00E+00	5.50E-06	ccA
TCGA-B0-4842	3.14E-06	1.00E+00	ccB
TCGA-B0-4843	3.99E-08	1.00E+00	ccB
TCGA-B0-4848	9.94E-13	1.00E+00	ccB
TCGA-B0-4849	1.00E+00	1.30E-08	ccA
TCGA-B0-4852	1.00E+00	3.44E-05	ccA
TCGA-B0-4945	9.99E-01	5.53E-04	ccA
TCGA-B0-5075	3.07E-01	6.93E-01	ccB
TCGA-B0-5077	1.00E+00	5.66E-07	ccA
TCGA-B0-5081	1.19E-11	1.00E+00	ccB
TCGA-B0-5083	4.23E-08	1.00E+00	ccB
TCGA-B0-5085	1.00E+00	3.82E-10	ccA
TCGA-B0-5088	2.13E-06	1.00E+00	ccB
TCGA-B0-5095	1.98E-10	1.00E+00	ccB
TCGA-B0-5096	2.63E-12	1.00E+00	ccB
TCGA-B0-5097	2.51E-13	1.00E+00	ccB
TCGA-B0-5098	1.04E-07	1.00E+00	ccB
TCGA-B0-5099	1.00E+00	3.38E-08	ccA
TCGA-B0-5100	1.11E-09	1.00E+00	ccB
TCGA-B0-5102	1.00E+00	3.32E-04	ccA
TCGA-B0-5104	1.00E+00	1.22E-10	ccA
TCGA-B0-5106	1.00E+00	3.76E-08	ccA
TCGA-B0-5108	2.95E-09	1.00E+00	ccB
TCGA-B0-5109	7.79E-11	1.00E+00	ccB
TCGA-B0-5110	1.00E+00	5.36E-09	ccA
TCGA-B0-5113	1.00E+00	4.42E-08	ccA
TCGA-B0-5116	1.00E+00	1.14E-05	ccA
TCGA-B0-5117	2.03E-03	9.98E-01	ccB
TCGA-B0-5119	1.00E+00	3.18E-10	ccA
TCGA-B0-5120	9.15E-01	8.47E-02	ccA
TCGA-B0-5121	1.00E+00	2.64E-08	ccA
TCGA-B0-5399	9.84E-01	1.55E-02	ccA
TCGA-B0-5400	1.09E-07	1.00E+00	ccB
TCGA-B0-5402	1.00E+00	2.69E-07	ccA
TCGA-B0-5690	1.00E+00	2.83E-09	ccA

TCGA-B0-5691	1.24E-03	9.99E-01	ccB
TCGA-B0-5692	1.00E+00	9.34E-08	ccA
TCGA-B0-5693	1.00E+00	2.20E-09	ccA
TCGA-B0-5694	2.78E-02	9.72E-01	ccB
TCGA-B0-5695	1.00E+00	7.12E-12	ccA
TCGA-B0-5696	1.00E+00	8.42E-09	ccA
TCGA-B0-5697	2.95E-07	1.00E+00	ccB
TCGA-B0-5698	1.00E+00	8.88E-08	ccA
TCGA-B0-5699	1.00E+00	2.19E-08	ccA
TCGA-B0-5701	9.12E-04	9.99E-01	ccB
TCGA-B0-5703	1.00E+00	9.80E-08	ccA
TCGA-B0-5705	1.00E+00	3.01E-11	ccA
TCGA-B0-5706	2.24E-09	1.00E+00	ccB
TCGA-B0-5709	1.13E-08	1.00E+00	ccB
TCGA-B0-5710	1.00E+00	1.90E-07	ccA
TCGA-B0-5711	1.00E+00	9.26E-09	ccA
TCGA-B0-5713	1.00E+00	1.63E-10	ccA
TCGA-B0-5812	1.00E+00	2.59E-04	ccA
TCGA-B2-3923	6.02E-03	9.94E-01	ccB
TCGA-B2-3924	1.00E+00	1.23E-08	ccA
TCGA-B2-4098	4.11E-04	1.00E+00	ccB
TCGA-B2-4099	1.00E+00	4.01E-08	ccA
TCGA-B2-4101	1.00E+00	2.72E-04	ccA
TCGA-B2-4102	1.00E+00	6.06E-07	ccA
TCGA-B2-5633	6.78E-06	1.00E+00	ccB
TCGA-B2-5635	1.00E+00	4.31E-06	ccA
TCGA-B2-5636	9.53E-10	1.00E+00	ccB
TCGA-B2-5641	4.04E-03	9.96E-01	ccB
TCGA-B4-5378	3.87E-08	1.00E+00	ccB
TCGA-B4-5832	1.28E-06	1.00E+00	ccB
TCGA-B4-5834	1.00E+00	2.34E-09	ccA
TCGA-B4-5835	8.80E-03	9.91E-01	ccB
TCGA-B4-5836	1.00E+00	9.62E-08	ccA
TCGA-B4-5838	1.19E-04	1.00E+00	ccB
TCGA-B4-5843	9.69E-01	3.14E-02	ccA
TCGA-B4-5844	1.00E+00	4.50E-10	ccA
TCGA-B8-4146	1.00E+00	5.46E-07	ccA
TCGA-B8-4148	1.00E+00	6.52E-09	ccA
TCGA-B8-4151	1.00E+00	4.23E-13	ccA
TCGA-B8-4153	1.00E+00	3.87E-11	ccA

TCGA-B8-4154	1.00E+00	4.24E-08	ccA
TCGA-B8-4619	1.31E-07	1.00E+00	ccB
TCGA-B8-4620	2.58E-05	1.00E+00	ccB
TCGA-B8-4621	2.55E-03	9.97E-01	ccB
TCGA-B8-5158	7.03E-11	1.00E+00	ccB
TCGA-B8-5159	9.99E-01	7.33E-04	ccA
TCGA-B8-5163	2.39E-12	1.00E+00	ccB
TCGA-B8-5164	1.00E+00	3.26E-06	ccA
TCGA-B8-5165	9.19E-01	8.14E-02	ccA
TCGA-B8-5545	1.38E-08	1.00E+00	ccB
TCGA-B8-5546	5.31E-02	9.47E-01	ccB
TCGA-B8-5549	9.99E-01	1.16E-03	ccA
TCGA-B8-5550	2.18E-06	1.00E+00	ccB
TCGA-B8-5551	2.38E-11	1.00E+00	ccB
TCGA-B8-5552	4.14E-03	9.96E-01	ccB
TCGA-B8-5553	1.00E+00	1.25E-05	ccA
TCGA-BP-4158	1.00E+00	8.72E-11	ccA
TCGA-BP-4159	9.99E-01	1.07E-03	ccA
TCGA-BP-4160	8.68E-01	1.32E-01	ccA
TCGA-BP-4161	4.06E-01	5.94E-01	ccB
TCGA-BP-4162	1.00E+00	8.63E-07	ccA
TCGA-BP-4163	4.72E-09	1.00E+00	ccB
TCGA-BP-4164	1.00E+00	8.58E-10	ccA
TCGA-BP-4165	1.00E+00	2.33E-09	ccA
TCGA-BP-4166	1.00E+00	4.94E-06	ccA
TCGA-BP-4167	5.59E-11	1.00E+00	ccB
TCGA-BP-4169	9.68E-09	1.00E+00	ccB
TCGA-BP-4170	1.00E+00	3.81E-09	ccA
TCGA-BP-4173	1.14E-08	1.00E+00	ccB
TCGA-BP-4174	1.00E+00	2.33E-05	ccA
TCGA-BP-4176	2.63E-09	1.00E+00	ccB
TCGA-BP-4177	2.94E-08	1.00E+00	ccB
TCGA-BP-4325	1.00E+00	2.72E-10	ccA
TCGA-BP-4326	9.65E-09	1.00E+00	ccB
TCGA-BP-4327	1.00E+00	9.32E-06	ccA
TCGA-BP-4329	8.31E-01	1.69E-01	ccA
TCGA-BP-4330	9.93E-01	7.08E-03	ccA
TCGA-BP-4332	1.00E+00	2.40E-05	ccA
TCGA-BP-4334	1.65E-05	1.00E+00	ccB
TCGA-BP-4337	1.27E-07	1.00E+00	ccB

TCGA-BP-4338	3.07E-11	1.00E+00	ccB
TCGA-BP-4340	1.00E+00	5.21E-10	ccA
TCGA-BP-4341	1.00E+00	9.48E-09	ccA
TCGA-BP-4343	1.93E-08	1.00E+00	ccB
TCGA-BP-4345	5.04E-10	1.00E+00	ccB
TCGA-BP-4346	2.47E-05	1.00E+00	ccB
TCGA-BP-4347	1.00E+00	7.47E-10	ccA
TCGA-BP-4349	1.00E+00	7.59E-09	ccA
TCGA-BP-4351	1.17E-04	1.00E+00	ccB
TCGA-BP-4355	9.98E-01	2.32E-03	ccA
TCGA-BP-4756	1.90E-02	9.81E-01	ccB
TCGA-BP-4758	1.00E+00	2.27E-07	ccA
TCGA-BP-4759	1.00E+00	1.65E-04	ccA
TCGA-BP-4760	5.28E-11	1.00E+00	ccB
TCGA-BP-4761	1.14E-09	1.00E+00	ccB
TCGA-BP-4762	7.14E-06	1.00E+00	ccB
TCGA-BP-4763	4.78E-06	1.00E+00	ccB
TCGA-BP-4765	9.71E-01	2.93E-02	ccA
TCGA-BP-4766	1.00E+00	4.81E-10	ccA
TCGA-BP-4768	1.00E+00	8.72E-07	ccA
TCGA-BP-4769	8.92E-10	1.00E+00	ccB
TCGA-BP-4770	1.32E-08	1.00E+00	ccB
TCGA-BP-4774	1.00E+00	2.96E-11	ccA
TCGA-BP-4775	1.00E+00	9.99E-09	ccA
TCGA-BP-4777	1.00E+00	4.67E-04	ccA
TCGA-BP-4781	1.38E-08	1.00E+00	ccB
TCGA-BP-4782	1.25E-05	1.00E+00	ccB
TCGA-BP-4784	4.28E-11	1.00E+00	ccB
TCGA-BP-4789	1.00E+00	4.19E-04	ccA
TCGA-BP-4790	1.40E-07	1.00E+00	ccB
TCGA-BP-4795	1.82E-10	1.00E+00	ccB
TCGA-BP-4797	3.59E-09	1.00E+00	ccB
TCGA-BP-4799	1.91E-05	1.00E+00	ccB
TCGA-BP-4801	1.00E+00	4.28E-05	ccA
TCGA-BP-4803	1.00E+00	1.16E-04	ccA
TCGA-BP-4804	4.99E-11	1.00E+00	ccB
TCGA-BP-4807	9.99E-01	1.25E-03	ccA
TCGA-BP-4959	6.36E-01	3.64E-01	ccA
TCGA-BP-4960	1.05E-06	1.00E+00	ccB
TCGA-BP-4961	9.70E-01	3.01E-02	ccA

TCGA-BP-4962	2.91E-07	1.00E+00	ccB
TCGA-BP-4963	8.94E-01	1.06E-01	ccA
TCGA-BP-4964	8.29E-01	1.71E-01	ccA
TCGA-BP-4967	7.18E-03	9.93E-01	ccB
TCGA-BP-4968	1.00E+00	1.50E-08	ccA
TCGA-BP-4969	1.00E+00	8.14E-11	ccA
TCGA-BP-4970	1.91E-06	1.00E+00	ccB
TCGA-BP-4971	4.41E-07	1.00E+00	ccB
TCGA-BP-4972	1.00E+00	2.31E-04	ccA
TCGA-BP-4973	1.00E+00	1.07E-09	ccA
TCGA-BP-4975	1.00E+00	1.17E-06	ccA
TCGA-BP-4976	1.00E+00	1.75E-10	ccA
TCGA-BP-4977	9.23E-01	7.72E-02	ccA
TCGA-BP-4981	1.00E+00	3.83E-09	ccA
TCGA-BP-4982	1.00E+00	1.08E-05	ccA
TCGA-BP-4983	1.91E-11	1.00E+00	ccB
TCGA-BP-4985	2.23E-11	1.00E+00	ccB
TCGA-BP-4987	1.00E+00	1.00E-10	ccA
TCGA-BP-4988	4.45E-07	1.00E+00	ccB
TCGA-BP-4989	8.18E-03	9.92E-01	ccB
TCGA-BP-4991	1.00E+00	3.29E-06	ccA
TCGA-BP-4992	1.51E-03	9.98E-01	ccB
TCGA-BP-4993	9.99E-01	1.15E-03	ccA
TCGA-BP-4994	8.78E-02	9.12E-01	ccB
TCGA-BP-4995	9.72E-01	2.79E-02	ccA
TCGA-BP-4998	6.58E-08	1.00E+00	ccB
TCGA-BP-4999	1.00E+00	8.86E-09	ccA
TCGA-BP-5000	8.55E-06	1.00E+00	ccB
TCGA-BP-5001	1.00E+00	7.98E-09	ccA
TCGA-BP-5004	1.00E+00	5.64E-08	ccA
TCGA-BP-5006	1.00E+00	9.84E-10	ccA
TCGA-BP-5007	1.00E+00	6.39E-10	ccA
TCGA-BP-5008	1.03E-02	9.90E-01	ccB
TCGA-BP-5009	1.72E-07	1.00E+00	ccB
TCGA-BP-5010	9.95E-10	1.00E+00	ccB
TCGA-BP-5168	1.00E+00	1.20E-10	ccA
TCGA-BP-5169	3.27E-10	1.00E+00	ccB
TCGA-BP-5170	4.32E-06	1.00E+00	ccB
TCGA-BP-5173	1.00E+00	9.98E-06	ccA
TCGA-BP-5174	1.00E+00	7.51E-05	ccA

TCGA-BP-5175	8.67E-07	1.00E+00	ccB
TCGA-BP-5176	1.00E+00	1.03E-09	ccA
TCGA-BP-5177	9.99E-01	9.35E-04	ccA
TCGA-BP-5180	5.22E-01	4.78E-01	ccA
TCGA-BP-5181	1.00E+00	6.48E-11	ccA
TCGA-BP-5182	9.01E-08	1.00E+00	ccB
TCGA-BP-5183	1.00E+00	4.02E-04	ccA
TCGA-BP-5187	8.32E-01	1.68E-01	ccA
TCGA-BP-5189	2.62E-07	1.00E+00	ccB
TCGA-BP-5190	1.00E+00	1.07E-06	ccA
TCGA-BP-5191	9.92E-08	1.00E+00	ccB
TCGA-BP-5192	1.00E+00	1.89E-11	ccA
TCGA-BP-5194	1.00E+00	2.06E-07	ccA
TCGA-BP-5195	8.54E-01	1.46E-01	ccA
TCGA-BP-5196	2.65E-10	1.00E+00	ccB
TCGA-BP-5198	6.13E-13	1.00E+00	ccB
TCGA-BP-5199	1.14E-07	1.00E+00	ccB
TCGA-BP-5200	1.00E+00	5.64E-08	ccA
TCGA-BP-5202	1.00E+00	1.77E-10	ccA
TCGA-CJ-4634	1.00E+00	5.42E-12	ccA
TCGA-CJ-4635	9.96E-01	4.22E-03	ccA
TCGA-CJ-4636	1.03E-04	1.00E+00	ccB
TCGA-CJ-4639	1.00E+00	1.68E-09	ccA
TCGA-CJ-4640	3.95E-02	9.61E-01	ccB
TCGA-CJ-4643	1.00E+00	1.31E-10	ccA
TCGA-CJ-4869	2.02E-07	1.00E+00	ccB
TCGA-CJ-4872	1.92E-05	1.00E+00	ccB
TCGA-CJ-4873	1.50E-07	1.00E+00	ccB
TCGA-CJ-4874	1.00E+00	2.08E-10	ccA
TCGA-CJ-4876	5.23E-01	4.77E-01	ccA
TCGA-CJ-4878	1.00E+00	1.90E-04	ccA
TCGA-CJ-4881	1.90E-09	1.00E+00	ccB
TCGA-CJ-4882	2.23E-10	1.00E+00	ccB
TCGA-CJ-4884	3.30E-01	6.70E-01	ccB
TCGA-CJ-4886	1.00E+00	2.07E-06	ccA
TCGA-CJ-4889	1.56E-06	1.00E+00	ccB
TCGA-CJ-4891	3.09E-09	1.00E+00	ccB
TCGA-CJ-4892	1.00E+00	2.84E-09	ccA
TCGA-CJ-4893	1.00E+00	4.41E-08	ccA
TCGA-CJ-4894	9.91E-01	9.14E-03	ccA

TCGA-CJ-4897	1.00E+00	1.19E-09	ccA
TCGA-CJ-4899	5.75E-04	9.99E-01	ccB
TCGA-CJ-4901	1.87E-11	1.00E+00	ccB
TCGA-CJ-4902	7.72E-07	1.00E+00	ccB
TCGA-CJ-4903	1.00E+00	2.29E-06	ccA
TCGA-CJ-4905	1.00E+00	1.93E-09	ccA
TCGA-CJ-4907	2.95E-03	9.97E-01	ccB
TCGA-CJ-4908	8.59E-02	9.14E-01	ccB
TCGA-CJ-4912	3.50E-02	9.65E-01	ccB
TCGA-CJ-4916	1.00E+00	9.26E-07	ccA
TCGA-CJ-4920	9.53E-08	1.00E+00	ccB
TCGA-CJ-5671	1.08E-10	1.00E+00	ccB
TCGA-CJ-5672	9.46E-01	5.44E-02	ccA
TCGA-CJ-5675	1.00E+00	3.77E-07	ccA
TCGA-CJ-5676	2.99E-06	1.00E+00	ccB
TCGA-CJ-5679	1.32E-08	1.00E+00	ccB
TCGA-CJ-5683	1.00E+00	1.85E-09	ccA
TCGA-CJ-5684	1.00E+00	7.67E-08	ccA
TCGA-CJ-5686	6.50E-01	3.50E-01	ccA
TCGA-CJ-5689	1.65E-04	1.00E+00	ccB
TCGA-CJ-6027	5.63E-10	1.00E+00	ccB
TCGA-CJ-6030	4.37E-07	1.00E+00	ccB
TCGA-CJ-6031	2.17E-11	1.00E+00	ccB
TCGA-CJ-6032	1.00E+00	9.40E-10	ccA
TCGA-CW-5581	1.00E+00	1.41E-07	ccA
TCGA-CW-5583	1.00E+00	2.95E-06	ccA
TCGA-CW-5584	1.00E+00	1.87E-06	ccA
TCGA-CW-5587	1.00E+00	2.70E-06	ccA
TCGA-CW-5589	1.00E+00	1.34E-06	ccA
TCGA-CW-6088	1.00E+00	1.26E-08	ccA
TCGA-CW-6090	1.00E+00	9.89E-05	ccA
TCGA-CW-6093	1.00E+00	5.34E-09	ccA
TCGA-CW-6097	1.05E-12	1.00E+00	ccB
TCGA-CZ-4853	1.00E+00	2.49E-09	ccA
TCGA-CZ-4854	3.69E-11	1.00E+00	ccB
TCGA-CZ-4856	1.00E+00	2.94E-07	ccA
TCGA-CZ-4858	3.84E-11	1.00E+00	ccB
TCGA-CZ-4859	1.00E+00	3.69E-11	ccA
TCGA-CZ-4862	2.13E-04	1.00E+00	ccB
TCGA-CZ-4863	1.00E+00	8.64E-06	ccA

TCGA-CZ-4864	1.00E+00	1.02E-09	ccA
TCGA-CZ-4866	9.99E-01	1.42E-03	ccA
TCGA-CZ-5452	8.37E-01	1.63E-01	ccA
TCGA-CZ-5453	1.00E+00	3.47E-12	ccA
TCGA-CZ-5457	1.00E+00	1.73E-09	ccA
TCGA-CZ-5458	6.02E-01	3.98E-01	ccA
TCGA-CZ-5463	1.00E+00	9.60E-10	ccA
TCGA-CZ-5465	1.00E+00	1.20E-09	ccA
TCGA-CZ-5467	1.00E+00	1.26E-08	ccA
TCGA-CZ-5469	4.50E-09	1.00E+00	ccB
TCGA-CZ-5470	9.21E-01	7.90E-02	ccA
TCGA-CZ-5982	1.00E+00	1.88E-08	ccA
TCGA-CZ-5984	3.70E-11	1.00E+00	ccB
TCGA-CZ-5985	1.48E-02	9.85E-01	ccB
TCGA-CZ-5986	1.00E+00	5.49E-10	ccA
TCGA-CZ-5988	8.10E-08	1.00E+00	ccB
TCGA-CZ-5989	1.00E+00	7.98E-07	ccA
TCGA-DV-5565	6.59E-02	9.34E-01	ccB
TCGA-DV-5566	9.99E-01	7.05E-04	ccA
TCGA-DV-5567	7.58E-10	1.00E+00	ccB
TCGA-DV-5569	4.36E-01	5.64E-01	ccB
TCGA-DV-5574	2.17E-09	1.00E+00	ccB
TCGA-DV-5576	6.37E-09	1.00E+00	ccB

Table 2.4A: PAM classification of Clinical cohort.

Sample ID	ccA Probability	ccB Probability	Subtype Classification
57	2.05E-01	7.95E-01	ccB
45	5.22E-01	4.78E-01	ccA
71	6.18E-01	3.82E-01	ccA
163	6.08E-01	3.92E-01	ccA
197	6.56E-01	3.44E-01	ccA
219	7.43E-01	2.57E-01	ccA
247	4.21E-01	5.79E-01	ccB
601	1.47E-01	8.53E-01	ccB
578	4.39E-01	5.61E-01	ccB
641	2.33E-01	7.67E-01	ccB
787	6.92E-01	3.08E-01	ccA
625	1.37E-01	8.63E-01	ccB
94	7.55E-01	2.45E-01	ccA
62	5.34E-01	4.66E-01	ccA
266	2.35E-01	7.65E-01	ccB
485	3.38E-01	6.62E-01	ccB
737	5.37E-01	4.63E-01	ccA
753	3.19E-01	6.81E-01	ccB
138	7.95E-01	2.05E-01	ccA
570	6.85E-01	3.15E-01	ccA
581	7.14E-01	2.86E-01	ccA
785	8.16E-02	9.18E-01	ccB
642	7.67E-02	9.23E-01	ccB
244	1.88E-01	8.12E-01	ccB
743	7.18E-01	2.82E-01	ccA
296	8.74E-02	9.13E-01	ccB
311	1.40E-01	8.60E-01	ccB
436	1.16E-01	8.84E-01	ccB
49	5.46E-08	1.00E+00	ccB
87	3.04E-06	1.00E+00	ccB
187	1.48E-04	1.00E+00	ccB
209	9.99E-01	1.38E-03	ccA
282	9.99E-01	6.16E-04	ccA
358	1.83E-05	1.00E+00	ccB
431	1.66E-06	1.00E+00	ccB
47	3.57E-07	1.00E+00	ccB
48	4.26E-06	1.00E+00	ccB

59	9.70E-04	9.99E-01	ccB
76	9.98E-01	1.72E-03	ccA
88	5.69E-02	9.43E-01	ccB
92	9.47E-01	5.29E-02	ccA
128	6.16E-02	9.38E-01	ccB
143	4.47E-05	1.00E+00	ccB
160	1.36E-04	1.00E+00	ccB
162	8.20E-08	1.00E+00	ccB
173	1.94E-02	9.81E-01	ccB
181	1.72E-02	9.83E-01	ccB
186	1.76E-02	9.82E-01	ccB
191	1.82E-04	1.00E+00	ccB
201	9.99E-01	6.30E-04	ccA
250	9.62E-01	3.76E-02	ccA
258	9.97E-01	2.86E-03	ccA
260	9.28E-01	7.20E-02	ccA
280	9.74E-01	2.58E-02	ccA
486	8.51E-01	1.49E-01	ccA
494	9.86E-01	1.40E-02	ccA
549	3.12E-03	9.97E-01	ccB
559	9.38E-01	6.16E-02	ccA
560	9.32E-05	1.00E+00	ccB
561	9.99E-01	1.16E-03	ccA
571	1.00E+00	9.98E-05	ccA
576	9.74E-01	2.59E-02	ccA
587	1.00E+00	3.54E-05	ccA
598	4.86E-03	9.95E-01	ccB
600	4.35E-03	9.96E-01	ccB
610	9.12E-01	8.77E-02	ccA
668	8.34E-01	1.66E-01	ccA
44	1.80E-03	9.98E-01	ccB
63	1.49E-06	1.00E+00	ccB
64	9.98E-01	2.37E-03	ccA
83	1.98E-04	1.00E+00	ccB
104	9.98E-01	2.34E-03	ccA
127	9.14E-03	9.91E-01	ccB
144	9.95E-01	4.55E-03	ccA
145	9.92E-01	7.70E-03	ccA
150	1.08E-02	9.89E-01	ccB
154	8.78E-01	1.22E-01	ccA

188	9.61E-01	3.94E-02	ccA
193	8.70E-04	9.99E-01	ccB
286	9.09E-01	9.07E-02	ccA
287	1.00E+00	1.47E-04	ccA
301	9.98E-01	2.21E-03	ccA
318	9.77E-01	2.33E-02	ccA
408	1.00E+00	7.71E-05	ccA
428	9.57E-01	4.32E-02	ccA
487	1.00E+00	2.67E-05	ccA
512	9.99E-01	5.32E-04	ccA
537	9.83E-01	1.73E-02	ccA
579	9.98E-01	1.81E-03	ccA
586	9.99E-01	9.34E-04	ccA
591	9.03E-01	9.71E-02	ccA
657	9.98E-01	1.60E-03	ccA
704	3.66E-02	9.63E-01	ccB
788	9.82E-01	1.81E-02	ccA
840	9.94E-01	6.32E-03	ccA
75	9.85E-01	1.54E-02	ccA
77	9.83E-01	1.71E-02	ccA
99	1.00E+00	4.89E-04	ccA
158	5.85E-04	9.99E-01	ccB
109	9.04E-02	9.10E-01	ccB
147	5.91E-04	9.99E-01	ccB
149	1.38E-03	9.99E-01	ccB
185	3.54E-07	1.00E+00	ccB
223	9.12E-01	8.80E-02	ccA
228	4.11E-02	9.59E-01	ccB
252	4.21E-04	1.00E+00	ccB
279	2.48E-06	1.00E+00	ccB
455	1.27E-03	9.99E-01	ccB
461	4.90E-06	1.00E+00	ccB
509	1.00E+00	2.59E-06	ccA
569	6.81E-04	9.99E-01	ccB
607	1.00E+00	2.23E-04	ccA
644	4.26E-06	1.00E+00	ccB
794	5.73E-06	1.00E+00	ccB
823	9.99E-01	7.19E-04	ccA
227	2.25E-02	9.78E-01	ccB
433	9.99E-01	7.22E-04	ccA

440	1.00E+00	1.67E-05	ccA
550	4.21E-02	9.58E-01	ccB
566	9.99E-01	1.44E-03	ccA
758	8.46E-08	1.00E+00	ccB
40	4.64E-07	1.00E+00	ccB
74	9.08E-07	1.00E+00	ccB
112	1.85E-07	1.00E+00	ccB
165	1.02E-03	9.99E-01	ccB
167	6.92E-08	1.00E+00	ccB
189	5.17E-05	1.00E+00	ccB
249	2.26E-07	1.00E+00	ccB
261	1.00E+00	4.93E-04	ccA
274	3.40E-05	1.00E+00	ccB
292	1.66E-04	1.00E+00	ccB
337	4.45E-04	1.00E+00	ccB
357	9.40E-07	1.00E+00	ccB
366	1.55E-05	1.00E+00	ccB
370	2.30E-05	1.00E+00	ccB
395	8.54E-05	1.00E+00	ccB
396	1.22E-03	9.99E-01	ccB
398	6.01E-02	9.40E-01	ccB
427	1.85E-03	9.98E-01	ccB
463	1.92E-07	1.00E+00	ccB
466	8.85E-08	1.00E+00	ccB
478	3.14E-06	1.00E+00	ccB
490	1.43E-04	1.00E+00	ccB
499	5.46E-04	9.99E-01	ccB
515	2.02E-02	9.80E-01	ccB
544	7.48E-06	1.00E+00	ccB
562	9.35E-01	6.55E-02	ccA
584	9.99E-01	9.22E-04	ccA
620	1.00E+00	2.31E-04	ccA
623	2.82E-05	1.00E+00	ccB
661	4.55E-04	1.00E+00	ccB
687	1.00E+00	2.89E-04	ccA
719	1.00E+00	4.00E-04	ccA
763	2.02E-05	1.00E+00	ccB
779	9.99E-01	7.72E-04	ccA
815	1.00E+00	7.27E-07	ccA
126	6.95E-03	9.93E-01	ccB

242	9.75E-03	9.90E-01	ccB
413	7.87E-05	1.00E+00	ccB
439	1.35E-03	9.99E-01	ccB
452	6.11E-07	1.00E+00	ccB
630	1.27E-02	9.87E-01	ccB
183	4.68E-06	1.00E+00	ccB
541	8.95E-01	1.05E-01	ccA
297	8.86E-06	1.00E+00	ccB
693	5.59E-07	1.00E+00	ccB

Chapter 3

Basic MR/PET physics

In PET imaging, a radiotracer compound labeled with a positron emitting radionuclide, e.g. ^{18}F-FDG, is injected into the patient. The radiotracer decays by emitting a positron, which annihilates with an electron. The annihilation produces two 511 KeV photons traveling in opposite directions along a straight line. The PET scintillation detectors surrounding the patient as coincidence events, which, subsequently, are reconstructed as tomographic images, may detect these photons. PET images show the tracer distribution in the tissue. MR imaging relies on an interaction between magnetic field and magnetic moment of protons. Radio-frequency pulses are usually applied to alter magnetization to create magnetic flux that induces electrical current, aka MR signal, in MR receiving coils. MRI can provide high-resolution anatomical images with excellent soft tissue contrast, which complement the high sensitivity of PET imaging in detecting physiological and molecular process of biological systems. In addition to the structural information, MR can also provide physiological, functional and metabolic information using novel MR Blood oxygenation level dependent (BOLD), functional MRI, MR perfusion, Diffusion Tensor Imaging (DTI), MR spectroscopy/chemical shift imaging techniques. More importantly, MR does not impose a risk of ionizing radiation to patients.

MR/PET mechanism

MR-PET, developed over the past 5 years, is a new tool for identifying and staging cancer treatment. Similar to CT-PET, functional images are superimposed over static images. MR-PET has been reported feasible in several small populations (Czerin). In retrospective studies, MR-PET was equal in diagnostic accuracy to CT-PET (Czerin). MR-

PET in has been reported superior to CT-PET in identification of liver metastases, malignant bone lesions and accurate assessment of T stage in a mixed tumor population[41, 159, 160]. Diffusion imaging was reported as particularly valuable. Large prospective studies have not yet been performed. MR-PET is of particular value in children and young women to avoid ionizing radiation.

PET images are obtained simultaneously or in adjacent scanners and fused during a single imaging session. Multiple pulse sequences and imaging planes in tandem with Gd chelates and PET tracers provide excellent anatomic and functional imaging in the brain and pelvis. Fusion of ultra-fast MR sequences and PET images obtained during quiet breathing can be problematic in abdomen although less so in the retroperitoneum.

Table 3.1A: Demographics of patients used in MRI/PET-FDG study.

Sample Name	Tumor Size (cm)	Grade	Stage	Number of primary sites	Number of metastatic sites
Patient 1	8.6	2	II	5	NA
Patient 2	8.9	2	II	3	NA
Patient 3	8	3	IV	2	4
Patient 4	3.5	2	I	2	NA
Patient 5	3.6	2	I	2	NA
Patient 6	4.2	3	III	6	NA
Patient 7	6.3	2	I	4	NA
Patient 8	17	4	IV	4	4

Table 3.2A Standard uptake values (SUV) and ccRCC subtype classifications for MR/PET-FDG samples.

Sample Name	Tumor Site	Tumor Mean (SUV)	Max SUV	Subtype
Patient 1		2.33		
	Site 1		2.3	ccA
	Site 2		2.4	ccA
	Site 3		2.8	ccA
	Site 4		2.8	ccA
	Site 5		2.5	ccB
Patient 2		2.26		
	Site 1		4	ccB
	Site 2		2.6	ccA
	Site 3		2.2	ccA
Patient 3		1.27		
	Site 1		3	ccA
	Site 2		3.5	ccA
	Met 1		3.5	ccB
	Met 2		3.3	ccB
	Met 3		3	ccA
	Met 4		2.8	ccB
Patient 4		1.79		
	Site 1		3	ccA
	Site 2		2.8	ccA
Patient 5		1.4		
	Site 1		2.3	ccA
	Site 2		1.8	ccA
Patient 6		2.17		
	Site 1		2.6	ccB
	Site 2		2.8	ccB
	Site 3		3.2	ccB
	Site 4		3.5	ccB
	Site 5		2.7	ccB
	Site 6		2.3	ccB
Patient 7		2.48		
	Site 1		3.4	ccB
	Site 2		2.9	ccA
	Site 3		3	ccB
	Site 4		3.2	ccB
Patient 8		4.87		
	Site 1		6.4	ccB
	Site 2		6.2	ccB
	Site 3		5.2	ccB
	Site 4		6.2	ccB
	Met 1		NA	ccB
	Met 2		NA	ccB
	Met 3		NA	ccB
	Met 4		NA	ccB

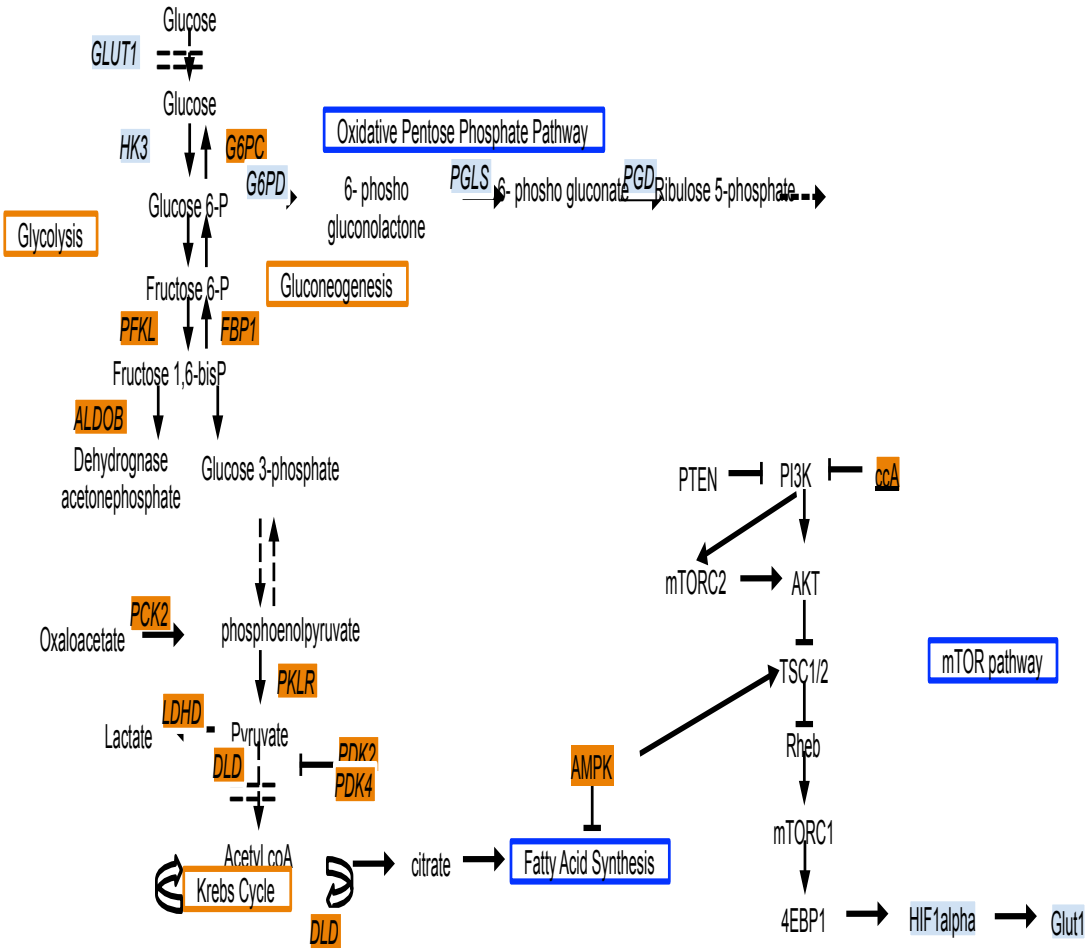

Figure 3.1A: Clear cell A and B subtypes obtain energy through distinct metabolic pathways. Clear cell A (orange)-typed samples tend to produce energy through glycolysis and the Krebs Cycle, while ccB samples (blue) enhance fatty acid synthesis and increase activity of the oxidative pentose phosphate pathway, shutting down glycogen synthesis to support enhanced metabolism. Genes highlighted in orange are significantly higher (p-value<0.05) in samples classified as ccA and those in blue are higher in ccB samples.

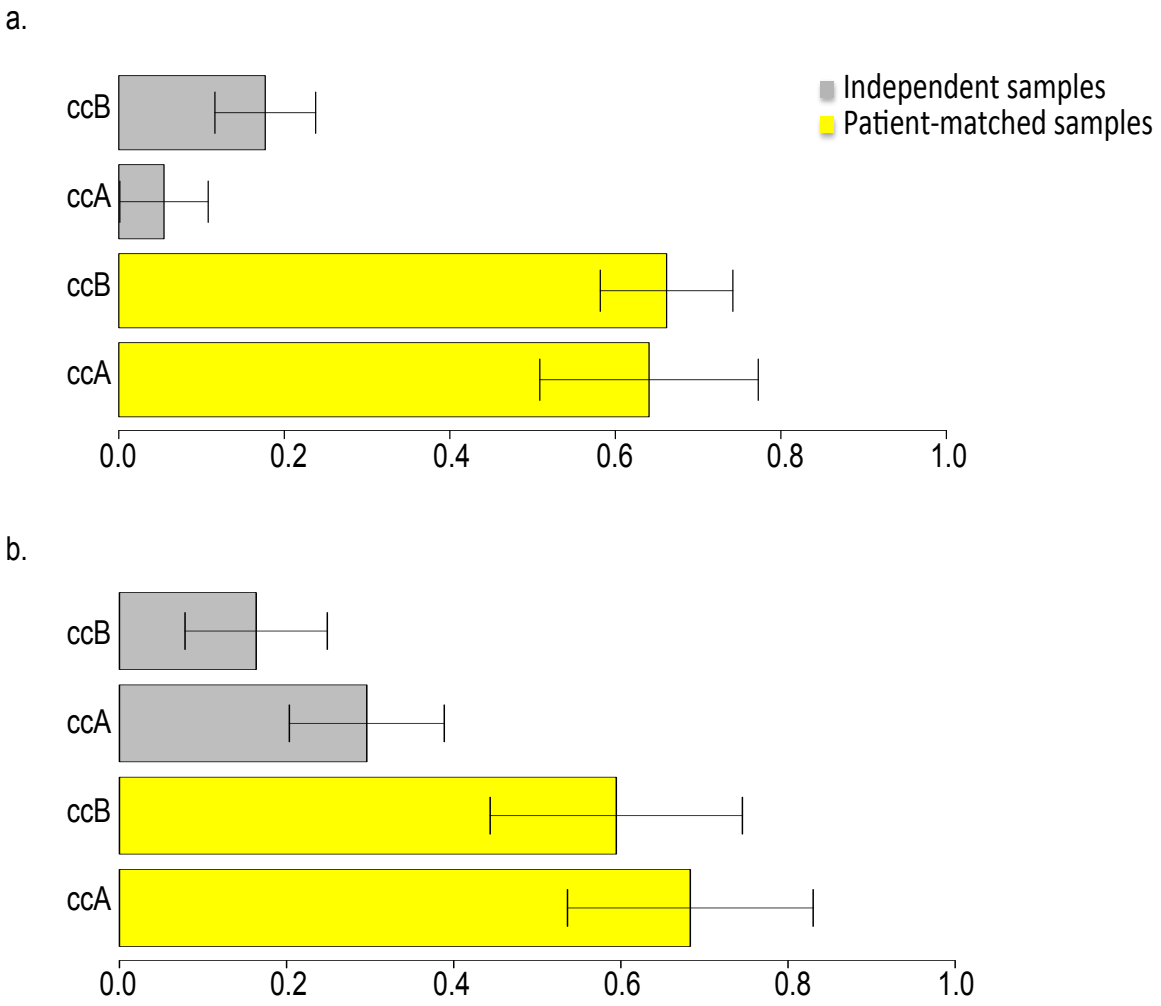

Figure 3.2A: ccRCC subtypes have intra-tumor genomic similarities.
Intra-class correlation analysis, with 95% confidence intervals, was performed on samples biopsied from eight ccRCC patients. a, Expression profiles of all expressed genes from microarray analysis were more similar among ccA and ccB-typed samples from the same patient (yellow) compared to those from individuals (grey). b, Similar to expression profiles including all genes, profiles of the 34-gene subtype classifier used to assign ccA/ccB classification, ClearCode34, exhibited stronger concordance with identically typed samples from the same tumor compared to those between different patients, suggesting core gene expression profiles are evident even in the presence of tumor heterogeneity.

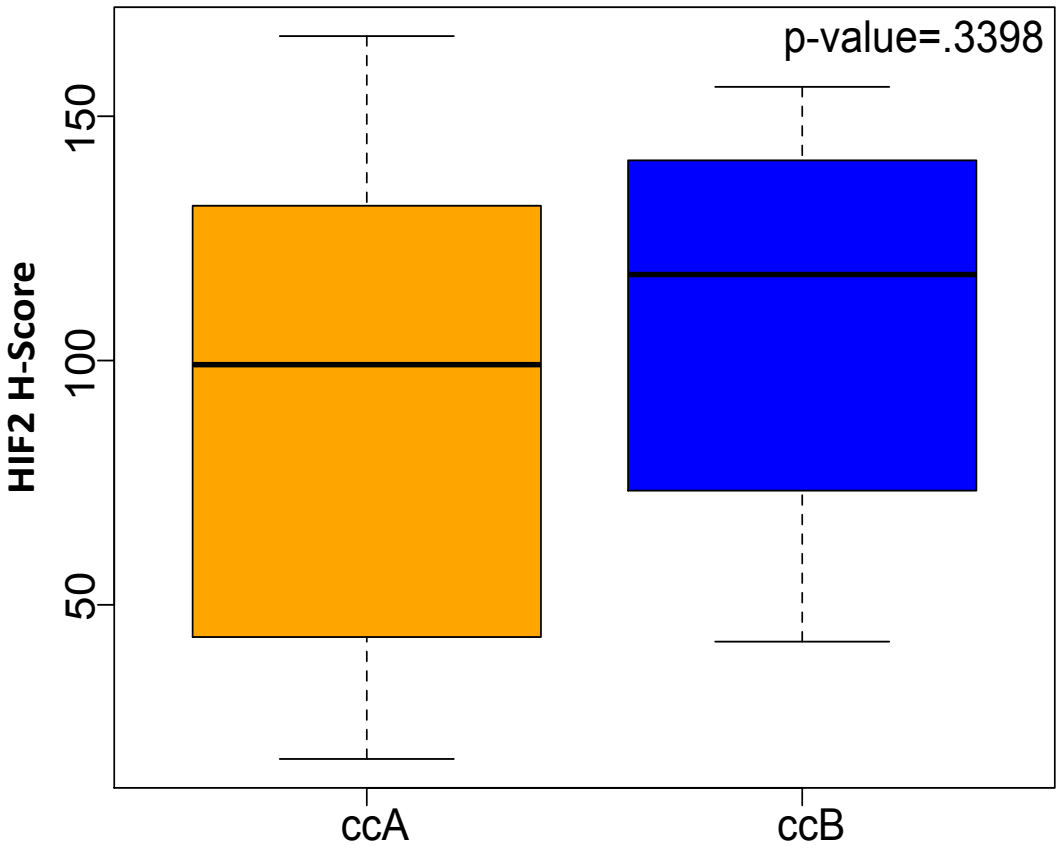

Figure 3.3A: HIF2 expression in ccA and ccB-typed samples.
Samples of the ccA and ccB subtype express similar HIF2 protein levels compared to higher HIF1 protein expression in ccB samples (Figure 2d).

REFERENCES

1. Khandani AH, Cowey CL, Moore DT, Gohil H, Rathmell WK. Primary renal cell carcinoma: relationship between 18F-FDG uptake and response to neoadjuvant sorafenib. Nucl Med Commun. 2012;33(9):967-73. Epub 2012/06/21. doi: 10.1097/MNM.0b013e3283561837. PubMed PMID: 22714005.

2. Powles T, Blank C, Chowdhury S, Horenblas S, Peters J, Shamash J, et al. The outcome of patients treated with sunitinib prior to planned nephrectomy in metastatic clear cell renal cancer. European Urology. 2011;60(3):448-54. Epub 2011/05/27. doi: 10.1016/j.eururo.2011.05.028. PubMed PMID: 21612860.

3. Cancer facts and figures 2015. American Cancer Society. 2015.

4. Arjumand W, Sultana S. Role of VHL gene mutation in human renal cell carcinoma. Tumour Biol. 2012;33(1):9-16. Epub 2011/11/30. doi: 10.1007/s13277-011-0257-3. PubMed PMID: 22125026.

5. Haase VH. Renal cancer: oxygen meets metabolism. Exp Cell Res. 2012;318(9):1057-67. Epub 2012/03/13. doi: 10.1016/j.yexcr.2012.02.026. PubMed PMID: 22406000; PubMed Central PMCID: PMC3334413.

6. Heng DY, Xie W, Regan MM, Warren MA, Golshayan AR, Sahi C, et al. Prognostic factors for overall survival in patients with metastatic renal cell carcinoma treated with vascular endothelial growth factor-targeted agents: results from a large, multicenter study. J Clin Oncol. 2009;27(34):5794-9. Epub 2009/10/15. doi: 10.1200/JCO.2008.21.4809. PubMed PMID: 19826129.

7. Brooks SA, Brannon AR, Parker JS, Fisher JC, Sen O, Kattan MW, et al. ClearCode34: A prognostic risk predictor for localized clear cell renal cell carcinoma. European Urology. 2014;66(1):77-84. Epub 2014/03/13. doi: 10.1016/j.eururo.2014.02.035. PubMed PMID: 24613583; PubMed Central PMCID: PMC4058355.

8. Keefe SM, Nathanson KL, Rathmell WK. The molecular biology of renal cell carcinoma. Semin Oncol. 2013;40(4):421-8. Epub 2013/08/27. doi: 10.1053/j.seminoncol.2013.05.006. PubMed PMID: 23972705.

9. Volpe A, Patard JJ. Prognostic factors in renal cell carcinoma. World Journal of Urology. 2010;28(3):319-27. doi: 10.1007/s00345-010-0540-8.

10. Brooks SA, Rathmell WK. Uniting Molecular Biomarkers to Advance the Science and Care of Clear Cell Renal Cell Carcinoma. The Journal of OncoPathology. 2014;1(4):45-54. doi: 10.13032/tjop.2052-5931.100053.

11. Oosterwijk E, Rathmell WK, Junker K, Brannon AR, Pouliot F, Finley DS, et al. Basic research in kidney cancer. European Urology. 2011;60(4):622-33. Epub 2011/07/12. doi: 10.1016/j.eururo.2011.06.048. PubMed PMID: 21741760.

12. Jonasch E, Futreal PA, Davis IJ, Bailey ST, Kim WY, Brugarolas J, et al. State of the Science: An Update on Renal Cell Carcinoma. Mol Cancer Res. 2012. Epub 2012/05/29. doi: 10.1158/1541-7786.MCR-12-0117. PubMed PMID: 22638109.

13. Brannon AR, Haake SM, Hacker KE, Pruthi RS, Wallen EM, Nielsen ME, et al. Meta-analysis of Clear Cell Renal Cell Carcinoma Gene Expression Defines a Variant Subgroup and Identifies Gender Influences on Tumor Biology. European Urology. 2012;61(2):258-68. doi: 10.1016/j.eururo.2011.10.007.

14. Brannon AR, Reddy A, Seiler M, Arreola A, Moore DT, Pruthi RS, et al. Molecular Stratification of Clear Cell Renal Cell Carcinoma by Consensus Clustering Reveals Distinct Subtypes and Survival Patterns. Genes & Cancer. 2010;1(2):152-63. doi: 10.1177/1947601909359929.

15. Network TCGR. Comprehensive molecular characterization of clear cell renal cell carcinoma. Nature. 2013;499(7456):43-9. Epub 2013/06/25. doi: 10.1038/nature12222. PubMed PMID: 23792563; PubMed Central PMCID: PMC3771322.

16. Latif F, Tory K, Gnarra J, Yao M, Duh FM, Orcutt ML, et al. Identification of the von Hippel-Lindau disease tumor suppressor gene. Science. 1993;260(5112):1317-20. Epub 1993/05/28. PubMed PMID: 8493574.

17. Nickerson ML, Jaeger E, Shi Y, Durocher JA, Mahurkar S, Zaridze D, et al. Improved identification of von Hippel-Lindau gene alterations in clear cell renal tumors. Clin Cancer Res. 2008;14(15):4726-34. Epub 2008/08/05. doi: 10.1158/1078-0432.CCR-07-4921. PubMed PMID: 18676741; PubMed Central PMCID: PMC2629664.

18. Pennacchietti S, Michieli P, Galluzzo M, Mazzone M, Giordano S, Comoglio PM. Hypoxia promotes invasive growth by transcriptional activation of the met protooncogene. Cancer Cell. 2003;3(4):347-61. Epub 2003/05/03. PubMed PMID: 12726861.

19. Petrella BL, Lohi J, Brinckerhoff CE. Identification of membrane type-1 matrix metalloproteinase as a target of hypoxia-inducible factor-2 alpha in von Hippel-Lindau renal cell carcinoma. Oncogene. 2005;24(6):1043-52. Epub 2004/12/14. doi: 10.1038/sj.onc.1208305. PubMed PMID: 15592504; PubMed Central PMCID: PMC1847637.

20. Smith K, Gunaratnam L, Morley M, Franovic A, Mekhail K, Lee S. Silencing of epidermal growth factor receptor suppresses hypoxia-inducible factor-2-driven VHL-/- renal cancer. Cancer Res. 2005;65(12):5221-30. Epub 2005/06/17. doi: 10.1158/0008-5472.CAN-05-0169. PubMed PMID: 15958567.

21. Staller P, Sulitkova J, Lisztwan J, Moch H, Oakeley EJ, Krek W. Chemokine receptor CXCR4 downregulated by von Hippel-Lindau tumour suppressor pVHL. Nature. 2003;425(6955):307-11. Epub 2003/09/19. doi: 10.1038/nature01874. PubMed PMID: 13679920.

22. Zagzag D, Krishnamachary B, Yee H, Okuyama H, Chiriboga L, Ali MA, et al. Stromal cell-derived factor-1alpha and CXCR4 expression in hemangioblastoma and clear cell-renal cell carcinoma: von Hippel-Lindau loss-of-function induces expression of a ligand and its receptor. Cancer Res. 2005;65(14):6178-88. Epub 2005/07/19. doi: 10.1158/0008-5472.CAN-04-4406. PubMed PMID: 16024619.

23. Hu CJ, Wang LY, Chodosh LA, Keith B, Simon MC. Differential roles of hypoxia-inducible factor 1alpha (HIF1Alpha) and HIF-2alpha in hypoxic gene regulation. Mol Cell Biol. 2003;23(24):9361-74. Epub 2003/12/04. PubMed PMID: 14645546; PubMed Central PMCID: PMC309606.

24. Gordan JD, Bertout JA, Hu CJ, Diehl JA, Simon MC. HIF-2alpha promotes hypoxic cell proliferation by enhancing c-myc transcriptional activity. Cancer Cell. 2007;11(4):335-47. Epub 2007/04/10. doi: 10.1016/j.ccr.2007.02.006. PubMed PMID: 17418410; PubMed Central PMCID: PMC3145406.

25. Gordan JD, Lal P, Dondeti VR, Letrero R, Parekh KN, Oquendo CE, et al. HIF-alpha effects on c-Myc distinguish two subtypes of sporadic VHL-deficient clear cell renal carcinoma. Cancer Cell. 2008;14(6):435-46. Epub 2008/12/09. doi: 10.1016/j.ccr.2008.10.016. PubMed PMID: 19061835; PubMed Central PMCID: PMC2621440.

26. Shen C, Beroukhim R, Schumacher SE, Zhou J, Chang M, Signoretti S, et al. Genetic and functional studies implicate HIF1alpha as a 14q kidney cancer suppressor gene. Cancer Discov. 2011;1(3):222-35. Epub 2011/11/01. doi: 10.1158/2159-8290.CD-11-0098. PubMed PMID: 22037472; PubMed Central PMCID: PMC3202343.

27. Sandlund J, Oosterwijk E, Grankvist K, Oosterwijk-Wakka J, Ljungberg B, Rasmuson T. Prognostic impact of carbonic anhydrase IX expression in human renal cell carcinoma. BJU Int. 2007;100(3):556-60. Epub 2007/07/05. doi: 10.1111/j.1464-410X.2007.07006.x. PubMed PMID: 17608827.

28. Patard JJ, Fergelot P, Karakiewicz PI, Klatte T, Trinh QD, Rioux-Leclercq N, et al. Low CAIX expression and absence of VHL gene mutation are associated with tumor aggressiveness and poor survival of clear cell renal cell carcinoma. Int J Cancer. 2008;123(2):395-400. Epub 2008/05/09. doi: 10.1002/ijc.23496. PubMed PMID: 18464292; PubMed Central PMCID: PMC2721857.

29. Bui MH, Visapaa H, Seligson D, Kim H, Han KR, Huang Y, et al. Prognostic value of carbonic anhydrase IX and KI67 as predictors of survival for renal clear cell carcinoma. J Urol. 2004;171(6 Pt 1):2461-6. Epub 2004/05/06. PubMed PMID: 15126876.

30. Belldegrun A. Prospective randomized double-blind phase III study of adjuvant cG250 (Rencarex®) vs placebo in 864 pts with high-risk ccRCC. ASCO Abstract. 2013.

31. Harris AL. Hypoxia--a key regulatory factor in tumour growth. Nat Rev Cancer. 2002;2(1):38-47. Epub 2002/03/21. doi: 10.1038/nrc704. PubMed PMID: 11902584.

32. Claesson-Welsh L, Welsh M. VEGFA and tumour angiogenesis. J Intern Med. 2013;273(2):114-27. Epub 2012/12/12. doi: 10.1111/joim.12019. PubMed PMID: 23216836.

33. Mendel DB, Laird AD, Xin X, Louie SG, Christensen JG, Li G, et al. In vivo antitumor activity of SU11248, a novel tyrosine kinase inhibitor targeting vascular endothelial growth factor and platelet-derived growth factor receptors: determination of a pharmacokinetic/pharmacodynamic relationship. Clin Cancer Res. 2003;9(1):327-37. Epub 2003/01/23. PubMed PMID: 12538485.

34. Polyzos A. Activity of SU11248, a multitargeted inhibitor of vascular endothelial growth factor receptor and platelet-derived growth factor receptor, in patients with metastatic renal cell carcinoma and various other solid tumors. J Steroid Biochem Mol Biol. 2008;108(3-5):261-6. Epub 2007/10/20. doi: 10.1016/j.jsbmb.2007.09.004. PubMed PMID: 17945482.

35. Motzer RJ, Michaelson MD, Redman BG, Hudes GR, Wilding G, Figlin RA, et al. Activity of SU11248, a multitargeted inhibitor of vascular endothelial growth factor receptor and platelet-derived growth factor receptor, in patients with metastatic renal cell carcinoma. J Clin Oncol. 2006;24(1):16-24. Epub 2005/12/07. doi: 10.1200/JCO.2005.02.2574. PubMed PMID: 16330672.

36. Motzer RJ, Hutson TE, Tomczak P, Michaelson MD, Bukowski RM, Rixe O, et al. Sunitinib versus interferon alfa in metastatic renal-cell carcinoma. N Engl J Med. 2007;356(2):115-24. Epub 2007/01/12. doi: 10.1056/NEJMoa065044. PubMed PMID: 17215529.

37. Scartozzi M, Bianconi M, Faloppi L, Loretelli C, Bittoni A, Del Prete M, et al. VEGF and VEGFR polymorphisms affect clinical outcome in advanced renal cell carcinoma patients receiving first-line sunitinib. Br J Cancer. 2013;108(5):1126-32. Epub 2013/03/21. doi: 10.1038/bjc.2012.501. PubMed PMID: 23511629; PubMed Central PMCID: PMC3619056.

38. Jonasch E, Thakur, S., Sircar, K., Tamboli, P., Tannir, NM., Monzon, FA. Impact of chromosomal copy number variation on outcome in metastatic clear cell renal cell carcinoma patients treated with antiangiogenic agents. J Clin Oncol. 2013;31 Suppl:Abstr 393.

39. Escudier B, Eisen T, Stadler WM, Szczylik C, Oudard S, Staehler M, et al. Sorafenib for treatment of renal cell carcinoma: Final efficacy and safety results of the phase III treatment approaches in renal cancer global evaluation trial. J Clin Oncol. 2009;27(20):3312-8. Epub 2009/05/20. doi: 10.1200/JCO.2008.19.5511. PubMed PMID: 19451442.

40. Tran HT, Liu Y, Zurita AJ, Lin Y, Baker-Neblett KL, Martin AM, et al. Prognostic or predictive plasma cytokines and angiogenic factors for patients treated with pazopanib for metastatic renal-cell cancer: a retrospective analysis of phase 2 and phase 3 trials. The Lancet Oncology. 2012;13(8):827-37. Epub 2012/07/05. doi: 10.1016/S1470-2045(12)70241-3. PubMed PMID: 22759480.

41. Motzer RJ, Bukowski RM. Targeted therapy for metastatic renal cell carcinoma. J Clin Oncol. 2006;24(35):5601-8. Epub 2006/12/13. doi: 10.1200/JCO.2006.08.5415. PubMed PMID: 17158546.

42. Velickovic M, Delahunt B, McIver B, Grebe SK. Intragenic PTEN/MMAC1 loss of heterozygosity in conventional (clear-cell) renal cell carcinoma is associated with poor patient prognosis. Mod Pathol. 2002;15(5):479-85. Epub 2002/05/16. doi: 10.1038/modpathol.3880551. PubMed PMID: 12011252.

43. Atkins MB, Hidalgo M, Stadler WM, Logan TF, Dutcher JP, Hudes GR, et al. Randomized phase II study of multiple dose levels of CCI-779, a novel mammalian target of rapamycin kinase inhibitor, in patients with advanced refractory renal cell carcinoma. J Clin Oncol. 2004;22(5):909-18. Epub 2004/03/03. doi: 10.1200/JCO.2004.08.185. PubMed PMID: 14990647.

44. Motzer RJ, Hudes GR, Curti BD, McDermott DF, Escudier BJ, Negrier S, et al. Phase I/II trial of temsirolimus combined with interferon alfa for advanced renal cell carcinoma. J Clin Oncol. 2007;25(25):3958-64. Epub 2007/09/01. doi: 10.1200/JCO.2006.10.5916. PubMed PMID: 17761980.

45. Armstrong AJ, George DJ, Halabi S. Serum lactate dehydrogenase predicts for overall survival benefit in patients with metastatic renal cell carcinoma treated with inhibition of mammalian target of rapamycin. J Clin Oncol. 2012;30(27):3402-7. Epub 2012/08/15. doi: 10.1200/JCO.2011.40.9631. PubMed PMID: 22891270.

46. Mueller-Pillasch F, Pohl B, Wilda M, Lacher U, Beil M, Wallrapp C, et al. Expression of the highly conserved RNA binding protein KOC in embryogenesis. Mech Dev. 1999;88(1):95-9. Epub 1999/10/19. PubMed PMID: 10525192.

47. Jiang Z, Chu PG, Woda BA, Rock KL, Liu Q, Hsieh CC, et al. Analysis of RNA-binding protein IMP3 to predict metastasis and prognosis of renal-cell carcinoma: a retrospective study. The Lancet Oncology. 2006;7(7):556-64. Epub 2006/07/04. doi: 10.1016/S1470-2045(06)70732-X. PubMed PMID: 16814207.

48. Hoffmann NE, Sheinin Y, Lohse CM, Parker AS, Leibovich BC, Jiang Z, et al. External validation of IMP3 expression as an independent prognostic marker for metastatic progression and death for patients with clear cell renal cell carcinoma. Cancer. 2008;112(7):1471-9. Epub 2008/02/09. doi: 10.1002/cncr.23296. PubMed PMID: 18260086; PubMed Central PMCID: PMC2792740.

49. Zamparese R, Pannone G, Santoro A, Lo Muzio L, Corsi F, Pedicillo MC, et al. Survivin expression in renal cell carcinoma. Cancer Invest. 2008;26(9):929-35. Epub 2008/11/27. doi: 10.1080/07357900802017553. PubMed PMID: 19034775.

50. Sato A, Oya M, Ito K, Mizuno R, Horiguchi Y, Umezawa K, et al. Survivin associates with cell proliferation in renal cancer cells: regulation of survivin expression by insulin-like growth factor-1, interferon-gamma and a novel NF-kappaB inhibitor. Int J Oncol. 2006;28(4):841-6. Epub 2006/03/10. PubMed PMID: 16525632.

51. Lei Y, Geng Z, Guo-Jun W, He W, Jian-Lin Y. Prognostic significance of survivin expression in renal cell cancer and its correlation with radioresistance. Mol Cell Biochem. 2010;344(1-2):23-31. Epub 2010/06/22. doi: 10.1007/s11010-010-0525-3. PubMed PMID: 20563741.

52. Dalgliesh GL, Furge K, Greenman C, Chen L, Bignell G, Butler A, et al. Systematic sequencing of renal carcinoma reveals inactivation of histone modifying genes. Nature. 2010;463(7279):360-3. Epub 2010/01/08. doi: 10.1038/nature08672. PubMed PMID: 20054297; PubMed Central PMCID: PMC2820242.

53. Varela I, Tarpey P, Raine K, Huang D, Ong CK, Stephens P, et al. Exome sequencing identifies frequent mutation of the SWI/SNF complex gene PBRM1 in renal carcinoma. Nature. 2011;469(7331):539-42. Epub 2011/01/21. doi: 10.1038/nature09639. PubMed PMID: 21248752; PubMed Central PMCID: PMC3030920.

54. Pena-Llopis S, Vega-Rubin-de-Celis S, Liao A, Leng N, Pavia-Jimenez A, Wang S, et al. BAP1 loss defines a new class of renal cell carcinoma. Nat Genet. 2012;44(7):751-9. Epub 2012/06/12. doi: 10.1038/ng.2323. PubMed PMID: 22683710.

55. Kapur P, Pena-Llopis S, Christie A, Zhrebker L, Pavia-Jimenez A, Rathmell WK, et al. Effects on survival of BAP1 and PBRM1 mutations in sporadic clear-cell renal-cell carcinoma: a retrospective analysis with independent validation. The Lancet Oncology. 2013;14(2):159-67. Epub 2013/01/22. doi: 10.1016/S1470-2045(12)70584-3. PubMed PMID: 23333114.

56. Pawlowski R, Muhl SM, Sulser T, Krek W, Moch H, Schraml P. Loss of PBRM1 expression is associated with renal cell carcinoma progression. Int J Cancer. 2013;132(2):E11-7. Epub 2012/09/06. doi: 10.1002/ijc.27822. PubMed PMID: 22949125.

57. Hakimi AA, Chen YB, Wren J, Gonen M, Abdel-Wahab O, Heguy A, et al. Clinical and pathologic impact of select chromatin-modulating tumor suppressors in clear cell renal cell carcinoma. European Urology. 2013;63(5):848-54. Epub 2012/10/06. doi: 10.1016/j.eururo.2012.09.005. PubMed PMID: 23036577; PubMed Central PMCID: PMC3615105.

58. Hakimi AA, Ostrovnaya I, Reva BA, Schultz N, Chen YB, Gonen M, et al. Adverse Outcomes in Clear Cell Renal Cell Carcinoma with Mutations of 3p21 Epigenetic Regulators BAP1 and SETD2: a Report by MSKCC and the KIRC TCGA Research Network. Clin Cancer Res. 2013. Epub 2013/04/27. doi: 10.1158/1078-0432.CCR-12-3886. PubMed PMID: 23620406.

59. Simon JM, Hacker KE, Singh D, Brannon AR, Parker JS, Weiser M, et al. Variation in chromatin accessibility in human kidney cancer links H3K36 methyltransferase loss with widespread RNA processing defects. Genome Res. 2014;24(2):241-50. Epub 2013/10/26. doi: 10.1101/gr.158253.113. PubMed PMID: 24158655; PubMed Central PMCID: PMC3912414.

60. Gulati S, Martinez P, Joshi T, Birkbak NJ, Santos CR, Rowan AJ, et al. Systematic evaluation of the prognostic impact and intratumour heterogeneity of clear cell renal cell carcinoma biomarkers. European Urology. 2014;66(5):936-48. Epub 2014/07/23. doi: 10.1016/j.eururo.2014.06.053. PubMed PMID: 25047176.

61. La Rochelle J, Klatte T, Dastane A, Rao N, Seligson D, Said J, et al. Chromosome 9p deletions identify an aggressive phenotype of clear cell renal cell carcinoma. Cancer. 2010;116(20):4696-702. Epub 2010/07/16. doi: 10.1002/cncr.25279. PubMed PMID: 20629029.

62. Monzon FA, Alvarez K, Peterson L, Truong L, Amato RJ, Hernandez-McClain J, et al. Chromosome 14q loss defines a molecular subtype of clear-cell renal cell carcinoma associated with poor prognosis. Mod Pathol. 2011;24(11):1470-9. Epub 2011/07/05. doi: 10.1038/modpathol.2011.107. PubMed PMID: 21725288.

63. Meskawi M, Sun M, Trinh QD, Bianchi M, Hansen J, Tian Z, et al. A review of integrated staging systems for renal cell carcinoma. European Urology. 2012;62(2):303-14. Epub 2012/05/12. doi: 10.1016/j.eururo.2012.04.049. PubMed PMID: 22575911.

64. Thompson RH, Gillett MD, Cheville JC, Lohse CM, Dong H, Webster WS, et al. Costimulatory B7-H1 in renal cell carcinoma patients: Indicator of tumor aggressiveness and potential therapeutic target. Proc Natl Acad Sci U S A. 2004;101(49):17174-9. Epub 2004/12/01. doi: 10.1073/pnas.0406351101. PubMed PMID: 15569934; PubMed Central PMCID: PMC534606.

65. Thompson RH, Kuntz SM, Leibovich BC, Dong H, Lohse CM, Webster WS, et al. Tumor B7-H1 is associated with poor prognosis in renal cell carcinoma patients with long-term follow-up. Cancer Res. 2006;66(7):3381-5. Epub 2006/04/06. doi: 10.1158/0008-5472.CAN-05-4303. PubMed PMID: 16585157.

66. Krambeck AE, Thompson RH, Dong H, Lohse CM, Park ES, Kuntz SM, et al. B7-H4 expression in renal cell carcinoma and tumor vasculature: associations with cancer progression and survival. Proc Natl Acad Sci U S A. 2006;103(27):10391-6. Epub 2006/06/27. doi: 10.1073/pnas.0600937103. PubMed PMID: 16798883; PubMed Central PMCID: PMC1502468.

67. Valera VA, Merino MJ. Misdiagnosis of clear cell renal cell carcinoma. Nat Rev Urol. 2011;8(6):321-33. Epub 2011/05/19. doi: 10.1038/nrurol.2011.64. PubMed PMID: 21587224.

68. Fisher R, Larkin J, Swanton C. Inter and intratumour heterogeneity: a barrier to individualized medical therapy in renal cell carcinoma? Front Oncol. 2012;2:49. Epub 2012/06/02. doi: 10.3389/fonc.2012.00049. PubMed PMID: 22655275; PubMed Central PMCID: PMC3356118.

69. Ljungber B, et al. Heterogeneity in renal cell carcinoma and its impact on prognosis-a flow cytometric study. Br J Cancer. 1996;74:123-7.

70. Ruiz-Cerda JL, Hernandez M, Sempere A, O'Connor JE, Kimler BF, Jimenez-Cruz F. Intratumoral heterogeneity of DNA content in renal cell carcinoma and its prognostic significance. Cancer. 1999;86(4):664-71. Epub 1999/08/10. PubMed PMID: 10440695.

71. Gerlinger M, Rowan AJ, Horswell S, Larkin J, Endesfelder D, Gronroos E, et al. Intratumor heterogeneity and branched evolution revealed by multiregion sequencing. N Engl J Med. 2012;366(10):883-92. Epub 2012/03/09. doi: 10.1056/NEJMoa1113205. PubMed PMID: 22397650.

72. Dirkes S. Acute kidney injury: not just acute renal failure anymore? Crit Care Nurse. 2011;31(1):37-49; quiz 50. Epub 2011/02/03. doi: 10.4037/ccn2011946. PubMed PMID: 21285464.

73. Fuchs TC, Hewitt P. Biomarkers for drug-induced renal damage and nephrotoxicity- an overview for applied toxicology. Aaps J. 2011;13(4):615-31. Epub 2011/10/05. doi: 10.1208/s12248-011-9301-x. PubMed PMID: 21969220; PubMed Central PMCID: PMC3231866.

74. Humphreys BD, Soiffer RJ, Magee CC. Renal failure associated with cancer and its treatment: an update. J Am Soc Nephrol. 2005;16(1):151-61. Epub 2004/12/03. doi: 10.1681/ASN.2004100843. PubMed PMID: 15574506.

75. Lameire N, Kruse V, Rottey S. Nephrotoxicity of anticancer drugs--an underestimated problem? Acta Clin Belg. 2011;66(5):337-45. Epub 2011/12/08. PubMed PMID: 22145268.

76. Lane BR. Molecular markers of kidney injury. Urol Oncol. 2011. Epub 2011/07/05. doi: 10.1016/j.urolonc.2011.05.007. PubMed PMID: 21723753.

77. Casciano DA. The use of genomics in model in vitro systems. Adv Exp Med Biol. 2012;745:210-20. Epub 2012/03/23. doi: 10.1007/978-1-4614-3055-1_12. PubMed PMID: 22437820.

78. Shiao YH. Genetic signature for human risk assessment: lessons from trichloroethylene. Environ Mol Mutagen. 2009;50(1):68-77. Epub 2008/11/26. doi: 10.1002/em.20432. PubMed PMID: 19031419; PubMed Central PMCID: PMC2630226.

79. Doll R. Tobacco: an overview of health effects. IARC Sci Publ. 1986;(74):11-22. Epub 1986/01/01. PubMed PMID: 3305329.

80. Trzcinka-Ochocka M, Jakubowski M, Razniewska G, Halatek T, Gazewski A. The effects of environmental cadmium exposure on kidney function: the possible influence of age. Environ Res. 2004;95(2):143-50. Epub 2004/05/19. doi: 10.1016/j.envres.2003.10.003. PubMed PMID: 15147919.

81. Hartwig A. Mechanisms in cadmium-induced carcinogenicity: recent insights. Biometals. 2010;23(5):951-60. Epub 2010/04/15. doi: 10.1007/s10534-010-9330-4. PubMed PMID: 20390439.

82. Liu ES, Ye YN, Shin VY, Yuen ST, Leung SY, Wong BC, et al. Cigarette smoke exposure increases ulcerative colitis-associated colonic adenoma formation in mice. Carcinogenesis. 2003;24(8):1407-13. Epub 2003/06/17. doi: 10.1093/carcin/bgg094. PubMed PMID: 12807736.

83. Zhu BQ, Heeschen C, Sievers RE, Karliner JS, Parmley WW, Glantz SA, et al. Second hand smoke stimulates tumor angiogenesis and growth. Cancer Cell. 2003;4(3):191-6. Epub 2003/10/03. PubMed PMID: 14522253.

84. Wang B, Li Y, Shao C, Tan Y, Cai L. Cadmium and its epigenetic effects. Curr Med Chem. 2012;19(16):2611-20. Epub 2012/04/05. PubMed PMID: 22471978.

85. Satarug S, Garrett SH, Sens MA, Sens DA. Cadmium, environmental exposure, and health outcomes. Environ Health Perspect. 2010;118(2):182-90. Epub 2010/02/04. doi: 10.1289/ehp.0901234. PubMed PMID: 20123617; PubMed Central PMCID: PMC2831915.

86. Bull S. Cadmium Toxicological Overview. Health Protection Agency. 2010;3:1-15.

87. Suzuki KT. Studies of Cadmium Uptake and Metabolism by the Kidney. Environ Health Perspect. 1984;54:21-30.

88. Bertin G, Averbeck D. Cadmium: cellular effects, modifications of biomolecules, modulation of DNA repair and genotoxic consequences (a review). Biochimie. 2006;88(11):1549-59. Epub 2006/10/31. doi: 10.1016/j.biochi.2006.10.001. PubMed PMID: 17070979.

89. Waalkes MP. Cadmium carcinogenesis. Mutat Res. 2003;533(1-2):107-20. Epub 2003/12/04. PubMed PMID: 14643415.

90. Cancer IAfRo. Berrylium, cadmium, mercury and exposures in the glass manufacturing industry. International Agency for Research on Cancer Monographs on the Evaluation of Carcinogenic Risks to Humans. 1993;58(IARC Scientific Publications, Lyon):119-237.

91. Waisberg M, Joseph P, Hale B, Beyersmann D. Molecular and cellular mechanisms of cadmium carcinogenesis. Toxicology. 2003;192(2-3):95-117. Epub 2003/10/29. PubMed PMID: 14580780.

92. Koizumi T, Shirakura H, Kumagai H, Tatsumoto H, Suzuki KT. Mechanism of cadmium-induced cytotoxicity in rat hepatocytes: cadmium-induced active oxygen-related permeability changes of the plasma membrane. Toxicology. 1996;114(2):125-34. Epub 1996/12/02. PubMed PMID: 8947611.

93. Masini A, Trenti T, Ventura E, Ceccarelli D, Muscatello U. The effect of ferric iron complex on Ca2+ transport in isolated rat liver mitochondria. Biochem Biophys Res Commun. 1985;130(1):207-13. Epub 1985/07/16. PubMed PMID: 4026827.

94. Bindoli A. Lipid peroxidation in mitochondria. Free Radic Biol Med. 1988;5(4):247-61. Epub 1988/01/01. PubMed PMID: 3075952.

95. Takeyama N, Miki S, Hirakawa A, Tanaka T. Role of the mitochondrial permeability transition and cytochrome C release in hydrogen peroxide-induced apoptosis. Exp Cell Res. 2002;274(1):16-24. Epub 2002/02/22. doi: 10.1006/excr.2001.5447. PubMed PMID: 11855853.

96. Lutzen A, Liberti SE, Rasmussen LJ. Cadmium inhibits human DNA mismatch repair in vivo. Biochem Biophys Res Commun. 2004;321(1):21-5. Epub 2004/09/11. doi: 10.1016/j.bbrc.2004.06.102. PubMed PMID: 15358209.

97. Hartmann M, Hartwig A. Disturbance of DNA damage recognition after UV-irradiation by nickel(II) and cadmium(II) in mammalian cells. Carcinogenesis. 1998;19(4):617-21. Epub 1998/05/26. PubMed PMID: 9600346.

98. McNeill DR, Narayana A, Wong HK, Wilson DM, 3rd. Inhibition of Ape1 nuclease activity by lead, iron, and cadmium. Environ Health Perspect. 2004;112(7):799-804. Epub 2004/05/26. PubMed PMID: 15159209; PubMed Central PMCID: PMC1241995.

99. Szuster-Ciesielska A, Stachura A, Slotwinska M, Kaminska T, Sniezko R, Paduch R, et al. The inhibitory effect of zinc on cadmium-induced cell apoptosis and reactive oxygen species (ROS) production in cell cultures. Toxicology. 2000;145(2-3):159-71. Epub 2000/04/20. PubMed PMID: 10771141.

100. Watjen W, Haase H, Biagioli M, Beyersmann D. Induction of apoptosis in mammalian cells by cadmium and zinc. Environ Health Perspect. 2002;110 Suppl 5:865-7. Epub 2002/11/12. PubMed PMID: 12426148; PubMed Central PMCID: PMC1241262.

101. Jimi S, Uchiyama M, Takaki A, Suzumiya J, Hara S. Mechanisms of cell death induced by cadmium and arsenic. Ann N Y Acad Sci. 2004;1011:325-31. Epub 2004/05/06. PubMed PMID: 15126309.

102. Hecht SS. Lung carcinogenesis by tobacco smoke. Int J Cancer. 2012;131(12):2724-32. Epub 2012/09/05. doi: 10.1002/ijc.27816. PubMed PMID: 22945513; PubMed Central PMCID: PMC3479369.

103. Letasiova S, Medve'ova A, Sovcikova A, Dusinska M, Volkovova K, Mosoiu C, et al. Bladder cancer, a review of the environmental risk factors. Environ Health. 2012;11 Suppl 1:S11. Epub 2012/07/13. doi: 10.1186/1476-069X-11-S1-S11. PubMed PMID: 22759493; PubMed Central PMCID: PMC3388449.

104. Loeb LA, Ernster VL, Warner KE, Abbotts J, Laszlo J. Smoking and lung cancer: an overview. Cancer Res. 1984;44(12 Pt 1):5940-58. Epub 1984/12/01. PubMed PMID: 6388830.

105. Pogribny IP, Rusyn I. Environmental toxicants, epigenetics, and cancer. Adv Exp Med Biol. 2013;754:215-32. Epub 2012/09/08. doi: 10.1007/978-1-4419-9967-2_11. PubMed PMID: 22956504.

106. Sankpal UT, Pius H, Khan M, Shukoor MI, Maliakal P, Lee CM, et al. Environmental factors in causing human cancers: emphasis on tumorigenesis. Tumour Biol. 2012;33(5):1265-74. Epub 2012/05/23. doi: 10.1007/s13277-012-0413-4. PubMed PMID: 22614680.

107. Torti SV, Torti FM. Iron and cancer: more ore to be mined. Nat Rev Cancer. 2013;13(5):342-55. Epub 2013/04/19. doi: 10.1038/nrc3495. PubMed PMID: 23594855.

108. Carmeliet P, Jain RK. Molecular mechanisms and clinical applications of angiogenesis. Nature. 2011;473(7347):298-307. Epub 2011/05/20. doi: 10.1038/nature10144. PubMed PMID: 21593862.

109. Il'yasova D, Schwartz GG. Cadmium and renal cancer. Toxicol Appl Pharmacol. 2005;207(2):179-86. Epub 2005/08/17. doi: 10.1016/j.taap.2004.12.005. PubMed PMID: 16102569.

110. Maxwell P, Salnikow K. HIF-1: an oxygen and metal responsive transcription factor. Cancer Biol Ther. 2004;3(1):29-35. Epub 2004/01/17. PubMed PMID: 14726713.

111. Sabolic I. Common mechanisms in nephropathy induced by toxic metals. Nephron Physiol. 2006;104(3):p107-14. Epub 2006/08/31. doi: 10.1159/000095539. PubMed PMID: 16940748.

112. Van Vleet TR, Schnellmann RG. Toxic nephropathy: environmental chemicals. Semin Nephrol. 2003;23(5):500-8. Epub 2003/09/19. PubMed PMID: 13680539.

113. Wang YF, Shyu HW, Chang YC, Tseng WC, Huang YL, Lin KH, et al. Nickel (II)-induced cytotoxicity and apoptosis in human proximal tubule cells through a ROS- and mitochondria-mediated pathway. Toxicol Appl Pharmacol. 2012;259(2):177-86. Epub 2012/01/17. doi: 10.1016/j.taap.2011.12.022. PubMed PMID: 22245127.

114. Sabath E, Robles-Osorio ML. Renal health and the environment: heavy metal nephrotoxicity. Nefrologia. 2012;32(3):279-86. Epub 2012/04/18. doi: 10.3265/Nefrologia.pre2012.Jan.10928. PubMed PMID: 22508139.

115. Cheng TF, Choudhuri S, Muldoon-Jacobs K. Epigenetic targets of some toxicologically relevant metals: a review of the literature. J Appl Toxicol. 2012;32(9):643-53. Epub 2012/02/16. doi: 10.1002/jat.2717. PubMed PMID: 22334439.

116. Chervona Y, Arita A, Costa M. Carcinogenic metals and the epigenome: understanding the effect of nickel, arsenic, and chromium. Metallomics. 2012;4(7):619-27. Epub 2012/04/05. doi: 10.1039/c2mt20033c. PubMed PMID: 22473328; PubMed Central PMCID: PMC3687545.

117. Martinez-Zamudio R, Ha HCH. Environmental epigenetics in metal exposure. Epigenetics. 2011;6(7):820-7. doi: 10.4161/epi.6.7.16250.

118. Guo X, Lu J, Wang Y, Gui Y, Duan X, Cai Z. Ascorbate antagonizes nickel ion to regulate JMJD1A expression in kidney cancer cells. Acta Biochim Biophys Sin (Shanghai). 2012;44(4):330-8. Epub 2012/02/10. doi: 10.1093/abbs/gms004. PubMed PMID: 22318714.

119. Ellis LM. The role of neuropilins in cancer. Mol Cancer Ther. 2006;5(5):1099-107. Epub 2006/05/30. doi: 10.1158/1535-7163.MCT-05-0538. PubMed PMID: 16731741.

120. Goel S, Duda DG, Xu L, Munn LL, Boucher Y, Fukumura D, et al. Normalization of the vasculature for treatment of cancer and other diseases. Physiol Rev 2011 91:1071-121. doi: 10.1152/physrev.00038.2010.-New.

121. Vasudev NS, Selby PJ, Banks RE. Renal cancer biomarkers: the promise of personalized care. BMC Med. 2012;10:112. Epub 2012/09/29. doi: 10.1186/1741-7015-10-112. PubMed PMID: 23016578; PubMed Central PMCID: PMC3521191.

122. Wright TM, Brannon A, Gordon J, Mikels A, Mitchell C, Chen S, et al. Ror2, a developmentally regulated kinase, promotes tumor growth potential in renal cell carcinoma. Oncogene. 2009;28:2513-23.

123. Yao M, Huang Y, Shioi K, Hattori K, Murakami T, Sano F, et al. A three-gene expression signature model to predict clinical outcome of clear cell renal carcinoma. Int J Cancer. 2008;123(5):1126-32. Epub 2008/06/12. doi: 10.1002/ijc.23641. PubMed PMID: 18546273.

124. Network CGA. Integrative analysis of genomic and molecular alterations in clear cell renal cell carcinoma. Nature. 2013.

125. Zisman A. Risk Group Assessment and Clinical Outcome Algorithm to Predict the Natural History of Patients With Surgically Resected Renal Cell Carcinoma. Journal of Clinical Oncology. 2002;20(23):4559-66. doi: 10.1200/jco.2002.05.111.

126. Zigeuner R, Hutterer G, Chromecki T, Imamovic A, Kampel-Kettner K, Rehak P, et al. External validation of the Mayo Clinic stage, size, grade, and necrosis (SSIGN) score for clear-cell renal cell carcinoma in a single European centre applying routine pathology. European Urology. 2010;57(1):102-9. Epub 2008/12/09. doi: 10.1016/j.eururo.2008.11.033. PubMed PMID: 19062157.

127. Ellis MJ, Perou CM. The genomic landscape of breast cancer as a therapeutic roadmap. Cancer Discov. 2013;3(1):27-34. Epub 2013/01/16. doi: 10.1158/2159-8290.CD-12-0462. PubMed PMID: 23319768; PubMed Central PMCID: PMC3553590.

128. Network CGA. Comprehensive molecular portraits of human breast tumours. Nature. 2012;490(7418):61-70. Epub 2012/09/25. doi: 10.1038/nature11412. PubMed PMID: 23000897; PubMed Central PMCID: PMC3465532.

129. Parker JS, Mullins M, Cheang MC, Leung S, Voduc D, Vickery T, et al. Supervised risk predictor of breast cancer based on intrinsic subtypes. J Clin Oncol. 2009;27(8):1160-7. Epub 2009/02/11. doi: 10.1200/JCO.2008.18.1370. PubMed PMID: 19204204; PubMed Central PMCID: PMC2667820.

130. Puvvada S, Kendrick S, Rimsza L. Molecular classification, pathway addiction, and therapeutic targeting in diffuse large B cell lymphoma. Cancer Genet. 2013. Epub 2013/10/02. doi: 10.1016/j.cancergen.2013.07.003. PubMed PMID: 24080457.

131. De Sousa EMF, Wang X, Jansen M, Fessler E, Trinh A, de Rooij LP, et al. Poor-prognosis colon cancer is defined by a molecularly distinct subtype and develops from serrated precursor lesions. Nat Med. 2013;19(5):614-8. Epub 2013/04/16. doi: 10.1038/nm.3174. PubMed PMID: 23584090.

132. Sadanandam A, Lyssiotis CA, Homicsko K, Collisson EA, Gibb WJ, Wullschleger S, et al. A colorectal cancer classification system that associates cellular phenotype and responses to therapy. Nat Med. 2013;19(5):619-25. Epub 2013/04/16. doi: 10.1038/nm.3175. PubMed PMID: 23584089; PubMed Central PMCID: PMC3774607.

133. Rini BI, Zhou, M., Aydin, H., Elson, P., Maddala, T., Knezevic, D., Parodi, L., Bukowski, R. M., Novotny, W. F., Cowens, J. W. . Identification of prognostic genomic markers in patients with localized clear cell renal cell carcinoma (ccRCC). 2010.

134. Geiss GK, Bumgarner RE, Birditt B, Dahl T, Dowidar N, Dunaway DL, et al. Direct multiplexed measurement of gene expression with color-coded probe pairs. Nat Biotechnol. 2008;26(3):317-25. Epub 2008/02/19. doi: 10.1038/nbt1385. PubMed PMID: 18278033.

135. Tibshirani R, Hastie T, Narasimhan B, Chu G. Diagnosis of multiple cancer types by shrunken centroids of gene expression. Proc Natl Acad Sci U S A. 2002;99(10):6567-72. Epub 2002/05/16. doi: 10.1073/pnas.082099299. PubMed PMID: 12011421; PubMed Central PMCID: PMC124443.

136. Seiler M, Huang CC, Szalma S, Bhanot G. ConsensusCluster: a software tool for unsupervised cluster discovery in numerical data. Omics. 2010;14(1):109-13. Epub 2010/02/10. doi: 10.1089/omi.2009.0083. PubMed PMID: 20141333.

137. Gerlinger M, Horswell S, Larkin J, Rowan AJ, Salm MP, Varela I, et al. Genomic architecture and evolution of clear cell renal cell carcinomas defined by multiregion sequencing. Nat Genet. 2014;46(3):225-33. Epub 2014/02/04. doi: 10.1038/ng.2891. PubMed PMID: 24487277.

138. Catana C, Drzezga A, Heiss WD, Rosen BR. PET/MRI for neurologic applications. J Nucl Med. 2012;53(12):1916-25. Epub 2012/11/13. doi: 10.2967/jnumed.112.105346. PubMed PMID: 23143086; PubMed Central PMCID: PMC3806202.

139. Drzezga A, Souvatzoglou M, Eiber M, Beer AJ, Furst S, Martinez-Moller A, et al. First clinical experience with integrated whole-body PET/MR: comparison to PET/CT in

patients with oncologic diagnoses. J Nucl Med. 2012;53(6):845-55. Epub 2012/04/27. doi: 10.2967/jnumed.111.098608. PubMed PMID: 22534830.

140. Braunagel M, Graser A, Reiser M, Notohamiprodjo M. The role of functional imaging in the era of targeted therapy of renal cell carcinoma. World Journal of Urology. 2014;32(1):47-58. Epub 2013/04/17. doi: 10.1007/s00345-013-1074-7. PubMed PMID: 23588813.

141. Miyakita H, Tokunaga, M., Onda, H., Usui, Y., , Kinoshita H, Kawamura, N., Yasuda, S. Significance of 18F-fluorodeoxyglucose positron emission tomography (FDG-PET) for detection of renal cell carcinoma. International Journal of Urology. 2002;9:15-8.

142. Namura K, Minamimoto R, Yao M, Makiyama K, Murakami T, Sano F, et al. Impact of maximum standardized uptake value (SUVmax) evaluated by 18-Fluoro-2-deoxy-D-glucose positron emission tomography/computed tomography (18F-FDG-PET/CT) on survival for patients with advanced renal cell carcinoma: a preliminary report. BMC Cancer. 2010;10:667. Epub 2010/12/07. doi: 10.1186/1471-2407-10-667. PubMed PMID: 21129184; PubMed Central PMCID: PMC3016292.

143. Linehan WM, Rathmell WK. Kidney cancer. Urol Oncol. 2012;30(6):948-51. Epub 2012/12/12. doi: 10.1016/j.urolonc.2012.08.021. PubMed PMID: 23218074.

144. Li B, Qiu B, Lee DS, Walton ZE, Ochocki JD, Mathew LK, et al. Fructose-1,6-bisphosphatase opposes renal carcinoma progression. Nature. 2014;513(7517):251-5. Epub 2014/07/22. doi: 10.1038/nature13557. PubMed PMID: 25043030; PubMed Central PMCID: PMC4162811.

145. Tomaszewski JJ, Uzzo RG, Smaldone MC. Heterogeneity and renal mass biopsy: a review of its role and reliability. Cancer Biol Med. 2014;11(3):162-72. Epub 2014/11/05. doi: 10.7497/j.issn.2095-3941.2014.03.002. PubMed PMID: 25364577; PubMed Central PMCID: PMC4197425.

146. Volpe A, Finelli A, Gill IS, Jewett MA, Martignoni G, Polascik TJ, et al. Rationale for percutaneous biopsy and histologic characterisation of renal tumours. European Urology. 2012;62(3):491-504. Epub 2012/05/29. doi: 10.1016/j.eururo.2012.05.009. PubMed PMID: 22633318.

147. Clifford SC, Prowse, Amanda H., Affara, Nabeel A., Buys, Charles H.C.M., and Maher, Eamonn R. Inactivation of the von Hippel–Lindau (VHL) Tumour Suppressor Gene and Allelic Losses at Chromosome Arm 3p. GENES, CHROMOSOMES & CANCER. 1998;22:200-9.

148. Sternberg CN, Davis ID, Mardiak J, Szczylik C, Lee E, Wagstaff J, et al. Pazopanib in locally advanced or metastatic renal cell carcinoma: results of a randomized phase III trial. J Clin Oncol. 2010;28(6):1061-8. Epub 2010/01/27. doi: 10.1200/JCO.2009.23.9764. PubMed PMID: 20100962.

149. Sanjmyatav J, Steiner T, Wunderlich H, Diegmann J, Gajda M, Junker K. A specific gene expression signature characterizes metastatic potential in clear cell renal cell carcinoma. J Urol. 2011;186(1):289-94. Epub 2011/05/24. doi: 10.1016/j.juro.2011.03.033. PubMed PMID: 21600596.

150. Smaldone MC, Fung C, Uzzo RG, Haas NB. Adjuvant and neoadjuvant therapies in high-risk renal cell carcinoma. Hematol Oncol Clin North Am. 2011;25(4):765-91. Epub 2011/07/19. doi: 10.1016/j.hoc.2011.06.002. PubMed PMID: 21763967.

151. Network TCGR. The somatic genomic landscape of chromophobe renal cell carcinoma. Cancer Cell. 2014;26(3):319-30. Epub 2014/08/27. doi: 10.1016/j.ccr.2014.07.014. PubMed PMID: 25155756; PubMed Central PMCID: PMC4160352.

152. Network TCGAR. Comprehensive Molecular Characterization of Papillary Renal Cell Carcinoma. New England Journal of Medicine. 2015;Manuscript submitted.

153. Perou CM, Sorlie T, Eisen MB, van de Rijn M, Jeffrey SS, Rees CA, et al. Molecular portraits of human breast tumours. Nature. 2000;406(6797):747-52. Epub 2000/08/30. doi: 10.1038/35021093. PubMed PMID: 10963602.

154. Hakimi AA, Chen YB, Wren J, Gonen M, Abdel-Wahab O, Heguy A, et al. Clinical and Pathologic Impact of Select Chromatin-modulating Tumor Suppressors in Clear Cell Renal Cell Carcinoma. European Urology. 2012. Epub 2012/10/06. doi: 10.1016/j.eururo.2012.09.005. PubMed PMID: 23036577.

155. Kim WY, Kaelin WG, Jr. Molecular pathways in renal cell carcinoma--rationale for targeted treatment. Semin Oncol. 2006;33(5):588-95. Epub 2006/10/19. doi: 10.1053/j.seminoncol.2006.06.001. PubMed PMID: 17045088.

156. Mendell J, Dietz, HC. When the Message Goes Awry: Disease-Producing Mutations that Influence mRNA Content and Performance. Cell. 2001;107:411-4.

157. Gerber N, Brogioli R, Hattendorf B, Scheeder MR, Wenk C, Gunther D. Variability of selected trace elements of different meat cuts determined by ICP-MS and DRC-ICPMS. Animal. 2009;3(1):166-72. Epub 2009/01/01. doi: 10.1017/S1751731108003212. PubMed PMID: 22444183.

158. Scott CS, Chiu WA. Trichloroethylene cancer epidemiology: a consideration of select issues. Environ Health Perspect. 2006;114(9):1471-8. Epub 2006/09/13. PubMed PMID: 16966107; PubMed Central PMCID: PMC1570052.

159. Al-Nabhani KZ, Syed R, Michopoulou S, Alkalbani J, Afaq A, Panagiotidis E, et al. Qualitative and quantitative comparison of PET/CT and PET/MR imaging in clinical practice. J Nucl Med. 2014;55(1):88-94. Epub 2013/12/18. doi: 10.2967/jnumed.113.123547. PubMed PMID: 24337608.

160. Reiner CS, Stolzmann P, Husmann L, Burger IA, Hullner MW, Schaefer NG, et al. Protocol requirements and diagnostic value of PET/MR imaging for liver metastasis detection. Eur J Nucl Med Mol Imaging. 2014;41(4):649-58. Epub 2013/12/19. doi: 10.1007/s00259-013-2654-x. PubMed PMID: 24346415.